



UPPSALA
UNIVERSITET

UPTEC Q14 009

Examensarbete 30 hp
Juni 2014

Investigation of the dielectric breakdown strength of polymer nanocomposites

Mattias Karlsson



UPPSALA
UNIVERSITET

Teknisk- naturvetenskaplig fakultet
UTH-enheten

Besöksadress:
Ångströmlaboratoriet
Lägerhyddsvägen 1
Hus 4, Plan 0

Postadress:
Box 536
751 21 Uppsala

Telefon:
018 – 471 30 03

Telefax:
018 – 471 30 00

Hemsida:
<http://www.teknat.uu.se/student>

Abstract

Undersökning av dielektriska hållfastheten hos polymera nanokompositer

Investigation of the dielectric breakdown strength of polymer nanocomposites

Mattias Karlsson

The aim of this thesis is to investigate the possibility of enhancing the dielectric breakdown strength (DBS) of low density polyethylene (LDPE) with addition of voltage stabilizing additives. In the first part of the thesis, the influence of various process parameters on the alternating current DBS of pure LDPE and LDPE containing either 3 or 30 wt% magnesium oxide nanoparticles was investigated. It was found that the influence of moisture, crystalline structure and process stabilizing additives did not affect the DBS. In the second part of the thesis the effect of five different voltage stabilizing additives was investigated to enhance the DBS. No significant improvement in DBS could be seen for additives mixed with neat LDPE or LDPE nanocomposites by extrusion (typical DBS values ranged between 109-116 kV/mm for neat LDPE). However, the compounding by extrusion resulted in better stability of the breakdown data. A method to swell voltage stabilizing additives into the polymer matrix with solvents have been developed and evaluated. No significant improvements in breakdown strength could be seen for neat LDPE, but the DBS was increased by 15-20 % at low probability of failure for the LDPE nanocomposites. Further work is required to investigate if this increase is significant. It is believed that it is critical to dissolve a higher amount of the voltage stabilizing additives into the polymer matrix. The actual concentrations of the additives need to be quantified with chromatographic methods or infrared spectroscopy.

Handledare: Henrik Hillborg
Ämnesgranskare: Urban Wiklund
Examinator: Åsa Kassman
ISSN: 1401-5773, UPTec Q14 009

Undersökning av dielektriska hållfastheten hos polymera nanokompositer

Mattias Karlsson

Minimerade energiförluster vid överföring av elektricitet blir allt viktigare i dagens samhälle. Att förbättra isolationsmaterialet i kablarna gör att elektricitet kan överföras vid högre spänningar, vilket minskar energiförlusterna. Spänningen som ett elektriskt isolerande material kan utsättas för utan att gå sönder benämns som materialets dielektriska hållfasthet (DBS). Kabelisolation består antingen av papper impregnerat i olja eller av polyeten, som är en polymer. Elektricitet överförs antingen med växelström där strömmen varierar eller likström där strömmen är konstant. Växelström har störst energiförluster men är det vanligaste sättet att överföra elektricitet, speciellt över korta sträckor. För växelströmskablar har polyeten sedan länge använts som isolationsmaterial medan papper impregnerat i olja används för överföring med likström. Energiförlusterna blir mindre om överföringen sker med högre spänning och överföring av elektricitet långa sträckor sker därför med högspänd likström (HVDC). Den första undervattenskabeln med HVDC i världen använde oljeimpregnerat papper som isolationsmaterial och installerades 1954 mellan Gotland och Sveriges fastland. Det första kabelsystemet med HVDC i världen som använde polyeten som isolationsmaterial installerades 1999 på Gotland. Oljeimpregnerat papper som kabelisolation är pålitligt men kan vara miljöfarligt vid läckage. Överföring vid högre temperatur ökar effekten hos kabelsystemet och kablar med polymera isolationsmaterial klarar transmission av elektricitet vid högre temperaturer än oljeimpregnerat papper. Utvecklingen av polymera material som kabelisolation har därför tagit fart och fokus har riktats på att öka materialens DBS, dvs. spänning de klarar innan genomslag sker och materialen går sönder. Genomslag av polymera material beror på många parametrar och förklaras med olika mekanismer beroende på vad genomslaget orsakas av och hur det skadar materialet.

De viktigaste mekanismerna som beskriver genomslag av polymera material är beskrivna i första delen av litteraturstudien i detta examensarbete. I den andra delen av litteraturstudien beskrivs de metoder som används för att förbättra DBS hos polymerer och förbättringar som hittills har åstadkommit är summerade för respektive metod. Att använda polymerer där små partiklar har tillsatts, dvs. polymera kompositer, är en metod som används för att öka DBS. Att tillsätta mikrometerstora partiklar leder till försämrad eller oförändrad DBS medan nanopartiklar, som är tusen gånger mindre, kan leda till förbättrad DBS. Men för att förbättra DBS måste partiklarna vara jämt utspridda i materialet. Ytan av partiklarna interagerar med polymeren och egenskaperna nära detta interaktionsområde kan vara annorlunda än egenskaperna hos det polymera materialet. Ju mindre partiklarna blir desto större del av partiklarnas volym utgörs av denna interaktionsvolym. Om partiklarna är väl utspridda i polymeren så utgör denna interaktionsvolym en stor del av polymerens totala volym, redan vid små andelar iblandade partiklar. Partiklarna kan spridas ut bättre i materialet om dess yta behandlas på så sätt att den blir kompatibel med polymeren. Att tillsätta s.k. spänningsstabilisatorer är den andra metoden

för att öka DBS hos polymerer. Dessa additiv är molekyler som kan sänka elektronernas energi och på så sätt förhindra genomslag. Nanopartiklar och spänningsstabilisatorer kan även kombineras för att förbättra DBS.

Målet med detta examensarbete var att förbättra DBS hos lågdensitetspolyeten (LDPE) genom att blanda i olika spänningsstabilisatorer. En kombination av nanopartiklar och spänningsstabilisatorer har även använts för att förbättra DBS hos LDPE, dvs. spänningsstabilisatorer blandades i nanokompositer av LDPE. Nanopartiklarna bestod av magnesiumoxid. Spänningsstabilisatorerna blandades i LDPE eller nanokompositer av LDPE med två olika metoder: extrudering eller svällning. Under extrudering smälts material och smältan blandas mekaniskt av en roterande skruv. I svällningsmetoden svälls en homogen blandning av spänningsstabilisator upplöst i lösningsmedel in i LDPE. Efter svällningen så torkades materialen för att evaporera ut lösningsmedlet utan migration av spänningsstabilisatorn. När spänningsstabilisatorer blandats med LDPE eller nanokompositer av LDPE så pressades ~0.4-0.5 mm tjocka plattor av materialen. En sådan platta ledde till minst 20 prover som användes för att mäta DBS för ett material. Genomslagsmätningarna utfördes med växelström och resultaten av DBS varierar till viss del slumpmässigt beroende på lokala svagheter hos materialet. Därför måste DBS data för ett material utvärderas statistiskt och för att få pålitliga resultat så mättes DBS på minst 20 prover för utvärdering av ett material.

Först undersöktes spridningen i DBS för ett och samma material och det visade sig att material som extruderats har mindre spridning i DBS än material som inte extruderats. Det fastställdes även att torkning vid olika temperaturer (40 °C eller 70 °C) i vakuum före pressningen inte påverkar DBS. Spänningsstabilisatorer iblandade med extrudering eller svällning i LDPE eller nanokompositer av LDPE visade inga betydande skillnader i DBS jämfört med referenser av samma material. Men spänningsstabilisatorer iblandade i nanokompositer av LDPE med svällningsmetoden visade en ökad lägstanivå av DBS jämfört med referenser av samma material. Men mängden spänningsstabilisator i de pressade proverna måste analyseras, för mängden som svällts in under svällningen eller migrerat ut under torkningen är okänd. Framtida arbete är att komplettera dessa genomslagsmätningar under växelström med mätningar av DBS under likström för de mest lovande materialen, identifiera nya spänningsstabilisatorer och optimera svällningsprocessen.

Examensarbete 30 hp på civilingenjörsprogrammet

Teknisk fysik med materialvetenskap

Uppsala universitet, juni 2014

TABLE OF CONTENTS

1	INTRODUCTION	1
2	LITERATURE STUDY	2
2.1	BREAKDOWN MECHANISMS OF POLYMERS	2
2.1.1	Introduction	2
2.1.2	Intrinsic breakdown strength	3
2.1.3	Avalanche breakdown of polymeric materials	5
2.1.4	Thermal breakdown	9
2.1.5	Electromechanical breakdown	11
2.2	INFLUENCE OF NANOFILLERS	14
2.2.1	Dispersion and size of the filler	14
2.2.2	Influence of the interfacial region	15
2.2.3	Mechanical strength of the interfacial region	19
2.2.4	Particle shape	21
2.3	VOLTAGE STABILIZERS FOR ENHANCING BREAKDOWN STRENGTH	22
2.3.1	Voltage stabilizers used in polyolefine matrices	22
2.3.2	Voltage stabilizers used in polyolefine nanocomposite matrices	24
3	EXPERIMENTAL	26
3.1	MATERIALS	26
3.2	SAMPLE PREPARATION	27
3.2.1	Extrusion	27
3.2.2	Swelling	28
3.2.3	Drying	29
3.2.4	Pressing	29
3.3	MEASUREMENTS	30
3.4	METHOD FOR EVALUATION OF DBS MEASUREMENTS	32
4	RESULTS AND DISCUSSION	35
4.1	STABILITY OF AC DBS MEASUREMENTS	35
4.2	INFLUENCE OF PROCESS PARAMETERS ON BREAKDOWN STRENGTH	37
4.2.1	Different drying conditions	37
4.2.2	Influence of the extrusion process on breakdown strength	41
4.3	INFLUENCE OF NANOFILLERS ON BREAKDOWN STRENGTH	43
4.4	INFLUENCE OF VOLTAGE STABILIZING ADDITIVES ON BREAKDOWN STRENGTH	43
4.4.1	Additives mixed with PE matrices by extrusion	43
4.4.2	Additives mixed with PE matrices by swelling	46
4.5	INFLUENCE OF BOTH NANOFILLERS AND VOLTAGE STABILIZERS ON BREAKDOWN STRENGTH	48
4.5.1	Additives mixed with PE nanocomposite matrices by extrusion	48
4.5.2	Additives mixed with PE nanocomposite matrices by swelling	50
5	CONCLUSIONS	52
6	FUTURE WORK	52
7	ACKNOWLEDGEMENTS	53
8	REFERENCES	54

1 INTRODUCTION

Power is commonly transmitted and distributed short distances by using alternating current (AC) with extruded thermoplastics, e.g. polyethylene (PE), as cable insulation material. It is favorable to use high voltage direct current (HVDC) to transmit power over longer distances because of lower energy losses. Paper impregnated by oil has been used as insulation material for HVDC cables since 1954 when the first underground HVDC cable was installed between Gotland and the mainland of Sweden. One drawback with oil impregnated paper as cable insulation is contamination of the environment with oil if leakage occurs. To joint extruded thermoplastic cables together is easier than for oil impregnated paper cables and the experience for manufacturing and installing already exists for AC extruded cable systems. However, the main advantage for the development of extruded cable systems are the higher capacity that can be achieved because the systems can transmit power at higher temperatures than cables with oil impregnated paper insulation. The first HVDC cable with extruded thermoplastic as insulation material was installed 1999 at Gotland. It is desirable to operate the systems at as high voltage as possible in order to minimize energy losses and allowing transmission over longer distances. One of the limiting factors is the dielectric breakdown strength (DBS) of the insulation system. It is thus desirable to maximize the DBS, while at the same time minimizing the dielectric losses as well as operating the insulation system at as high temperature as possible. However, the mechanisms of dielectric breakdown are complex.¹

The first part of the following literature survey aims to summarize the most important breakdown mechanisms relevant for polymeric materials used for high voltage insulation applications. Polymer composites containing inorganic nanoparticles are promising materials to increase the DBS. The addition of micro sized particles decrease the DBS while the addition of nanoparticles can improve the DBS, if they are well dispersed in the polymer matrix. The incorporation of organic additives which can lower the energy of energetic electrons, called voltage stabilizing additives, are another promising way to improve the DBS of polymers. The most promising polymer nanocomposites and voltage stabilizing additives for polymers are summarized in the second part of the literature study. Those two methods can also be combined to improve the DBS.^{2,3}

The aim of this thesis work is to enhance the DBS of low density polyethylene (LDPE) with addition of voltage stabilizing additives. This was mainly performed after compounding by measuring the DBS under AC conditions, which is a fast measurement for screening of materials. Promising material candidates will be further evaluated with additional measurements. The experience from the literature survey was used to evaluate factors that could influence on the DBS, e.g. sample preparation, compounding parameters and sample thickness.

2 LITERATURE STUDY

2.1 Breakdown mechanisms of polymers

2.1.1 Introduction

The most important breakdown mechanisms for polymers are avalanche, thermal and electromechanical breakdown. Avalanche breakdown is divided into the three subclasses: fast avalanches, erosion breakdown and water treeing. Fast avalanches, thermal and electromechanical breakdown occur fast, while erosion and water treeing are mechanisms that degrade the material over time until failure occurs. This division into short and long term breakdown can be seen in **Table 1**. Typical times from initiation for each breakdown mechanism until failure occurs and at which conditions each breakdown mechanism dominates are also shown in **Table 1**. Fast avalanches dominate at low temperatures while electromechanical failure dominates at high temperatures where the mechanical properties of the polymer decrease. Thermal breakdown dominates in between this temperature interval but occurs often as a combination with fast avalanche or electromechanical breakdown. Erosion breakdown dominates at low voltages where failure occurs after degradation for a longer time. The polymer becomes degraded by partial discharges in the shape of a tree that grows slowly through the polymer. Water trees develop at similar conditions as erosion breakdown but when water is present in the material. This breakdown mechanism is typical for underground cables where water can diffuse into the material.^{4,5,6,7}

Table 1. Breakdown mechanisms divided into short and long term categories dependent on how fast failure occurs after the initiation of the breakdown mechanism. Typical criteria for when each breakdown mechanism dominates are also given, where T is the temperature.^{4,5}

	Short term breakdown			Long term breakdown	
Breakdown mechanism	Fast avalanches	Thermal	Electro-mechanical	Erosion	Water treeing
Time of the breakdown process	$10^{-9} - 10^{-6}$ s	$10^{-7} - 10^{-3}$ s	$10^{-6} - 10^{-3}$ s	$10^{-2} - 10^7$ s	hours-years
Dominating breakdown mechanism at:	low T	low T < T < high T	high T	low voltages over time	presence of water

The intrinsic breakdown strength is a theoretical value of the field required to cause breakdown in materials without defects or impurities. The measured breakdown strength is lower due to the influence of the polymer structure, as well as various additives. Dielectric breakdowns are described with different mechanism dependent on how the breakdown occurs. It is important to know which mechanism that dominates the failure to improve the DBS. For example: an increase in crystallinity results in a longer mean free path that will decrease the DBS, if fast avalanches dominate. However, the DBS can be improved with increased crystallinity due to the higher modulus, if an electromechanical failure occurs. Degradation of the polymer can be caused by partial discharges at low electrical fields, which can result in erosion breakdown in the form of tree shaped channels through the material over time. Locally elevated temperatures, caused by dielectric and joule heating, can result in thermal breakdown, if the temperature cannot be dissipated fast enough to avoid degradation of polymer. A breakdown mechanism rarely causes breakdown on its own, especially not at temperatures where different breakdown mechanisms have similar DBS. Different breakdown mechanisms interoperate at these temperatures and create a synergy effect, which lower the DBS. Thermal and electromechanical

breakdown can combined lower the DBS. This can occur when elevated temperatures caused by thermal losses lower the mechanical properties of the polymer which initiates electromechanical breakdown, as can be seen in more detail in section 2.1.4. The DBS depends mainly on the dominating breakdown mechanism but also on factors such as defects and impurities in the material, measuring conditions (electrodes, surrounding medium, AC, DC or impulse voltages), sample thickness and morphology.^{4,8,9,10,11}

2.1.2 Intrinsic breakdown strength

The intrinsic DBS is based on the theory of fast avalanche breakdown, i.e. electrons accelerated by the electric field causes ionization of molecules during impact and thus regenerating additional free electrons, creating an electron avalanche. Intrinsic DBS is a theoretical value of the maximum electric field before fast avalanche breakdown occurs in a “perfect material”, i.e. without any defects or impurities, and thus only dependent on the physical properties of the material and the temperature. The requirement of a “perfect material” is why intrinsic DBS is considered to be a theoretical value, difficult to reach during experiments. One method to study the intrinsic DBS for transparent materials is to use a focused laser pulse. This eliminates the use of electrodes to measure the DBS and minimizes the risk of defects in the material because only a small volume is tested. Damage in transparent materials can be analyzed optically with increased power of the laser, i.e. increased electric field, to determine when breakdown occurs. Several approaches to describe the intrinsic breakdown at quantum mechanical level have been seen over the past century. The first was formulated by Hippel¹² in 1932 and is called the low energy criterion. Electrons gain energy due to the applied electric field but they also lose energy due to interaction with phonons, i.e. lose energy to induce lattice vibrations. Hippel’s criterion describes that fast avalanche breakdown can only occur if the average energy gained of electrons are larger than the average energy losses of electrons. This criterion for breakdown has been implemented in a method that uses the density functional perturbation theory for estimating the intrinsic DBS for prototypical materials with ionic or covalent bonds. They conclude that the intrinsic DBS is improved for materials with large cut-off frequencies of phonons and large band gaps as can be seen in **Figure 1**. The increase of the intrinsic DBS for covalent and ionic materials is more dependent on the band gap and phonon cut-off frequencies, respectively. Note that the x-axes are scaled differently in **Figure 1** so the slopes cannot be directly compared to each other.^{8,13}

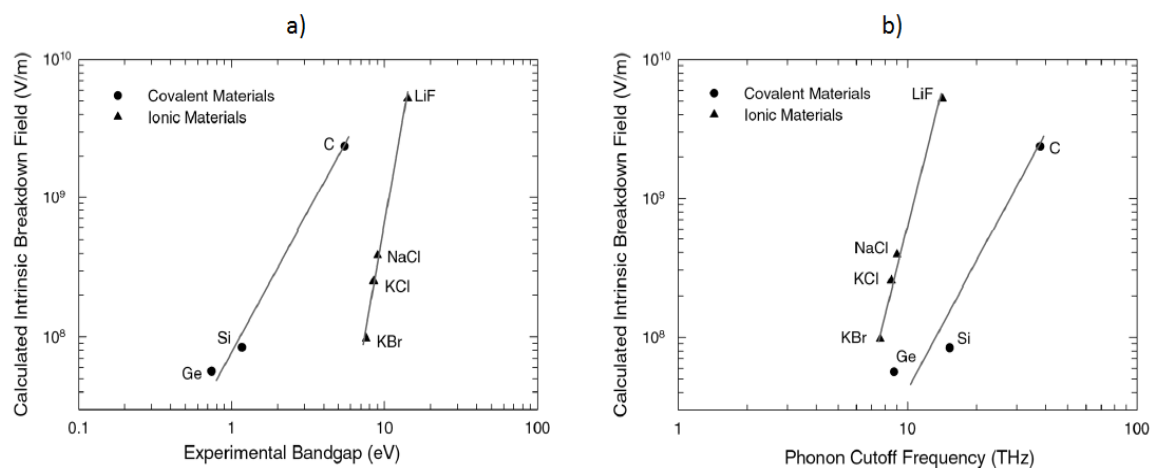


Figure 1. Results of the computed intrinsic DBS for prototypical ionic and covalent materials and their dependency of experimental band gap in a) and phonon cut-off frequency in b). These figures are reprinted with permission from reference 13. Copyright 2012, AIP Publishing LLC.

It is shown by Boggs et al.¹⁴ that PE containing impurities creates energy states within the band gap, which is responsible for the conduction at high field conditions. These states are called traps and the depths of the traps depend on how much energy it requires to release the charge carrier from the trap. Occupied energy states close to the valence band and unoccupied energy states close to the conduction band are called hole and electron traps, respectively. This can be seen in **Figure 2a** that shows the density of states for the chemical impurities that are shown in **Figure 2b** in PE. The further away from the respective band, i.e. further away from the conduction band if the state is unoccupied and vice versa, the deeper are the traps. The time an electron or a hole spends in a trap is dependent on the depth of the trap, i.e. it stays longer in a deep trap than a shallow. The unoccupied energy states closest to the conduction band are called hopping states if they are within 0.2 eV to the conduction band. These impurity states are caused by distortion of bonds in the chain of PE caused by the impurity atom. Shallow traps are defined for energy states between 0.2-0.6 eV from the respective band which also behaves more like hopping sites than traps due to the short time the electron or hole stays there. Both the hopping sites and shallow traps are created by single bonded impurity atoms. Deep traps are defined for energy states between 0.7-1.3 eV from the respective band and the trap with a depth of around 1 eV corresponds to experimental values of the activation energy required for conduction in PE. Deep traps are created by double bonded impurity atoms. The deepest traps have a depth larger than 1.4 eV and are responsible for injection of charges from electrodes into the material and thus the distribution of space charges. Examples of which impurities that correspond to the classification of traps can be seen in **Figure 2b**.

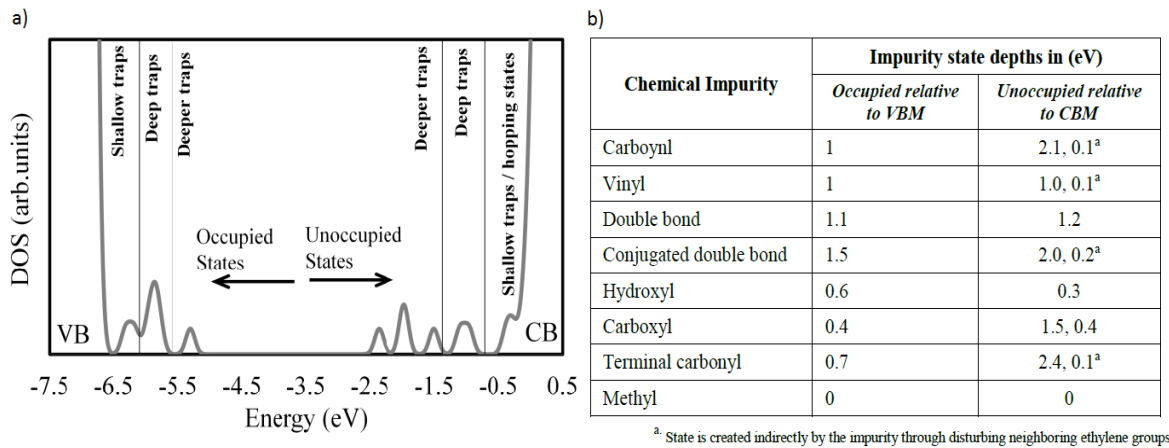


Figure 2. a) Occupied and unoccupied energy states close to the valence and conduction band of PE, respectively, caused by various impurities that create traps with different depths. b) The impurities used for creation of traps in PE. VBM and CBM in the table denotes valence and conduction band, respectively. These figures are reused from reference 14, copyright © 2013 IEEE.

Han et al.¹⁵ investigated how deep traps affect space charge and conduction in PE by adding 3 wt% NaY zeolite nanoparticles to LDPE. Zeolite was used because of its larger surface area compared to commonly used nanoparticles, e.g. TiO₂, due to its porous structure. The amount of space charges was much higher in the pure LDPE compared to the zeolite/LDPE nanocomposite. The space charges in the zeolite/LDPE nanocomposite remained constant over time and originated thus from charge carriers trapped in the two categories deep or deeper traps, as can be seen in **Figure 2a**. The space charges in the LDPE sample were due to charge carriers trapped in shallow traps because the amount of space charges was reduced over time. Both samples developed space charges near the electrodes with the same polarity as the electrode close by, i.e. formation of homo space charges. **Figure 3** illustrates the formation of

hetero and homo space charges. Injected electrons got trapped in the deep traps and created negative space charges close to the cathode. The potential of the interface between the cathode and the sample decreased by a local electric field generated by the deeply trapped electrons close to the cathode and therefore prevent further injection of electrons. This result in a much smaller conduction currents, i.e. decreased mobility of charge carriers, at high electric fields for zeolite/nanocomposite than for the LDPE sample. Ma et al.¹⁶ explain that deep traps can decrease the DBS by enhancing the electric field locally which can initiate breakdown of the polymer. Han et al. conclude that deep traps that create homo space charges can suppress the injection of charges from the electrodes, decrease the mobility of charge carriers and thus improve the DBS.¹

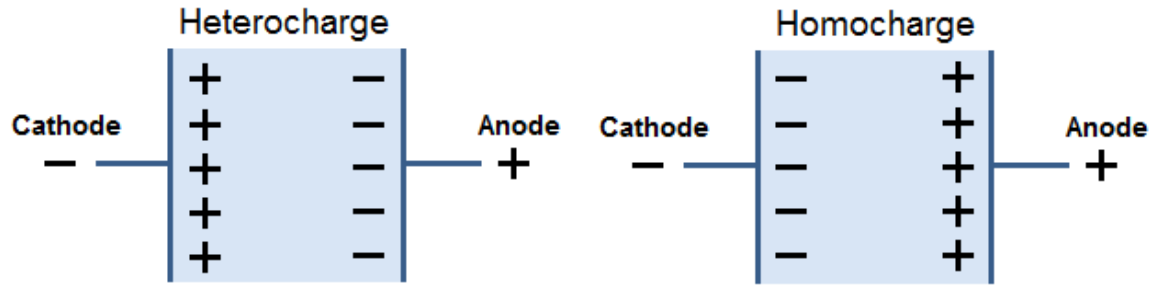


Figure 3. Distribution of hetero and homo space charge development near the electrodes.

2.1.3 Avalanche breakdown of polymeric materials

Avalanche breakdown can both occur slowly and rapidly depending on the magnitude of the applied voltage. Electrons are accelerated by the electric field and gain therefore kinetic energy. Electrons that gain sufficient energy will cause ionization during impact and generate more free electrons. If the process of impact ionization goes on, i.e. the generated electrons also causes impact ionization, then the polymer will undergo rapid breakdown due to an increased amount of highly energetic and mobile electrons. These electrons are distributed similar to an avalanche from the initiation of the first impact ionization. This rapid formation of a conduction path through the insulator is called fast avalanche breakdown. These conduction paths can also be created slowly over time during lower applied voltages and is then called trees. There are two categories of trees: water trees created due to water present in the material and electrical trees which is caused by erosion due to discharges of gas. Water treeing is a degradation mechanism of the polymer, which can be initiated if water is present in the material under high voltage conditions. It can be mitigated by including hydrophilic additives or modifying the size and number of spherulites. Breakdown caused by electrical trees are called erosion breakdown. Partial discharges in gas pockets damages the polymer locally by erosion, i.e. a bombardment of electrical arcs against the polymer in this case, which expands the electrical tree.^{7,17,18}

Fast avalanches

This mechanism of failure is often called avalanche or impact ionization breakdown but will be denoted with fast avalanche breakdown in this thesis. This because avalanche breakdown is used as a group name for the three breakdown mechanisms that damage the material in the shape of a tree, i.e. fast avalanches, erosion breakdown and water treeing. Electrons that have enough kinetic energy to cause ionization during a collision can initiate fast avalanches. This will generate an additional free electron if no electrons are recombined. The length between interactions of electrons and the polymer matrix is called the mean free path and electrons gain kinetic energy from the applied field during the movement over this path. This energy is then

reduced by interactions with the polymer matrix. The amount of additional mobile electrons generated by ionization during impact will rapidly increase and create a conduction path through the insulator similar to an avalanche, if the ionization process goes on. This breakdown mechanism depends therefore on the mean free path of the electrons and the magnitude of the applied electric field. The short mean free path in solid insulation materials (5-20 Å) makes it difficult for the average applied electric field to accelerate the electrons to a kinetic energy that causes ionization and thus fast avalanche failure. However, the magnitude of local fields in the material can be enhanced at the tip of electrical trees, by defects or by the formation of space charges near the electrodes. These enhanced local fields can thus initiate an avalanche of mobile electrons. Breakdown due to ionization which results in additional electrons is described by Kao et al. only to occur at regions with low density, which contain small voids where the mean free path is longer.^{7,9,19}

There usually exist voids of different sizes in a polymeric material. Small voids due to the free volume of the polymer chains correspond to the mean free path of electrons and are around 5-20 Å. Larger voids can be created in the polymer during processing of the material, e.g. incorporation of gas bubbles in melted PE during crosslinking. Other factors such as impurities and incorporation of additives in polymers can result in presence of larger voids. Also degradation mechanisms, e.g. electrical aging, creation of water and electrical trees, can result in larger cavities. The mean free path of electrons is much longer in gases than in solids and depends on the pressure of the gas. Voids inside the polymer filled with gas can therefore be ionized at lower voltages and initiate an avalanche of energetic electrons. Paschen made experiments of breakdown voltages for gases with different pressure of the gas and distances between the electrodes. The breakdown voltages for various distances and pressures can be used to compare at which voltages ionization of gas molecules will occur in voids of different sizes in the polymer. Those experimental results can be described by Paschen's law,

$$V_b = (Bpd) / (\ln(pd) + \ln\left(\frac{A}{\ln(1+\frac{1}{\gamma})}\right)), \quad (1)$$

where V_b is the breakdown voltage of the gas dependent on the pressure of the gas (p) and distance between the electrodes (d). A , B and γ are constants. A is related to the saturation ionization of the gas, B is related to the energies of excitation and ionization and γ is called Townsend's secondary ionization coefficient and is related to the electrode material.^{7,19,20}

Figure 4 shows Paschen's law for air at atmospheric pressure where the breakdown voltage is a function of the gap between the electrodes. The value of γ depends on the electrode material but also on surface conditions and purity of the gas and is therefore not constant for different magnitudes of electric fields between the electrodes and pressures of the gas. The Paschen curve in **Figure 4** is calculated with $\gamma=0.01$ which is for aluminum electrodes and corresponds to the interval of the minimum breakdown voltage. The minimum value of the breakdown voltage is around 300 V which occurs at an electrode distance of around 10 µm. These values are in agreement with values found in literature for air at atmospheric pressure. Voids with a size of around 10 µm are therefore most harmful to the polymer because of the higher probability for ionization of the gas to occur which can degrade the polymer. Smaller and larger voids are therefore to prefer which have higher breakdown voltages.^{7,21}

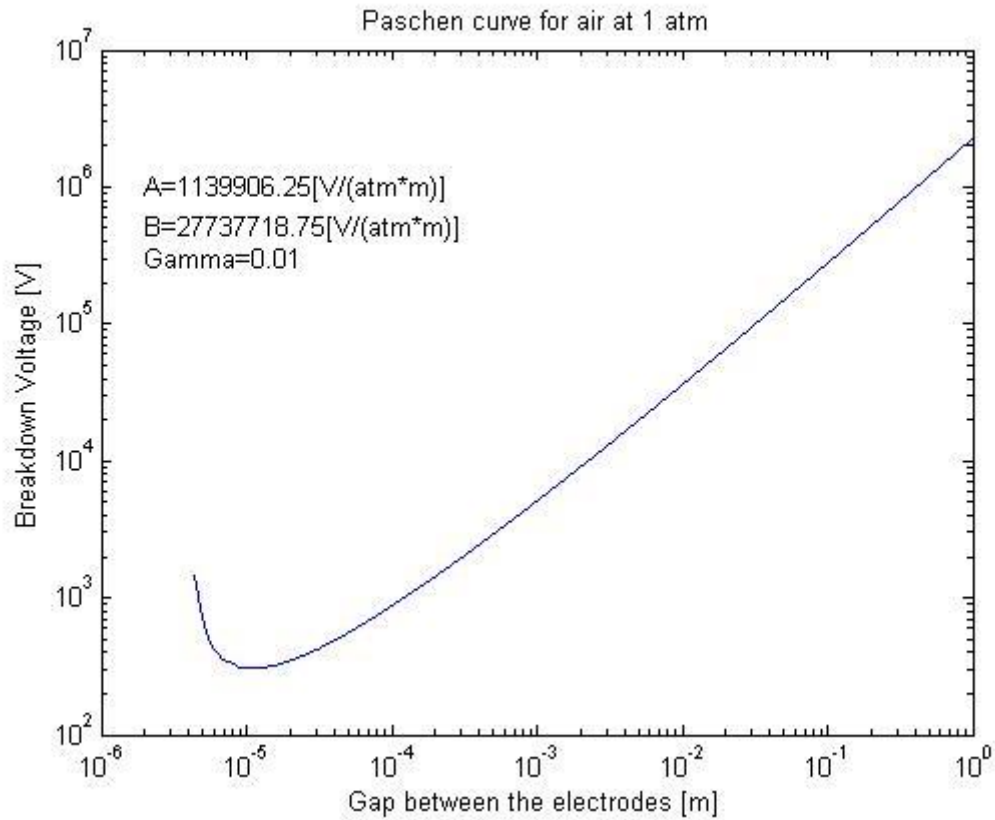


Figure 4. Breakdown voltages for air at atmospheric pressure as a function of the distance between the electrodes calculated by Paschen's law. The values of the constants A and B are for air, gamma is for aluminum electrodes and are taken from reference 20.

Fast avalanche breakdown is dependent on the thickness of the dielectric material. Thinner samples result in higher DBS than thicker samples because the probability that a thinner sample contains defects is smaller than for a thicker sample. This relationship between the DBS and the thickness of the sample have been described by an inverse power law equation, i.e. $E(d)=kd^{-n}$ where n and k are constants correlated to the material, which is derived from fitting of experimental results. Chen et al.²² have developed a model that describes how the DBS varies with thickness for breakdown under DC conditions based on the theory of bipolar charge injection, which is a theory that describes the transport of charges. The results of a simulation based on this model for PE is showed in **Figure 5** and the simulated values agree with experimental results.

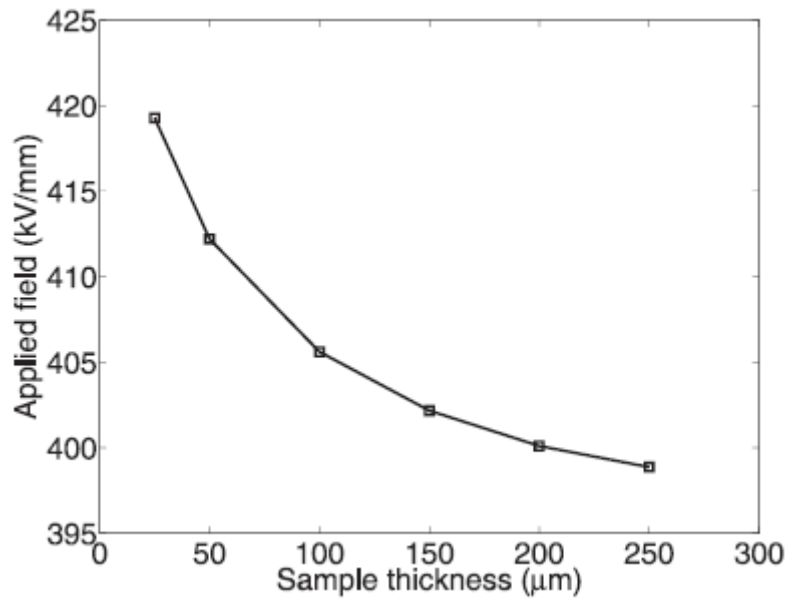


Figure 5. Simulated results of the DC DBS for PE as a function of the thickness of the sample. This figure is reprinted with permission from reference 22. Copyright 2012, AIP Publishing LLC.

Water treeing

Water can degrade insulation materials under high electric field conditions. Defects in the material locally enhance the electric field which water tends to diffuse to. The diffusion cause stresses in the material which creates micro sized cavities that form channels, called water trees. Degradation caused by water trees occur especially in underground cables where water can diffuse into the cable over time. It has been shown experimentally that two samples of PE with the same degree of crystallinity can develop water trees at different rates. This is due to that water tree propagation is dependent on the size and number of spherulites of the sample. The smaller and more spherulites results in slower propagation of water trees. Nucleation agents, e.g. phenolphthalein, methyl red and cresine, can be added to PE in order to decrease the size and increase the number of spherulites and therefore increase resistance against water trees. Hydrophilic additives, e.g. polyethylene glycol, can also increase the resistance against water trees by binding water to its surface, which reduces the amount of water in defects that could have initiated water tree growth. Yoshimura et al. observed spherulites in a domain with water trees destroyed by local forces resulting in fatigue. He drew the conclusion that Coulomb forces resulting in electrostatic pressure and forces from hydrated ions injected into the polymer are important factors during the formation of water trees. Water treeing occurs easiest in the amorphous domains of the polymer and water trees therefore tend to extend along amorphous domains between spherulite boundaries. Amorphous regions also exist between lamellae inside spherulites. Additives that cannot crystallize diffuse to these amorphous regions inside spherulites if they are compatible with the polymer and thus can be solved. Additives which have low solubility in the polymer diffuse to the other amorphous region between the spherulites. This explains the superior mechanical stress that the amorphous domains between the lamellae can withstand in comparison to the domains between the spherulites and that is why water trees grow in the latter domain around spherulites.^{6,17,23,24}

Erosion breakdown

Erosion breakdown, also called electrical trees, occur at low electric fields and grow slowly over time due to partial discharges that damages the polymer locally. The erosion DBS is measured with long endurance tests, usually with pin plane electrode geometry to initiate the growth of a tree at the tip of the pin. The rate of tree growth can be increased by applying higher voltages during the erosion breakdown measurements than the voltages cable insulation materials are exposed to during power transmission. Important parameters to measure for electrical trees are time to tree initiation and time to breakdown. Tanaka et al.¹⁸ describe the process of electrical treeing with three stages. The first stage is the initiation of a tree, second growth of the tree and third widening of the tree channel. The initiation of a tree is believed to be caused by charge injection from the electrodes. Solid dielectric breakdown at the top of the tree results in growth of the tree by formation of thin channels that corresponds to stage two of treeing. However, breakdown doesn't occur directly when a thin tree channel has grown to the other electrode. The channels of the trees are first widened by partial discharges of gas, which degrades the polymer by erosion of electric arcs. The much longer mean free paths in gaseous states of aggregation than the solid state result in electrons with sufficient energy to cause impact ionization of the gas. Electrical trees can propagate in different shapes and are divided into different types of trees, as can be seen in **Figure 6**.^{25,26}

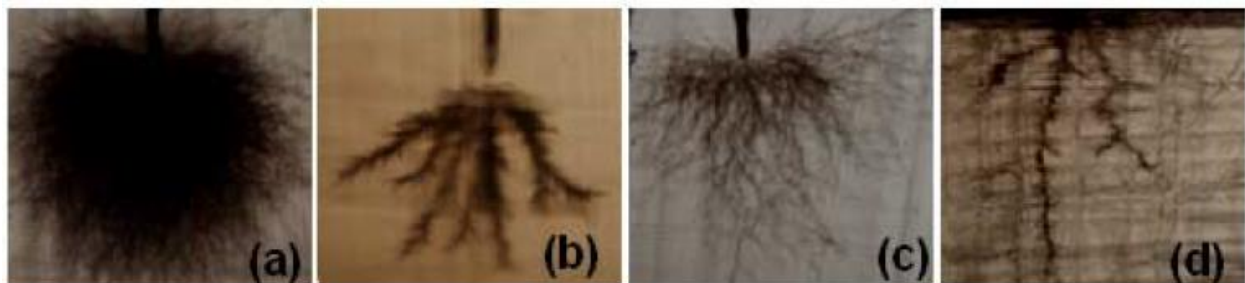


Figure 6. Different types of electrical trees in cross-linked polyethylene (XLPE): a) Bush b) tree like c) fibrillar d) intrinsic. This figure is reused from reference 25.

Nanocomposites can show better resistance against erosion breakdown than neat polymers if the nanoparticles are well dispersed. An interaction zone is created at the interface between nanoparticles and polymer in nanocomposites. The volume of this interaction zone becomes a big part of the material when nanoparticles are well dispersed, due to their large surface area. This interaction zone is believed to be an important factor for the understanding of the influence of nanoparticles on electrical treeing, but is not completely understood yet. The resistance against widening of tree channels caused by partial discharges can be significantly improved by well dispersed nanofillers, especially at low voltages. Resistance against partial discharges is important because widening of the tree channels can result in agglomeration of nanoparticles. Nanocomposites that reduce the amount of space charges could increase the resistance against tree initiation. Neat polymers usually show better resistance against erosion breakdown at higher voltages.¹⁸

2.1.4 Thermal breakdown

Thermal breakdown occur when thermal losses in the polymer cannot be dissipated fast enough and causes elevated temperatures that damages the polymer. Thermal losses are caused by joule heating during DC conditions or joule heating and heat from dielectric losses during AC conditions. Joule heating originates from small conduction currents that generate heat due to

the resistivity of the material. The quantity of heat generated by joule heating (Q_j) depends on the current I and on the resistivity R ,

$$Q_j = I^2 R . \quad (2)$$

The rate of heat generation can be expressed by

$$C_v \left(\frac{dT}{dt} \right) = \sigma(T, E) E^2 , \quad (3)$$

where C_v is the heat capacity, E is the electric field, T is the temperature, t is the time, σ is the conductivity. Typical for insulating materials such as polymers are low thermal conductivity and low dielectric losses which makes the heat generated by dielectric losses negligible and thus only heat generated by joule heating has to be considered. This assumption equals Eq. (2) and (3).^{11,19}

Claude et al.¹¹ showed that thermal breakdown occur at and below the glass transition temperature for a copolymer of polyvinylidene fluoride-chlorotrifluoroethylene (PVDF-CTFE), while electromechanical breakdown occur at higher temperatures. Values of conductivity as a function of electric field and temperature were measured for thin film samples of PVDF-CTFE. The glass transition temperature of this polymer is -24 °C. The thermal conductivity σ can be expressed as

$$\sigma = \sigma_0 e^{[gE + a(T - T_0)]} , \quad (4)$$

where E is the electric field, T is the temperature while T_0 , σ_0 , g and a are constants. Claude et al.¹¹ used Eq. (4) to calculate the temperature as a function of the electric field, which is shown in **Figure 7a**. The temperature rises abrupt when the critical temperature is reached for which thermal breakdown occurs. It can also be observed that the DBS increases with decreasing temperature. Defects in the material can enhance the effect of local elevated temperatures and thus lower DBS. This is believed to be the case for the different experimental and theoretical values of the thermal DBS in **Figure 7b** at low temperatures.

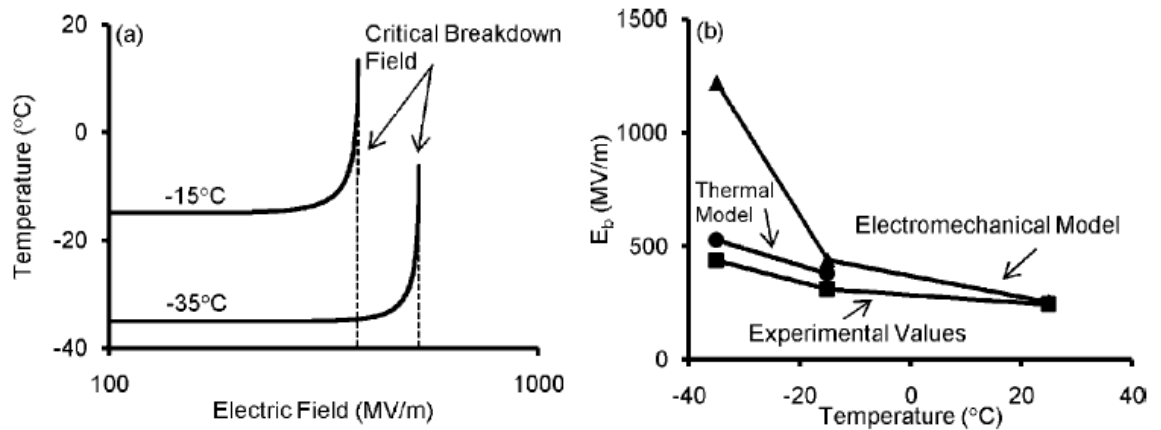


Figure 7. a) Theoretical computed values of the thermal DBS for PVDF-CTFE at -15 and -35 °C. b) Incorporation of a model for thermal and electromechanical DBS and experimental values dependent of the temperature for the same polymer as in a). These figures are reprinted by permission from reference 11. Copyright 2007, AIP Publishing LLC.

Electromechanical breakdown, which depends on the mechanical properties of the insulating material, dominates at higher temperatures. The theoretical DBS model for electromechanical breakdown, **Figure 7b**, agrees well with the experimental value at 25 °C. For temperatures in between, e.g. at -15 °C, the lower experimental DBS compared to values of the models is believed to be explained by a synergy effect of both thermal and electromechanical breakdown

which lowers the DBS. Electromechanical DBS is dependent on good mechanical properties, which can be decreased under elevated temperatures.¹¹

Yin et al.²⁷ have investigated which impact thermal aging of different polymers has on the DBS as well as mechanical and physical properties. The 1 mm thick samples consisted of polyimide with different amounts of Al_2O_3 nanoparticles. The DBS under AC and DC conditions only decreased significantly after aging if thermal degradation resulted in large defects. The mechanical properties were otherwise altered more by thermal aging than the DBS. The addition of Al_2O_3 nanoparticles decreased the rate of thermal degradation by preventing diffusion paths for oxygen. The temperature at which the thermal aging took place was 50-100 °C under the glass transition temperature.

Conduction currents exist in insulating materials, even at low fields and increases with increased electric field and temperature. Impurities and the disordered characteristics of amorphous domains in the material cause the conduction currents at high fields, over 10 kV/mm, by insertion of new possible energy states in the band gap of the insulator, called impurity states. This reduces the band gap which increases the mobility of charge carriers. The thermal conductivity of an insulating material are essential to disperse the heat in order prevent thermal breakdown. Theoretical estimations of the thermal DBS for LDPE containing different amounts of MgO nanoparticles has been made by Reddy et al.²⁸ from experimental data of thermal conductivity, leakage current and volume resistivity. These theoretical values of the thermal DBS estimated from experimental data are based on a plane parallel geometry of the sample. The conclusion is that the increase of thermal conductivity with an increased amount of MgO nanoparticles has a negligible influence on the estimated thermal DBS. However, variations in the volume resistivity and leakage current have a larger impact on the estimated thermal DBS.²⁹

Nagao et al.³⁰ have investigated how joule heating affects the breakdown under high DC conditions at room temperature for films of PE or ethyl-vinyl acetate (EVA). A thermograph was used to measure elevated temperatures to detect if joule heating occurred before breakdown took place and where it occurred. Joule heating was observed before breakdown and the breakdown was initiated at the point with the highest elevated temperature caused by joule heating. This was observed for both polymer films. However, no rapid rise in temperature with increased electric field could be observed. Thermal breakdown is therefore not believed to be the only breakdown mechanism resulting in breakdown in this study but a contributing mechanism. The other breakdown mechanisms contributing to failure of the samples in this study are either believed to be fast avalanche or electromechanical breakdown. Fast avalanche breakdown is commonly assumed to be the dominating breakdown mechanism for PE at room temperature and electromechanical breakdown can be initiated by decreased mechanical properties at elevated temperatures.

2.1.5 Electromechanical breakdown

The mechanical strength of polymers decreases with increasing temperature due to softening of the polymer. Electromechanical breakdown is dependent on the mechanical strength of the polymer and is responsible for the lower DBS values at elevated temperatures, which is shown by Claude et al.¹¹ in **Figure 7b**. The polymer can be compressed by the electrostatic force that is generated by the applied voltage between the electrodes. The electric field will increase, due to the shorter distance between the electrodes, if the electrostatic force decreases the thickness of the polymer. This results in an enhanced electrostatic force between the electrodes, further deformation of the polymer and eventually breakdown due to mechanical failure. Stark and

Garton have developed a simplified theory of electromechanical breakdown for polymer samples in the shape of a rectangle, i.e. with parallel sides. Elastic deformation of the polymer will occur and result in electromechanical breakdown, if the compressive stress due to electrostatic attraction between the electrodes becomes larger than the restoring elastic stress of the polymer. The balance between the electrostatic compressive stress and the restoring elastic stress can be expressed by

$$\frac{\epsilon_r \epsilon_0}{2} \left(\frac{V}{d}\right)^2 = Y \ln\left(\frac{d_0}{d}\right), \quad (5)$$

where V is the applied voltage and d is the compressed thickness of the polymer which is a function of V . Y is Young's modulus, d_0 is the initial thickness of the polymer, ϵ_r and ϵ_0 are the permittivity of the polymer and of vacuum, respectively. Equation (5) can be reorganized and express V as a function of d ,

$$V = d \sqrt{\left(\frac{2Y}{\epsilon_r \epsilon_0} \ln\left(\frac{d_0}{d}\right)\right)}. \quad (6)$$

The maximum value of V , i.e. when the thickness goes to zero, is obtained by taking the derivative of V with respect to d and equal the expression to zero,

$$\frac{dV}{d[d(V)]} = 0. \quad (7)$$

$d(V)$ is the compressed thickness as a function of the applied voltage. The maximum voltage where the thickness of the polymer goes to zero, i.e. the breakdown voltage when the electrostatic stress exceeds the restoring elastic stress of the polymer, is obtained when

$$\ln\left(\frac{d_0}{d}\right) = \frac{1}{2}. \quad (8)$$

The breakdown strength E_c for electromechanical breakdown according to the theory of Stark and Garton is therefore given by

$$E_c = \frac{V_c}{d_c} = \sqrt{\frac{Y}{\epsilon_r \epsilon_0}}, \quad (9)$$

where V_c is the applied voltage at breakdown and d_c is the thickness of the compressed polymer when breakdown occurs. This theory is an approximation which does not include plastic deformation of the polymer or variations of Young's modulus. The breakdown voltage is based on the assumption that the thickness due to deformation of the polymer goes to zero at the criterion for breakdown, which also is a theoretical approximation different from the real situation.⁷

Stark and Garton¹⁰ measured the DBS of uncrosslinked PE and PE crosslinked by radiation. One sample irradiated with 100 Mrad and the other with 300 Mrad that prevented softening of these samples at the melting point of PE, as can be seen in **Figure 8**. Theoretical DBS values for the three samples calculated with Eq. (9) are in agreement with the experimental values in **Figure 8** despite the approximations in this theory of electromechanical breakdown.

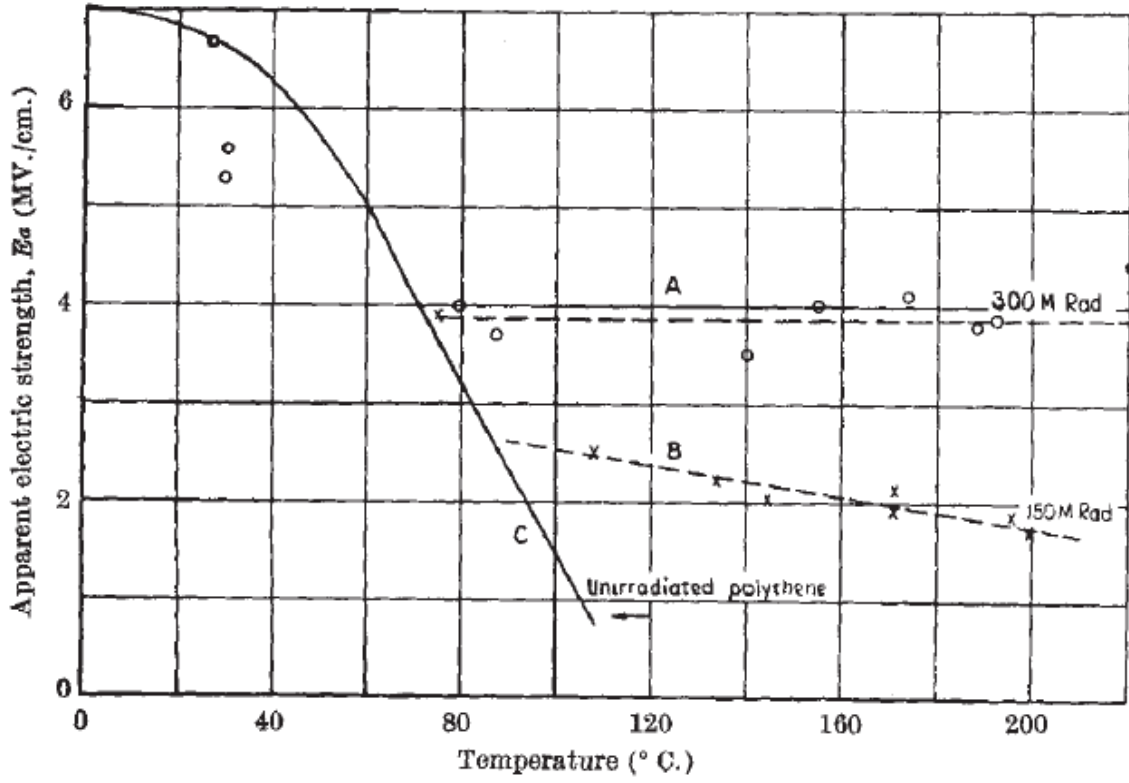


Figure 8. DBS measurements as a function of temperature for two irradiated samples and one sample without irradiation. This figure is reused from reference 10.

Claude et al.¹¹ have modified the theory of Stark and Garton by including the yield stress σ_y instead of Young's modulus. The breakdown field E_c can then be expressed as,

$$E_c = \sqrt{\frac{2\sigma_y}{\epsilon_r \epsilon_0}}. \quad (10)$$

The theory of Stark and Garton has also been modified by Zhou et al.³¹ who developed a power law model that takes plastic deformation into account. The power law model,

$$\sigma_y = K \ln\left(\frac{d_0}{d}\right)^N, \quad (11)$$

includes K which is dependent on the yield strength σ_y and N that describes the deviation from ideal plasticity. N=0 indicate ideal plasticity, N=1 linear elasticity and N=0.1-0.6 for polymers with crystalline regions. The criterion for breakdown according to the power law model is expressed as,

$$E_c = \frac{V_c}{d_c} = \sqrt{\frac{2K}{\epsilon_r \epsilon_0}} \left(\frac{N}{2}\right)^{N/2}. \quad (12)$$

Zhou et al.³¹ performed stress-strain measurements of poly(vinylidene fluoride-hexafluoropropylene) at various temperatures in order to fit these experimental results to the power law equation. The experimental values of the DBS as a function of temperature are shown in **Figure 9** and are compared to theoretical values of the DBS calculated by the Stark and Garton and the power law model. The values calculated from the model of Stark and Garton shows much higher values than both the experimental and theoretical values based on the power law model, which agrees well with each other.

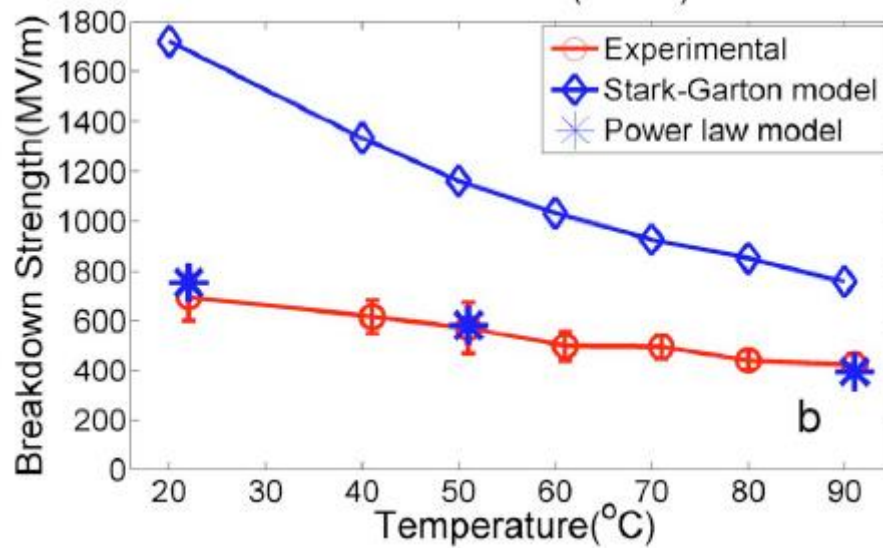


Figure 9. Experimental and theoretical values of the DBS, according to the Stark-Garton and power law model for poly(vinylidene fluoride-hexafluoropropylene) at different temperatures. This figure is reprinted with permission from reference 31. Copyright 2009, AIP Publishing LLC.

Blok and LeGrand³² developed a theory of electromechanical breakdown where the sample is deformed locally by shear forces caused by local enhancements in the electric field. The area that is deformed creates an indentation which generates an even more enhanced electric field close to the indentation. This increases the shear force of the indentation even more and results eventually in electromechanical breakdown or another contributing breakdown mechanism with lower DBS. The above mentioned theories of electromechanical breakdown only assumes that compressive forces act on the polymer during breakdown, while Blok and LeGrand also describes that local inhomogeneous electric fields exists which creates shear forces. Blok and LeGrand based their theory on experimental observations by transmitting polarized light through a sample during electromechanical breakdown and the fact that polymers which are subjected to shear forces are optically anisotropic normal to the plane of the sample. This is not the case for polymers only subjected to compressive, i.e. uniaxial, forces.⁷

2.2 Influence of nanofillers

2.2.1 Dispersion and size of the filler

Figure 10 illustrates that the interfacial zone becomes a larger part of the particle when the particle size decreases. The high surface area of the small nanoparticles is a problem during the dispersion into the polymer matrix. It is reduced by agglomeration of nanoparticles which minimizes the surface energy of the particles in comparison to the polymer matrix. The dispersion can be improved if coated nanoparticles which have compatible interfaces to the polymer matrix are used. The coatings must bond well to the nanoparticles to avoid too high dielectric losses and leakage currents in the nanocomposite. The DBS has both been improved and decreased by incorporation of various nanofillers in polymer matrices. Good dispersion of the filler is crucial to increase the DBS so the nanoparticles don't agglomerate into clusters and act like micro sized particles. Fillers can act as defects in the dielectric which locally distort the electric field and lower the DBS. The reason for these field distortions are differences in conductivity and permittivity between fillers and the polymer matrix under DC and AC conditions, respectively. Using nanoparticles as fillers can minimize this local distortion of the electric field.^{2,16,33,34}

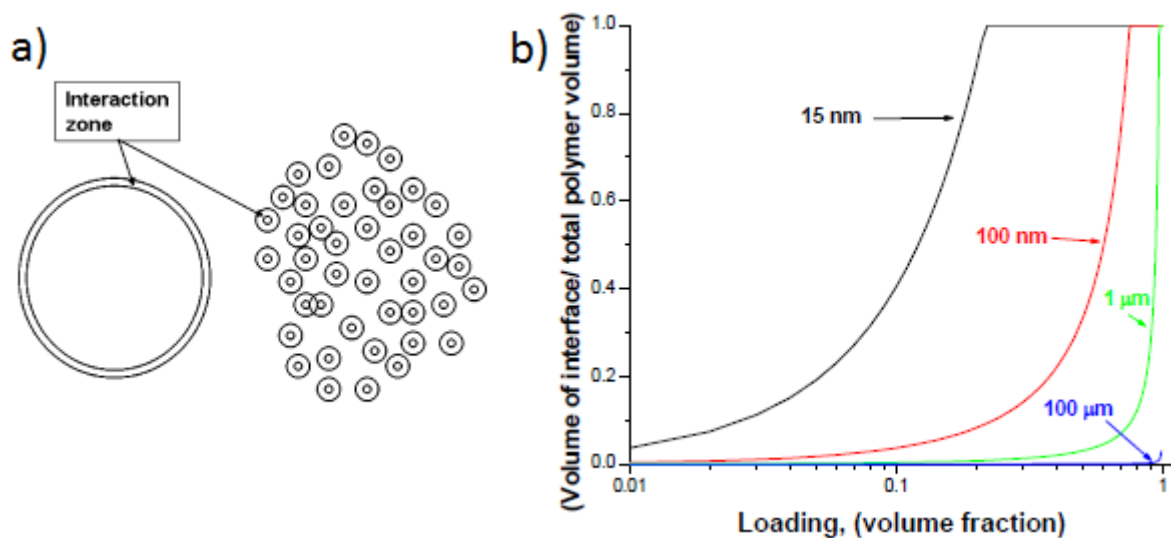


Figure 10. a) Illustrates the effect of increased volume ratio of the interaction zone and the volume of the particle when the particle size decreases. b) The volume of interface per total polymer volume as a function of the volume fraction of nanoparticles for different particle sizes. These figures are reused from reference 34.

2.2.2 Influence of the interfacial region

A lower concentration of nanoparticles correspond the same surface area as a higher concentration of micro sized particles. This is the reason why the interfacial region between the particle and the polymer network becomes more important as the size of the particle decreases, as can be seen in **Figure 10**. Coatings on the particles surface have therefore a larger impact on the dielectric properties of the composite and hence the DBS. Locally near the interfacial layer of the nanoparticle the properties of the matrix can be different than the macroscopic bulk properties of the matrix. Ma et al.¹⁶ coated TiO₂ nanoparticles with the polar silane AEAPS, N-(2-aminoethyl) 3-aminopropyl-trimethoxysilane), and dispersed them in a matrix of LDPE. The DBS of a nanocomposite containing 5 wt% AEAPS surface modified TiO₂ particles, average size of 23 nm, was improved with 40 % compared to the unmodified TiO₂ nanocomposite. However, the DBS of the neat polymer was higher than the surface modified TiO₂ nanocomposite, as can be seen in **Figure 11**. The increase in DBS compared to the unmodified TiO₂ nanocomposite is still interesting because several observed factors could have resulted in lower DBS for the surface modified nanocomposite. These factors were: worse dispersion into the polymer matrix, a more incompatible hydrophilic surface to the hydrophobic polymer matrix and more disordered spherulites compared to the uncoated sample. The reason for the higher DBS of the coated samples can therefore be attributed to the electronic characteristics of the polar AEAPS groups that were used for surface modification. The DC DBS measurements were carried out at room temperature and fast avalanche breakdown were therefore assumed to be the dominating failure mechanism. The higher DBS for the sample with polar groups are explained by reduction of electrons energies, due to creation of electron traps, scattering and excitation processes, which prevent the development of an avalanche.

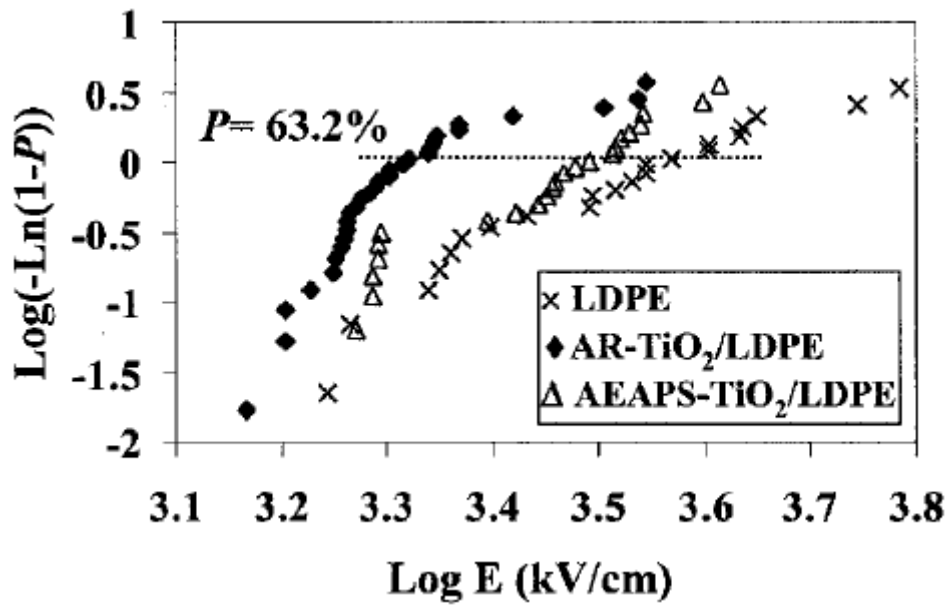


Figure 11. The DBS of LDPE and LDPE nanocomposites containing uncoated and AEAPS coated TiO₂ nanoparticles. The results are presented by a Weibull plot that shows the cumulative probability of failure as a function of the breakdown field. This figure is reused from reference 16.

Pulsed electro-acoustic measurements observed different distribution of space charges in the three samples. The creation of space charges is due to trapping of charge carriers. The sample containing uncoated TiO₂ nanoparticles created negative space charges close to the cathode and positive space charges close to the anode, i.e. creation of homo space charges which have the same polarity as the electrode close by. Both the pure LDPE and the LDPE sample with AEAPS coated TiO₂ nanoparticles showed a development of hetero space charges, i.e. creation of space charges with different polarity compared to the electrode close by. The homo space charge development for the uncoated sample showed an increase in charge injection from the electrodes. This is contradictory to Yamano³ in section 2.3.1 who concludes that a development of negative space charges near the cathode, i.e. homo space charges, will suppress the injection of charges. The amount of space charges was reduced for the coated sample compared to both other samples. However, these smaller amounts of space charges were observed to consist of deep traps. Ma et al.¹⁶ explain that breakdown could be caused by locally increased electrical fields around the deep traps. This assumption is also contradictory to Yamano who describes that his samples which contained the deepest traps resulted in the highest DBS. Yamano describes that the improvement in DBS for the sample with deepest traps is due to reducing the energy of electrons by trapping which creates a homo space charge distribution and reduces the injection of charges.

Smith et al.³⁵ investigated the DBS of SiO₂ micro- and nanoparticles added to a matrix of XLPE. The results for AC, DC and impulse DBS measurements are summarized in **Figure 12**. The SiO₂ nanoparticles are surface modified with triethoxyvinylsilane for one of the nanocomposite samples. The DBS of the surface modified sample compared to the untreated nanocomposite increases significantly for DC and impulse DBS measurements but remains almost constant for AC DBS measurements. Homo space charge development at the electrodes that prevents further charge injection attributes to the higher DC DBS for the surface modified nanocomposite. The main reason for higher impulse DBS of nanocomposites than AC and DC DBS are believed to be scattering of charges due to large interfacial areas of the nanoparticles. Homo space charges requires longer time to develop than for impulse breakdown to occur and scattering is therefore believed to be the main reason for higher impulse than AC and DC DBS.

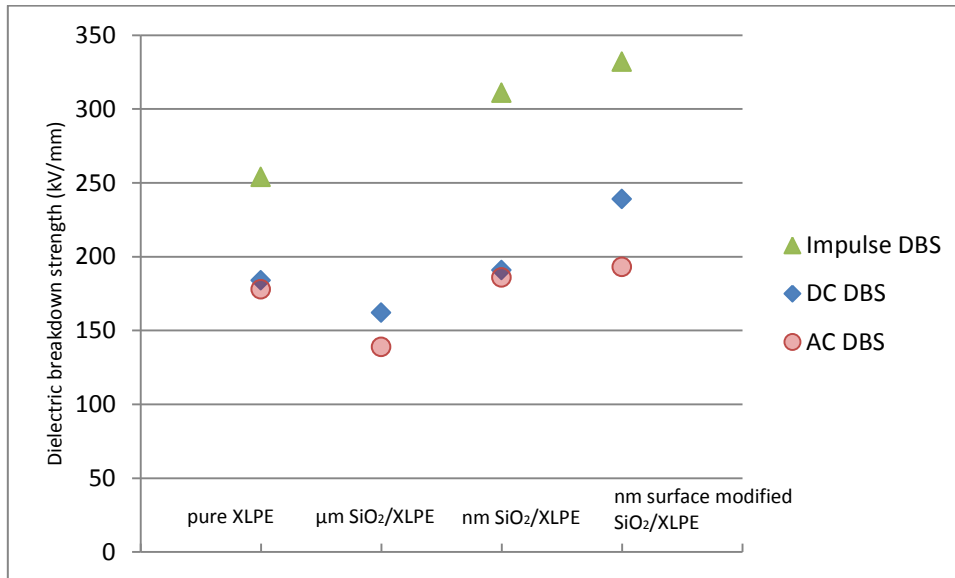


Figure 12. Comparison of the results from Smith et al.³⁵ for XLPE composites containing SiO₂ particles. The composites contain 12.5 wt% SiO₂ particles and the size of the micro- and nanoparticles are 6 μm and 12 nm, respectively.

Roy et al.³⁶ have compared the DC DBS for neat XLPE, XLPE silica microcomposite and XLPE silica nanocomposites with and without surface treatments of the silica particles. The three different surface modifications of the nanoparticles were hexamethyldisilazane (HDMS), triethoxyvinylsilane (TES) and N-(2-aminoethyl) 3-aminopropyl-trimethoxysilane (AEAPS). The XLPE silica nanocomposite with the TES surface modification showed the largest increase in DBS. Its DBS was 66 % higher than the neat XLPE at room temperature. The DBS decreases with increased temperature, which is shown in **Figure 13** for the XLPE silica nanocomposites and the neat XLPE. This is due to the influence of other breakdown mechanisms than fast avalanche breakdown at higher temperatures, e.g. thermal or electromechanical breakdown as described in section 2.1.4. The nanocomposites contained 5 wt% silica nanoparticles which had a diameter of 100 nm and the thickness of the samples were 15-150 μm. The DBS of XLPE decreases rapidly by addition of micro sized silica particles and this is mainly explained by the creation of defects caused by the microsilica particles. All nanocomposites showed an improvement in DBS at room temperature compared to the neat XLPE sample. The mobility of the charge carriers were decreased for all the nanocomposite samples, i.e. both modified and unmodified, while the mobility increases for the neat XLPE and microcomposite with an increased applied field. The explanation for this is that nanoparticles scatter charge carriers and thus reduce their energy which improves the DBS. An additional explanation to this is that the crystalline morphology can be changed by incorporation of nanoparticles. The DBS can be increased if the morphology changes result in less ordered crystalline domains, because the mobility of charge carriers are lower for amorphous than crystalline domains.

Two reasons contribute to the higher DBS for surface modified compared to unmodified silica nanocomposite samples. First, covalent bonding between nanoparticles and the XLPE matrix reduces the amount of defects present in the composite which is the case for the non-polar surface modification with TES. Second, silica particles with polar interfaces, i.e. AEAPS and HDMS surface modified silica particles, create deep traps which increase the threshold voltage for charge injection, decrease the mobility of charge carriers and thus improve the DBS. The nanocomposites also showed superior results compared to the pure XLPE during voltage endurance tests. The time to breakdown was 100 times longer for the nanocomposites and they

could also handle much higher fields than the pure XLPE. The TES composite with the highest DBS had a crystallinity of 60 % instead of 40 % as the other samples, even though the sample preparation and process conditions were the same. Larger total percent crystallinity has been shown by Tanaka et al. to decrease the DBS of LDPE during fast avalanche breakdown, due to longer mean free paths of the electrons. However, improved DBS with increasing degree of crystallinity indicates that the breakdown could be dominated by the electromechanical mechanism, which depends on good mechanical properties as described in section 2.1.5. Which breakdown mechanism that dominates is not discussed in this article by Roy et al.³⁶, but he refers to one of his previous articles³⁷ where he concluded that alteration of the amount crystallinity had no primary influence on the DBS. This conclusion was based on a comparison between the materials in **Figure 13** where all materials had ~40 % degree of crystallinity except for the TES-treated silica nanocomposite with 60 %. The TES nanocomposite with the highest degree of crystallinity also had the highest DBS. Roy et al. arguments that the degree of crystallinity have no primary influence on the DBS for his samples because the nanocomposites with 40% crystallinity had much higher DBS than the microcomposite, which also had 40% crystallinity. But it is well known that microcomposites exhibit lower DBS than nanocomposites, especially if the nanoparticles are well dispersed, so the basis of his argument is not describing the influence of crystallinity on the DBS. This discussion shows that the DBS can be influenced by many parameters which alter the DBS differently depending on which breakdown mechanism that is dominating. A discussion of dominating breakdown mechanism is therefore important especially when the measurements are carried out at different temperatures because many parameters, e.g. mechanical strength, varies with temperature which can induce another breakdown mechanisms.

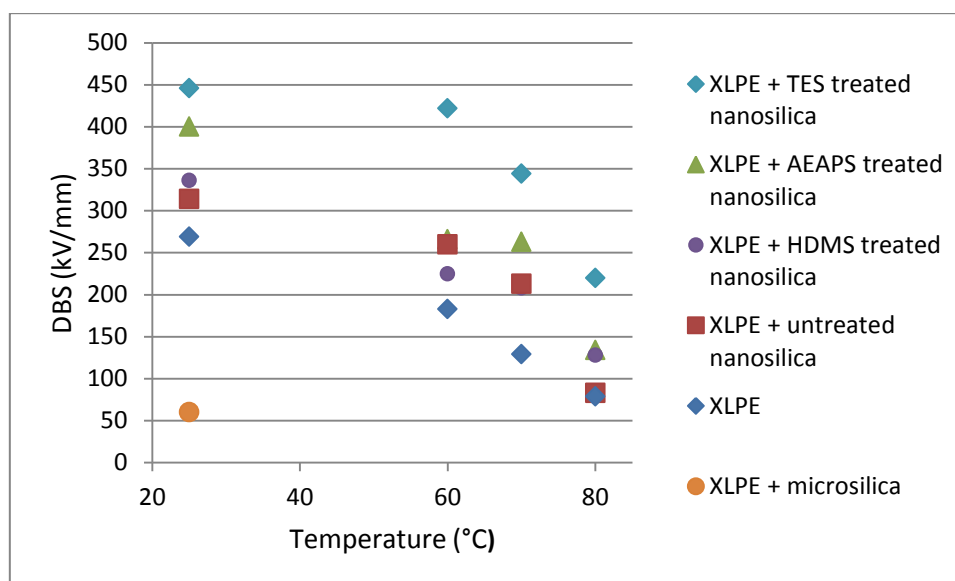


Figure 13. DC DBS of neat XLPE, XLPE silica microcomposite and of untreated and surface modified silica nanoparticles incorporated into a matrix of XLPE at various temperatures from the investigation made by Roy et al.³⁶

Nagao et al.³⁸ have improved the resistance against water trees of LDPE and XLPE by addition of MgO nanoparticles. The largest improvement was achieved at 5 wt% MgO and almost the same for both nanocomposites. However, the water tree resistance depended on the temperature and was more effective at 333 K than at 313 K.

2.2.3 Mechanical strength of the interfacial region

Dou et al.³³ have showed that a nanocomposite with barium titanite (BT) nanoparticles can improve the DBS. A volume content of 7 % BT particles with a diameter of 100 nm coated with titanite was dispersed into a matrix of polyvinylidene fluoride (PVDF). The thickness of the samples was 200 μm . The DBS of this nanocomposite, as can be seen in **Figure 14a**, was increased with 150 % compared to the nanocomposite with uncoated BT particles and to the pure PVDF. The titanite at the interface cross-linked the BT particles to the PVDF matrix which resulted in a potential barrier at the interface which prevents charge carriers to pass through the interface. This reduced the amount of space charges at the interface and increased the amount of space charges in the PVDF, which is described to be one of the reasons for improvement in DBS for the coated nanocomposite. The other reason is described by the creation of defects and edge dislocations when BT particles are added to PVDF which generates deep traps.

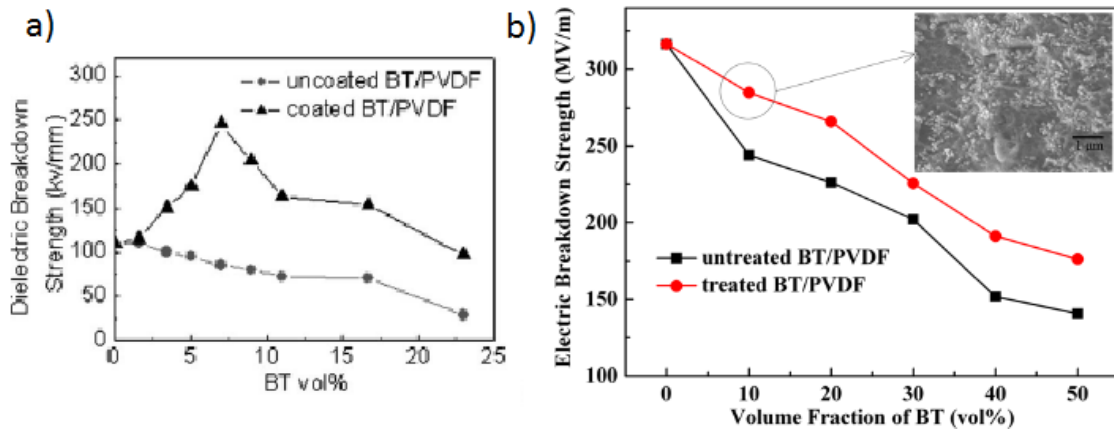


Figure 14. DBS of PVDF nanocomposites containing modified and unmodified BT nanoparticles as a function of volume fraction of BT particles. a) Measurements by Dou et al. with titanite coated BT particles. b) Measurements by Yu et al. with tetrafluorophthalic acid surface modified BT particles. Figure a) is reprinted with permission from reference 33. Copyright 2009, AIP Publishing LLC. Figure b) is reprinted with permission from reference 39. Copyright 2013, AIP Publishing LLC.

Yu et al.³⁹ have also investigated the DBS of BT nanoparticles dispersed into a PVDF matrix but the surface of their BT particles was modified with tetrafluorophthalic acid. The samples had a thickness of 12 μm and the BT particles a diameter of 100 nm. The DBS of the nanocomposite containing modified BT particles is 16 and 25 % higher than the nanocomposite without surface modification at volume contents of 10 and 50 %, respectively. However, the DBS of both these samples decreases with an increased concentration of BT particles and is lower than the DBS of the pure PVDF, as can be seen in **Figure 14b**. The surface modification with tetrafluorophthalic acid creates stable bonds between the BT particles and the PVDF matrix as described above by Dou et al. but also attributes to better dispersion. The DBS values of neat PVDF in **Figure 14a** and **b** cannot be directly compared to each other due to different sample thickness, no information if they measured DC or AC DBS and no measurements of crystallinity. Different process conditions can also contribute to different DBS values. The thicker sample of 200 μm in **Figure 14a** should result in a lower DBS than the sample in **Figure 14b** with a thickness of 12 μm , which also is the case. In conclusion, more information must be obtained from Dou and Yu et al. in order to evaluate if their references are relevant for comparison to their nanocomposite materials. The comparison between these two articles points out the importance of describing process parameters, material properties and test methods in order to present reliable references.

Shuman et al.⁴⁰ have showed that the DBS can be improved of a nanocomposite if the interface of the nanoparticle is bonded covalently to the polymer matrix. TiO₂ particles with a diameter of 32 nm and 5 wt% were coated with 2-aminoethyl dihydrogen phosphate (AEP) and dispersed into a polymer matrix of epoxy. The DC DBS was increased with 26 % for the TiO₂ AEP coated nanocomposite compared to the pure epoxy. The covalent bonding between the modified surface of the nanoparticle and epoxy matrix reduces the Maxwell-Wagner relaxation, which is believed to be the reason for a higher DBS by influencing the mobility of the charge carriers. TiO₂ particles surface modified with 2-Ethylhexyl phosphoric acid ester (EHP) were not able to create covalent bonds to the polymer matrix, which resulted in a lower glass transition temperature, increased free volume and lower DBS. AEP was preferable as a coating on TiO₂ particles for its ability to bond covalently to the epoxy matrix but also due to improved dispersion of the TiO₂ nanoparticles. Shuman et al.⁴¹ also modified BT nanoparticles with AEP which also bonded covalently to the epoxy matrix and improved the DBS. The BT particles surface was treated with hydrogen peroxide to synthesize hydroxyl groups which resulted in increased reactivity of the particles surface and thus its ability to bond to the AEP. The particle size was 30-50 nm and 5 wt% BT particles were dispersed into the epoxy matrix, which increased the DC DBS with 47 % compared to the neat epoxy.

Tanaka et al.⁹ decreased the DBS for LDPE films with 0.5 MV/cm, at both room temperature and -50°C, for a sample annealed at 90 °C compared to a sample without annealing. Thin films of LDPE were evaporated at a substrate of glass and the crystallinity was observed qualitatively with X-ray diffraction, optical microscopy and transmission electron microscopy for samples annealed at various temperatures. All these analysis methods showed an increase of crystallinity with increased annealing temperature. Thin films of LDPE were also evaporated to obtain the energy loss of electrons passing through the film dependent of various annealing temperatures, i.e. different degree of crystallinity. Electrons were accelerated towards the thin film sample and the distribution of its kinetic energy after passing through the sample was measured. The mean free path was calculated from these results by the assumption of exponential decay of the electrons energy as they passed through the LDPE film. The results of the computed mean free path as a function of annealing temperature are shown in **Figure 15a**. It can be seen that the mean free path increases with increased annealing temperature and thus with increased crystallinity. The DBS of 50 µm thick LDPE films were measured by using a spherical and a plane electrode surrounded by silicone oil and applying an impulse voltage. The results at room temperature and -50°C for different annealing temperatures are shown in **Figure 15b**. Enhanced annealing temperature results in increased degree of crystallinity and longer mean free path of the electrons which gives them time to gain more kinetic energy to cause fast avalanche breakdown at lower voltages. This result where the DBS is lowered with an increase of the mean free path indicates that fast avalanche breakdown is the dominating breakdown mechanism.

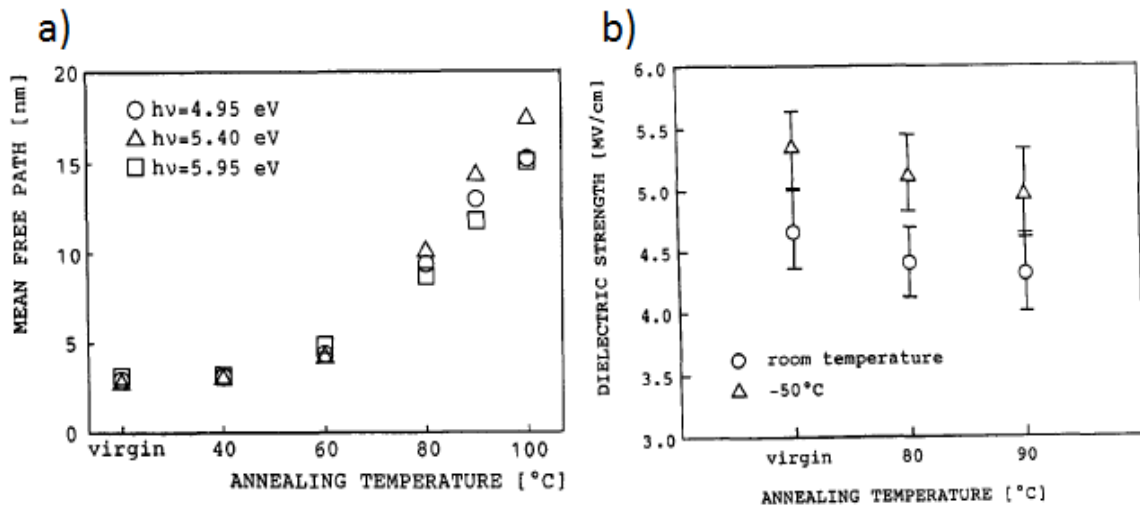


Figure 15. a) Calculated values of the mean free path, based on exponential decay of the electrons energy, as a function of annealing temperature for different phonon energies. b) Results of DBS measurements for 50 μm thick films of LDPE as a function of annealing temperature. These figures are reused from reference 9, copyright © 1991 IEEE.

2.2.4 Particle shape

Nanolaminates as additive in polymers has shown to increase the DBS at much higher volume contents compared to spherical inorganic nanoparticles. Fillery et al.⁴² dispersed montmorillonite (MMT) modified by dimethylditallowammonium in a polyvinyl butyral (PVB) matrix, which increased the AC DBS with 30 % compared to the pure PVB. The 30 % improvement was almost consistent over the volume fraction interval from 16 to 25 % of MMT, as can be seen in **Figure 16a**. The improvement of the DBS for much higher contents of additives in nanocomposites for MMT than for spherical inorganic particles was explained by more dense packing of the MMT. If the dense packed laminates are aligned perpendicular to the electrodes, then they can reduce the mobility of charge carriers and thus prevent breakdown. In the two figures with polymer rich areas, i.e. to the left hand side in **Figure 16b**, are the laminates of MMT well dispersed but starts to form tactoids with increasing amount of MMT in PVB. The blue areas between the laminates in a tactoid consist of intercalated PVB. This tendency with an increasing amount of tactoids continues up to a volume fraction of 25 % of MMT. At higher amounts of MMT become the intercalated areas between the laminates depleted from PVB. The intercalated PVB is believed to stabilize the bond of the hydroxyl groups to the laminates, reduce the mobility of charge carriers and thus improve the DBS.

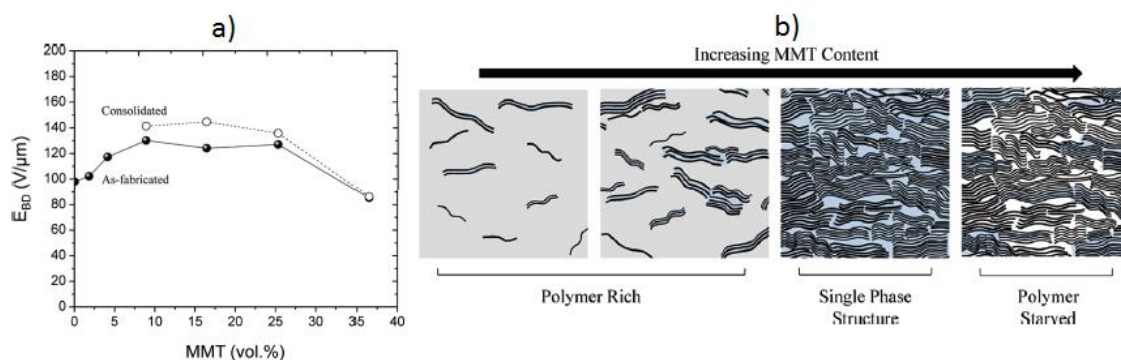


Figure 16. a) The DBS dependency of MMT volume content in a PVB nanocomposite. b) Schematic picture over the morphology in a PVB nanocomposite for different concentrations of MMT. The black lines are MMT laminates, grey areas PVB, blue represents regions of PVB intercalated between MMT layers and white represents regions depleted of PVB. These figures are reprinted with permission from reference 42. Copyright 2012, American Chemical Society.

2.3 Voltage stabilizers for enhancing breakdown strength

2.3.1 Voltage stabilizers used in polyolefine matrices

Voltage stabilizing additives are organic molecules that can reduce the energy of energetic electrons and thus prevent breakdown. These molecules usually consist of polycyclic aromatic compounds. Zhang et al.⁴³ have investigated the mechanisms that improve the DBS of XLPE containing aromatic carbonyl compounds, which acts as a voltage stabilizer additives. These compounds that contain delocalized π -electrons can create anions radicals, which are relatively stable, by trapping energetic electrons. The energy of the energetic electrons can be reduced by collision with aromatic carbonyl compounds if the collision results in an electron transition of the additive molecule. This electron transition process reduces the energy of the energetic electron so it doesn't contain sufficient energy to damage the single bond between carbon and carbon in the XLPE. The aromatic carbonyl additive that undergoes the electrical transition process creates an aliphatic cation radical. However, this radical can be transformed to a relatively stable aromatic cation due to the more delocalized π -electron in the aromatic than the aliphatic cation. This regeneration of the voltage stabilizer by transformation of the radical to its ground state has also been proposed by Ashcraft et al.⁴⁴ Acetophenone is an aromatic compound with a good ability to trap energetic electrons due to its delocalized π -electron and high electron affinity. It also has excitation energy lower than the energy it requires to break the single bond between carbon and carbon in XLPE, which is a demand to prevent degradation of the XLPE. The AC DBS has been improved with 50 % by the addition of Acetophenone in XLPE.

Yamano³ incorporated four different polycyclic benzene compounds into LDPE: naphthalene, anthracene, tetracene and pentacene, called group A additives as can be seen in **Figure 17a**. The DBS of LDPE with these compounds without radicals were measured in order to attach radicals to the compound with the highest DBS for further DBS measurements. The sample with anthracene showed the highest DBS, as can be seen in **Figure 17b** and its DBS increased with 50 % at a concentration of 0.1 wt% compared to the neat LDPE sample. The sample including tetracene increased the DBS with 14 % compared to the neat LDPE sample and the other two compounds showed no improvement in DBS. However, the dispersion of pentacene was not as good as the other compounds. The thickness of the samples was 10 μm and the DBS measurements were carried out at 8 °C. Halogen, electron donating and accepting radicals were attached to the anthracene compound to be used as additives with a concentration of 0.1

wt% for further measurements of the DC DBS (**Figure 17c**). The three compounds are 9-nitroanthracene (NO-An), 1-aminoanthracene (NH-An) and 9,10-dibromoanthracene (Br-An), called group B additives as can be seen in **Figure 17a**.

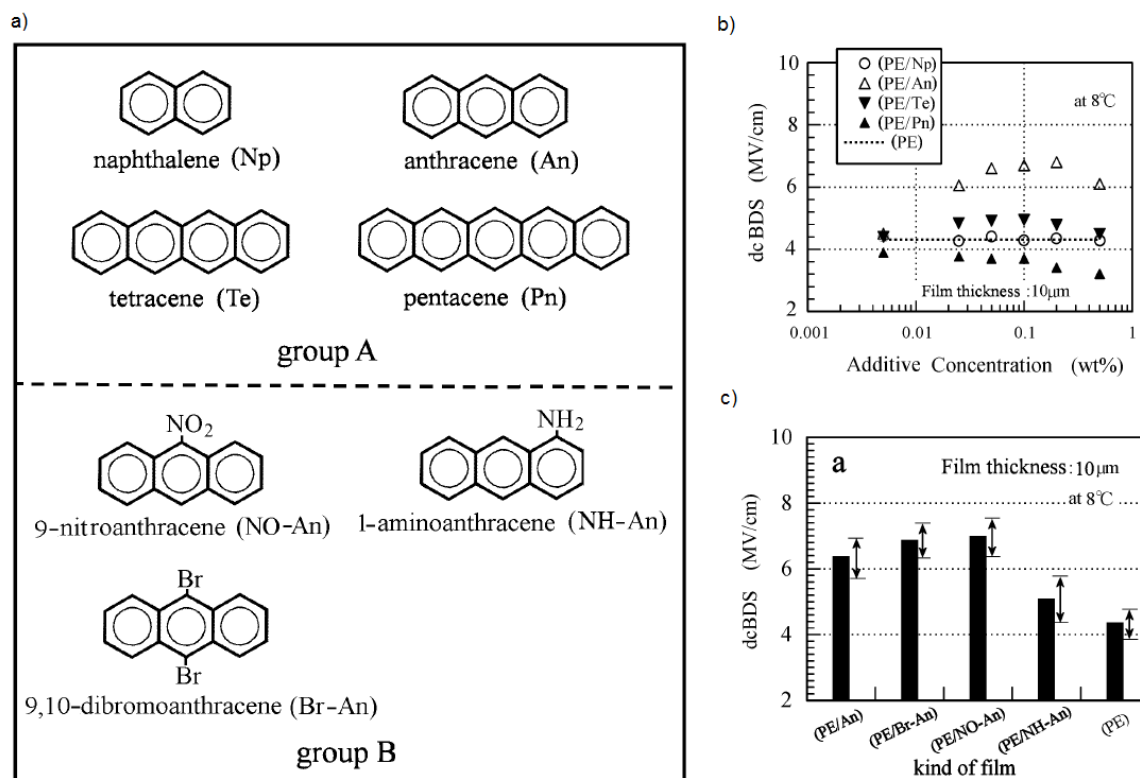


Figure 17. a) Four different polycyclic benzene compounds without radicals (group A additives) used as voltage stabilizers in LDPE. The three anthracene additives modified with an electron accepting radical (NO_2), electron donating radical (NH_2) and halogen radical (Br) are referred to as group B additives. b) DC DBS measurements of LDPE samples with the four additives of group A shown in a), dependent on the concentration of the additives. c) DC DBS measurements for neat LDPE, LDPE with anthracene without radicals and three LDPE samples containing the group B additives shown in a). These figures are reused from reference 3, copyright © 1991 IEEE.

The excitation energies of LDPE samples with the group B additives in **Figure 17a** were measured by UV absorption spectroscopy and showed no significant differences could be seen. The increase of DBS for (PE/NO-An) and (PE/Br-An) and the decrease for (PE/NH-An) compared to (PE-An) is therefore not dependent on the absorption of energy during excitation of π -electrons. Permittivity, dielectric losses and the degree of crystallinity were not changed significantly by adding group A or B additives, shown in **Figure 17a**, to an LDPE matrix. These variations of the DBS for the samples with radicals connected to anthracene are described by the creation of traps with various depths, which depends on the characteristic of the connected radical. Trapped electrons close to the cathode will suppress the injection of electrons due to the negative space charges, created by the trapped electrons, and thus prevent fast avalanche failure. The (PE/NO-An) shows the highest DBS and contains the electron-accepting radical NO_2 and is therefore believed to create deepest traps. The traps of the (PE/NH-An) sample may be shallower due to the electron donating NH_2 radicals and shows a reduction of the DBS compared to the (PE/An) sample. The DBS of (PE/Br-An) is almost as high as the (PE/NO-An) sample, which also is explained by creation of deep traps. This additive contains a dipole,

generated by the attraction of π -electrons to the Br radical, which creates deep traps where the polarization is positive.³

Jarvid et al.⁴⁵ showed that the voltage stabilizer 4,4'-didodecyloxybenzil added to XLPE can increase the tree initiation voltage (TIV), i.e. the voltage where electrical trees initiate to grow. The TIV was increased with 62 % compared to the neat XLPE sample at an additive concentration of 10 mmol/kg. The TIV was also improved by decreasing the ramp rate of the applied voltage. The 62 % increase in TIV was measured with a ramp rate of 20 V/s. Measurements of a sample containing 20 mmol/kg 4,4'-didodecyloxybenzil improved the TIV with 60 % when using a ramp rate of 80 V/s. These results indicate that the TIV can be increased by lowering the ramp rate or increasing the amount of voltage stabilizing additive to 20 mmol/kg.

A silane vinyl trimethoxy (VTMS) grafted onto chains of XLPE, 0.6 wt%, improved the resistance against water trees by decreasing the water tree length with 48 % compared to the neat XLPE. The grafted VTMS is more hydrophilic and absorbs more water than the neat XLPE which is the reason of the improvement in water tree resistance. Ethylene-vinyl acetate-vinyl alcohol (EVA-OH) has been shown to improve water tree resistance and DBS under AC conditions with increased amount hydroxyl groups, which results in an increase of hydrophilicity. It is also believed that hydrogen bonds, between hydroxyl groups and vinyl alcohol prevent diffusion of water through some of the amorphous domains and thus improve resistance against water trees. The water tree length decreased with 53 % and the DBS increased with 8 % at a conversion rate of hydroxyl groups at 52.2 % compared to the ethylene-vinyl acetate without hydroxyl groups.^{6,46}

2.3.2 Voltage stabilizers used in polyolefine nanocomposite matrices

To modify the surface of nanoparticles with organophosphate electropositive functional groups that withdraws electrons has been shown to improve the DBS, leakage current and dielectric losses when dispersed in an epoxy matrix. TiO₂ particles which surfaces were modified with chlorophenyl phosphate (CPP) and 4-nitrophenyl phosphate (NPP) and then dispersed into an epoxy matrix showed an improvement of the DC DBS with 18 and 28 %, respectively, compared to the neat epoxy polymer. A nanocomposite containing BT particles surface modified with NPP showed the largest increase of the DC BDS with 33 % compared to the neat epoxy. The molecule structure of the NPP and CPP organophosphate ligands are shown in **Figure 18**. The size of the TiO₂ and BT particles was 32 nm and 30-50 nm, respectively, and the volume fraction of TiO₂ and BT particles dispersed into epoxy was 5 %. The DBS of unmodified TiO₂ nanoparticles dispersed into an epoxy matrix showed a decrease in DBS and glass transition temperature, which indicates bad dispersion of the particles. The increase in DBS for particles coated with NPP and CPP is partly an effect of good dispersion of the particles but also due to a surface passivation effect and reduced surface conductivity of the particles. Charge carriers are prevented from desorbing or dissolving from the particles surface to the solvent as an effect of the passivation of the surface. The organophosphate ligands PP, APP and AEP that were used to modify surfaces of TiO₂ nanoparticles had a DBS around the neat epoxy polymer.⁴⁷

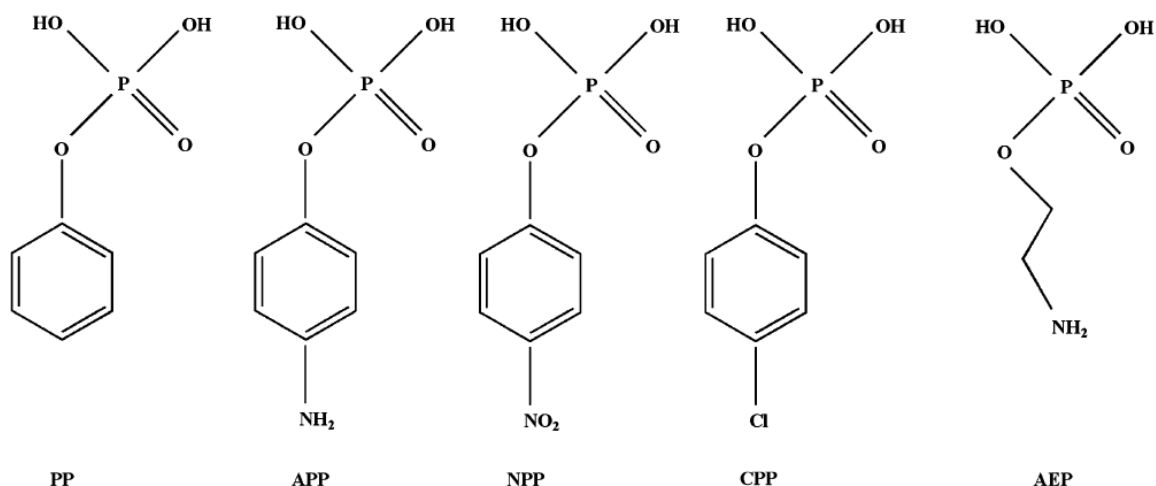


Figure 18. Phenyl phosphate (PP), aminophenyl phosphate (APP), 4-nitrophenyl phosphate (NPP), 2-aminoethyl dihydrogen phosphate (AEP) and chlorophenyl phosphate (CPP) are organophosphate ligands used to modify the surfaces of TiO_2 nanoparticles. Barium titanite nanoparticles were also surface modified with NPP to improve the DBS. This figure is reprinted from reference 47. Copyright 2013, American Chemical Society.

Yamano et al.⁴⁸ dispersed Al_2O_3 and nickel phthalocyanine (Pc) into LDPE and the tree initiation voltage (TIV) and the time to breakdown from tree initiation of the nanocomposite were investigated. **Figure 19** shows that LDPE compounded with Al_2O_3 and Pc resulted in a maximum improvement at 5 and 1.5 wt%, respectively. The TIV was increased with 80 % and time to breakdown from tree initiation with 600 % compared to the neat LDPE. The increase of TIV is due to absorbance of energetic electrons caused by excitation of π -electrons in Pc.

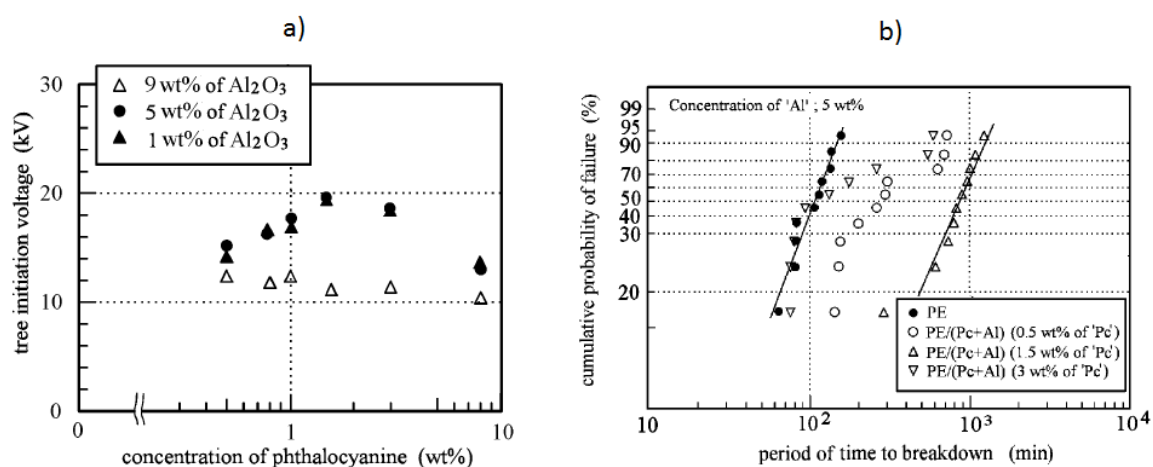


Figure 19. a) TIV for different concentrations of Al_2O_3 and Pc added in LDPE. An AC voltage of 9 kV was applied and then raised by 1 kV every minute until tree initiation occurred. b) Cumulative probability of failure for different concentrations of Al_2O_3 and Pc added in LDPE. An AC voltage of 10 kV was applied and raised with 1.2 times the TIV when tree initiation occurred. The figures are reused from reference 48, copyright © 2011 IEEE.

It can be seen in **Figure 19a** that an increased amount of Al_2O_3 in the nanocomposite results in no significant improvement in TIV, but a decrease in TIV for 9 wt% Al_2O_3 . However, various amounts of Pc in the nanocomposite have larger impact on the TIV and the optimal concentration is 1.5 wt% where the TIV is improved with 80% compared to the neat LDPE. The

TIV of the neat LDPE is not shown in **Figure 19**. Analysis with SEM showed large agglomeration of Al_2O_3 particles in the LDPE/ Al_2O_3 nanocomposite but not in the LDPE compounded with Al_2O_3 and Pc. These results are believed to be explained by the large π -electron cloud in Pc which creates a dipole moment larger than for the Al_2O_3 and attracts it to the Pc particle with Van der Waals forces. In this way becomes the Al_2O_3 particles better dispersed with addition of Pc to the LDPE/ Al_2O_3 nanocomposite and improves the time to breakdown from tree initiation compared to the neat LDPE, as can be seen in **Figure 19b**.⁴⁸

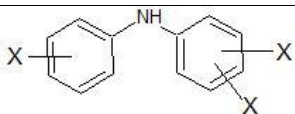
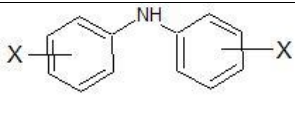
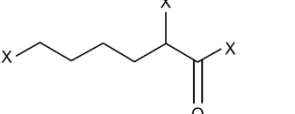
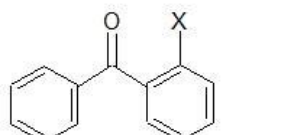
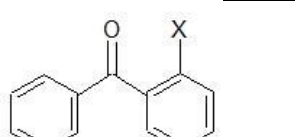
3 EXPERIMENTAL

3.1 Materials

LDPE and nanocomposites based on LDPE was used in this thesis work. The loading of magnesium oxide (MgO) nanoparticles in the LDPE nanocomposites was 3 or 30 wt% and will be referred to as PE+3% MgO and PE+30% MgO , respectively. PE will be used to denote LDPE in section 3 and 4.

The additives used as voltage stabilizers to enhance the DBS are summarized in **Table 2**. The voltage stabilizers that were experimentally evaluated in this thesis work were chosen with respect to their chemical structure and previous experience at ABB.

Table 2. Voltage stabilizing additives that was added to neat PE and PE nanocomposites in order to enhance the DBS.

Voltage stabilizing additives	Chemical structure*	Form at 20°C	Compatibility with PE
Additive A (A)		Liquid	Good
Additive B (B)		Liquid	Good
Additive C (C)		Liquid	Good
Additive D (D)		Liquid	Intermediate
Additive E (E)		Crystal	Intermediate

*Some functional groups have been denoted with "X" in the chemical structure of additives due to confidential reasons.

3.2 Sample preparation

Pellets of the polymer matrix, either neat PE or PE nanocomposites containing MgO nanoparticles, were mixed with the voltage stabilizing additives shown in **Table 2**. The additives were either mixed mechanically at high temperatures with an extrusion process or mixed chemically with diffusion by a swelling process. These processes are further described in sections 3.2.1 and 3.2.2. The materials, pellets of the polymer matrix mixed with additives, were then dried in a vacuum before they were pressed to ~0.4-0.5 mm thick plates.

3.2.1 Extrusion

A twin screw extruder (Thermo Fisher Prism eurolab 16) was used to compound polymer matrices with additives mechanically. The pellets of the polymer matrices were dried at 70°C for 18 h and the additives were weighed, added to the dried pellets and shaken before the extrusion process. The mixture of pellets and additive was first shaken by hand and then mechanically in a machine for 3 minutes.

The temperature profile at the different zones and rotation speed of the screw, shown in **Table 3**, are the same as in earlier projects for comparison without influence of different compounding parameters on the DBS. The pellets were fed manually into zone 1 because the automatic feeder is only made to handle dry pellets. The manual feed rate was adjusted to result in a torque of 80-90 %, which also was done in earlier projects. The temperature profile, rpm and torque of the screw in **Table 3** were chosen to obtain good mixing of the additives and polymer matrices along the screws with a short residence time and without degradation of the material. The materials were cooled in a bath with deionized water directly when they exited the die. The bath was cooled by several cooling blocks from the freezer. The extruded materials were chopped into pellets of 2.5 mm by a cutter directly after the cooling bath which generated new pellets that now consisted of the polymer matrix mixed with additive.

The maximum feed rate possible resulted for some materials only in a torque of 48-70 % with the predetermined temperature profile and screw speed of 150 rpm. The nanocomposite PE+30% MgO with 1.5 wt% additive C reached a torque of 100 % at 150 rpm so the rpm was lowered to 70 rpm where a torque of 80-90 % was obtained. However, this difference in rpm of the screw showed no difference in DBS, as can be seen in **Figure 42**.

Table 3. a) Process parameters of the extruder during compounding when the temperatures in b) were reached for all zones. b) Temperature profile.

a)	Feed rate	Manual feed	b)	Temperature profile	[°C]
	Screw rotation speed	150 rpm		Zone 1	140
	Torque	48-88 % *		Zone 2	140
	Pressure at die	16-24 bar		Zone 3	145
	Vent hole at die	Closed		Zone 4	145
	Pellet size	2.5 mm		Zone 5	148
				Die	150

* 12 Nm is the maximum torque for one screw.

3.2.2 Swelling

Voltage stabilizing additives were swelled into pellets of PE or PE nanocomposites by the use of the organic solvents heptane or cyclohexane. These solvents were chosen because they are soluble with the additives, can be absorbed and cause swelling of the PE matrix. Nanocomposites of PE were swelled with small amounts of solvent and additive while neat PE was swelled covered in solvent and additive. The amount of solvents used for the swelling of nanocomposites was 6-12 ml depending on the amount of additive used (1.6-3.2 g) while neat PE was swelled covered in a mixture of solvent and 9 wt% additive (around 70 g solvent and 7 g additive) enough to cover the pellets of neat PE. All swelling processes were performed at room temperature. The idea with the swelling process was to absorb a homogenous mixture of additive and solvent into the polymer matrix and then evaporate the solvent without diffusion of the additive out of the matrix. The amounts of additives that were present in the swelled samples have to be analyzed after the pellets were pressed to thin plates, because the amount of additive swelled into the pellets or lost during mixing and drying processes were unknown. Chromatographic methods will be used to quantify the amount of additives of some chosen materials with promising AC DBS.

Swelling of PE nanocomposites

The additives were first added to the organic solvents and mixed to a homogenous liquid with a high speed mixer, Speedmixer DAC 150 FV, and mixed 3*20 s with 24 000 rpm. The homogenous liquids were then added to pellets of the nanocomposite matrices and further mixed 4*20 s and 24 000 rpm with the high speed mixer before they were sealed in glass bottles to swell. The amounts of solvents per wt% additive were decided by testing to obtain pellets that looked dry enough to put in a clean vacuum oven after evaporation in a fume cupboard for ~7 h. Proportions of materials and swelling times are summarized in **Table 4** for additives swelled into PE nanocomposites.

Table 4. Summary of swelling parameters and proportions of materials.

Polymer matrix	Amount [wt%]	Additive [wt%]	Organic solvent [ml]	Swelling time [h]	Comments
PE+30%MgO	97	A 3	Heptane 6	117	Dried and tested
PE+30%MgO	94	A 6	Heptane 12	117	Never dried enough
PE+30%MgO	94	A 6	Heptane 18	67	Dried and tested
PE+3%MgO	97	A 3	Heptane 6	117	Dried and tested
PE+3%MgO	94	A 6	Heptane 12	117	Dried and tested
PE+3%MgO	94	A 6	Heptane 18	67	Dried and tested

Neat PE was also tried to be swelled with additives and small amounts of organic solvents but the pellets never became dry enough after evaporation in a fume cupboard to put in a clean vacuum oven. A thin layer of additive A could be seen at the surface of the pellets. Attempts to increase the absorption of solvent and additive A into the neat PE was performed by adding heat (50°C) and more solvent but without any success. Neat PE was therefore tried to be swelled covered in organic solvents. The PE+30% MgO swelled with 6 wt% additive A and 12 ml solvent also had a thin layer of additive A on the surface of the pellets so they couldn't be

dried in a vacuum oven. This is surprising because PE+3 wt% MgO swelled with 6 wt% additive A and 12 ml solvent looked more like dry pellets without this thin layer of additive A at the surface of the pellets after evaporation in a fume cupboard.

Swelling of neat PE

Neat PE pellets were swelled covered in a mixture of solvent and 9 wt% additives while stirred by a magnetic stirrer. Enough PE pellets to press one plate were first covered with solvents and additives were then added. The mixture was shaken by hand until the liquid became homogenous. The liquid was filtrated from the pellets after the swelling and the pellets were then put in a fume cupboard for ~7 h to evaporate, so they afterwards could be dried in a clean vacuum oven. A summary of neat PE swelled covered in a mixture of solvent and additive is shown in **Table 5**.

Table 5. Summary of swelling parameters and proportions of materials.

Polymer matrix	[g]	Additive [wt%]	Organic solvent	[wt%]	Swelling time [h]	Comments
PE	45	None ref.	Heptane	100	65	Dried and tested
PE	50	A 9	Heptane	91	65	Dried and tested
PE	45	None ref.	Cyclohexane	100	65	Dried and tested
PE	50	A 9	Cyclohexane	91	65	Dried and tested

3.2.3 Drying

Vacuum ovens (Thermo Scientific VT 6060 M) were used to dry materials in an atmosphere with low pressure. All materials where the additives were compounded with polymer matrices by extrusion have been dried at 70°C for 24 h at a pressure of less than 1 mbar. All swelled materials have been dried in vacuum oven at 40°C for 17 h at a pressure of less than 1 mbar. The swelled materials were dried at a lower temperature to evaporate the solvent without diffusion of the additives out of the pellets.

3.2.4 Pressing

Pellets were pressed to plates with a thickness of ~0.4-0.5 mm with a Servitec Polystat 300S hot press. The pressure and temperature of the plates were varied according to **Figure 20**. Other important settings of the press are: cooling rate of 66 %, initial temperature of 40 °C, initial pressure of 20 bar, the preference “HOLD” is chosen and a “HOLD temperature” of 80 °C. The press program, shown in **Figure 20**, starts when the temperature of the plates reaches 80 °C if “HOLD” is chosen and the “HOLD temperature” is 80 °C. A rectangular frame of stainless steel with a thickness of 0.5 mm was used as spacing between the press plates to determine the thickness and form of the pressed polymer plates. One mylar film made of PET with a thickness of 75 µm that fit inside the steel frame was used to further adjust the thickness of pressed polymer plates. Pellets were distributed evenly in the middle of the pressing plates in between two additional mylar films. The press program in **Figure 20**, preferences of the press and the use of mylar films were the same for all materials that were pressed to be able to compare them.

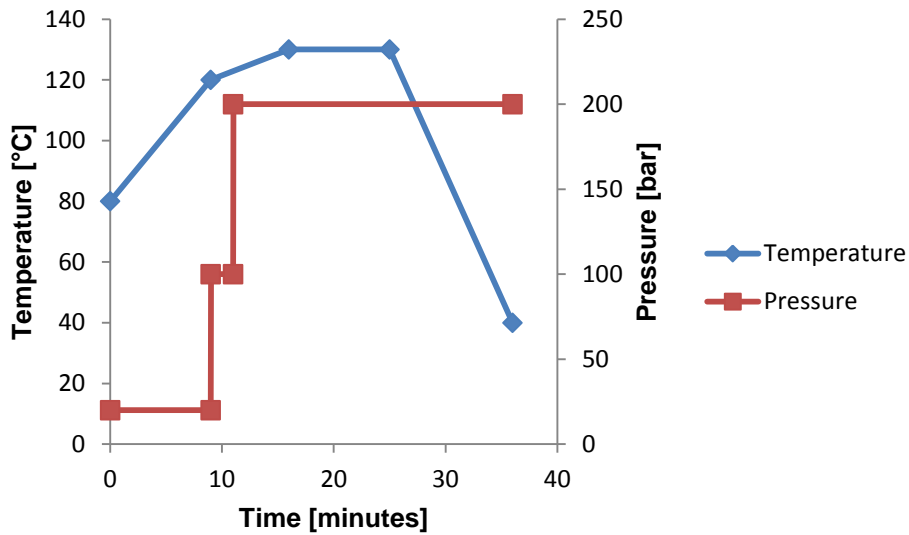


Figure 20. Temperature, pressure and time settings of the press program for the hot press.

3.3 Measurements

The AC DBS of different materials was measured and compared with a BA 100 breakdown analyzer from B2 for insulating oil. Castor oil, which has a dielectric constant of 4.5 at 26°C, surrounded the electrodes and the sample for all measurements to force the breakdown through the sample and not through the surrounding medium. The mushroom shaped electrodes shown in **Figure 21** were used to compare the DBS of different materials. The AC breakdown measurements were executed according to the standard IEC 60243-1, except for the use of the electrodes in **Figure 21**, instead of spherical IEC standard electrodes. The AC had a frequency of 50 Hz and the ramp rate of the voltage was 2 kV/s for all measurements. At least 20 samples were tested for one material to get reliable results from the statistical evaluation of the DBS data. Each plate pressed in the press resulted in 20-25 samples, i.e. enough samples for the DBS measurements. The DBS was always measured for two to four different materials at the same occasion. First the DBS of one sample from the material 1 was measured, then one sample from material 2 and so on. This was done to detect if contamination of the oil did influence the DBS along the measurements. Reference materials with known DBS were also tested to insure that the oil didn't influence differently on the DBS. The oil was changed continuously when contamination in the oil could be seen (around 8-10 materials), even if this showed no influence on the DBS. The thickness of the samples was measured with a micrometer at five places close the middle of the samples where breakdown occurred during the breakdown measurements. The average thickness was calculated and used to divide the breakdown voltage with because of thickness variations of the samples.



Figure 21. Mushroom shaped electrodes used during AC DBS measurements to screen different materials due to their DBS.

Differential scanning calorimetry (DSC) is a thermal analysis instrument where information of crystallinity, thermal history, melting- and crystallinity temperatures can be obtained. The temperature is changed with a predetermined rate during DSC measurements and the energy required or released during these temperature changes is registered. Energy is required or released if the thermal transitions involve endothermic or exothermic reactions, respectively. DSC measurements were carried out on some chosen materials to detect any differences in thermal history and total percent crystallinity, which can affect the DBS. The DSC measurements were performed in a nitrogen atmosphere with the temperature ranges and ramp rates described in **Table 6**. The enthalpy of 293 J/g for PE with 100% crystallinity was used to determine the degree of crystallinity.¹

Table 6. The ramp rate and ranges of the temperatures during the DSC measurements.

Step	Time [min]	Temperature ramp rate [°C/min]	Starting temperature [°C]	Ending temperature [°C]
1	5	0	-50	-50
2	25	10	-50	200
3	3	0	200	200
4	25	-10	200	-50
5	3	0	-50	-50
6	25	10	-50	200

Fourier transform infrared spectroscopy (FTIR) was performed on PE samples dried in vacuum at different drying conditions before the pressing process. The aim of this analysis was to determine if a process stabilizer in PE was consumed during the different drying processes (70 °C or 40 °C) and to conclude if this affects the DBS. The amount of this process stabilizing additive can be determined with FTIR by measuring the height of a specific absorption peak in the IR absorption spectrum of PE. The wavelength of the specific absorption peak, name and amount of the process stabilizing additive cannot be mentioned due to confidential reasons.

3.4 Method for evaluation of DBS measurements

The DBS data were evaluated with a two parameter Weibull distribution, as can be seen in Eq. (13), which is a statistical distribution of extreme values. Breakdown occurs at the weakest point in the material and the data obtained from the breakdown measurements therefore have to be evaluated statistically as smallest extreme values. The cumulative probability of failure $P(x)$ of a two parameter Weibull distribution (**Figure 22a**) is expressed by,

$$P(x) = \begin{cases} 1 - e^{-\left(\frac{x}{\alpha}\right)^\beta}, & x \geq 0, \\ 0, & x < 0 \end{cases} \quad (13)$$

where α is called the scale parameter and β the shape parameter and both are larger than zero. The scale parameter represents the probability of failure at 63.2 %,

$$P(x) = \left\{ 1 - \frac{1}{e} = 0.632, \quad x = \alpha \right. \quad (14)$$

The shape parameter β is the slope of a curve in a Weibull plot, as is described below and can be seen in **Figure 22b**. The parameters α and β are determined by estimating the failure rate of the number of samples tested. This was performed by using the median rank approximation (MR),

$$MR = \frac{i-0.3}{N+0.4}, \quad (15)$$

where N is the number of samples and i indicates the order of the N samples. The data from the breakdown measurements is first divided with the thickness of the sample to obtain the DBS (kV/mm). The DBS values must then be ranked from the lowest ($i=1$) to the highest ($i=N$) before the MR approximation can be used. The Weibull distribution function in Eq. (13) can be reorganized to obtain the form of a linear equation ($y=kx+m$),

$$\log(-\ln(1 - P(x))) = \beta * \log(x) - \beta * \log(\alpha), \quad (16)$$

where $P(x)=MR$ from Eq. (15) to include the median rank approximation. Equation (16) is the equation of a two parameter Weibull plot, which is shown in **Figure 22b** for different shape parameters. Note that β is the slope of the fitted line and α , that describes the DBS at 63.2 %, can be calculated from the last term in Eq. (16). The y-axis of the Weibull plot represents the probability of failure in percent. The cumulative probability of failure, **Figure 22a**, can be obtained by plotting $P(x)$ from the Weibull distribution function from Eq.(13) after estimation of the α and β parameters.^{7,49}

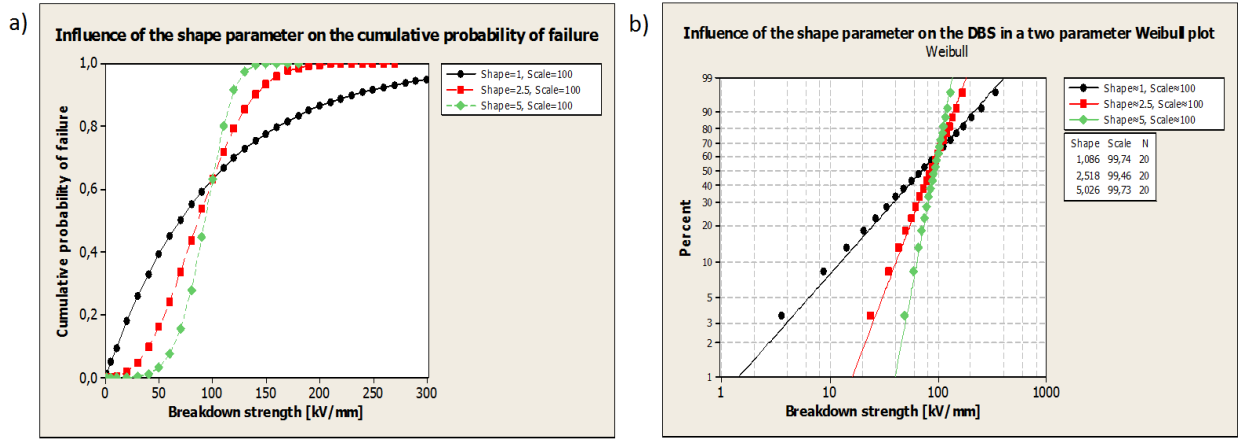


Figure 22. a) The Weibull distribution function $P(x)$ in Eq. (13), called the cumulative probability of failure, is plotted with $\alpha=100$ for different shape parameters. b) Two parameter Weibull plot described by Eq. (16) for $\alpha=100$ and the same values of β as in a). N indicates the number of samples.

The evaluation of AC DBS measurements, in the excess of the use of Weibull statistics, were performed by plotting DBS as a function of sample number, sample thickness as a function of sample number and DBS as a function of sample thickness. The Weibull plot from the AC DBS measurements of a PE nanocomposite without any drying of pellets before the pressing process is shown in **Figure 23**. Examples of plots for evaluation of the DBS data for this material are shown in **Figure 24**. The evaluation of the PE nanocomposite shown in this section is to illustrate the evaluation method. This method was used to evaluate all materials that were analyzed by AC breakdown measurements. The negative slope of the linear regression (blue line) in **Figure 24a** indicates that the DBS of the samples decreases during the measurements. This tendency could be caused by contamination of the surrounding oil but it can be concluded only to depend on the order the samples were tested in (**Figure 24b**) and the sample thickness dependency of the DBS (**Figure 24c**). Thinner samples result in higher DBS values, as can be seen by the negative slope of the linear regression in **Figure 24c**, because the probability that thinner samples contain defects is smaller than for thicker samples. **Figure 24b** shows that the thickness of samples was thinner in the beginning and thicker in the end of the measurements for this material.²²

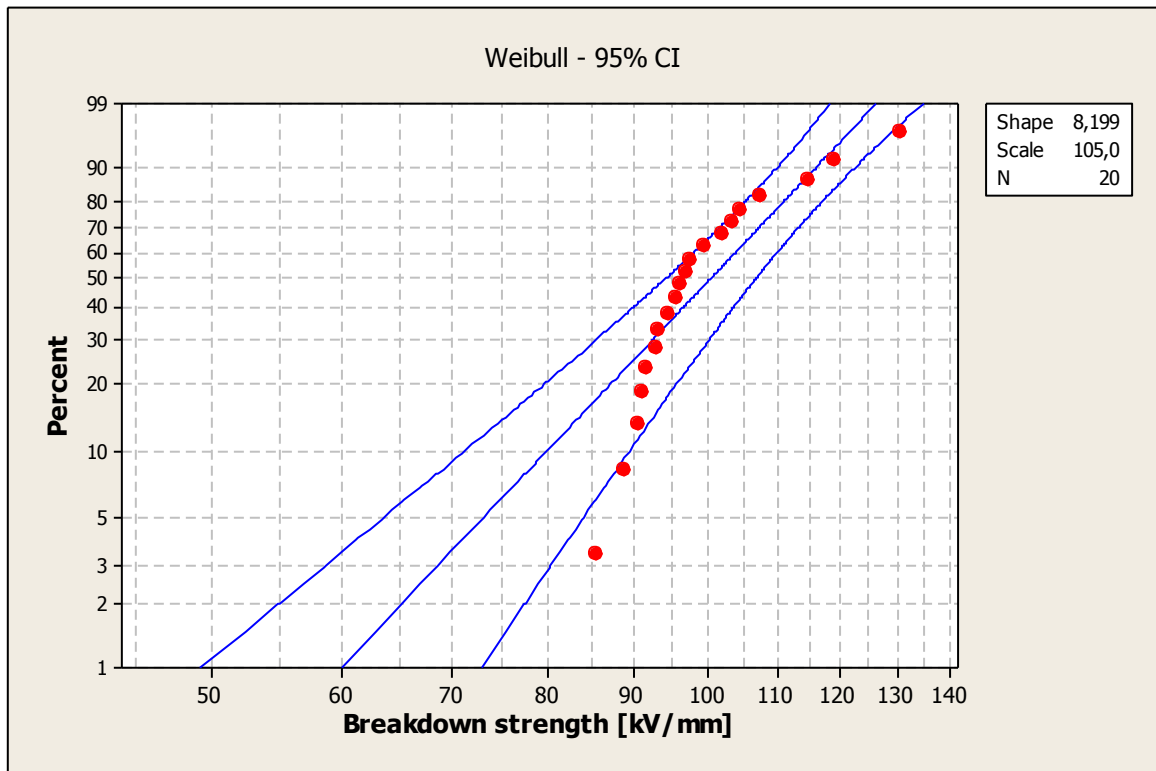


Figure 23. Weibull plot of PE+30% MgO without any drying of the pellets before the pressing process. The blue lines indicate a linear regression fit to the DBS values (middle line) and 95% confidence intervals of the DBS values (outer lines).

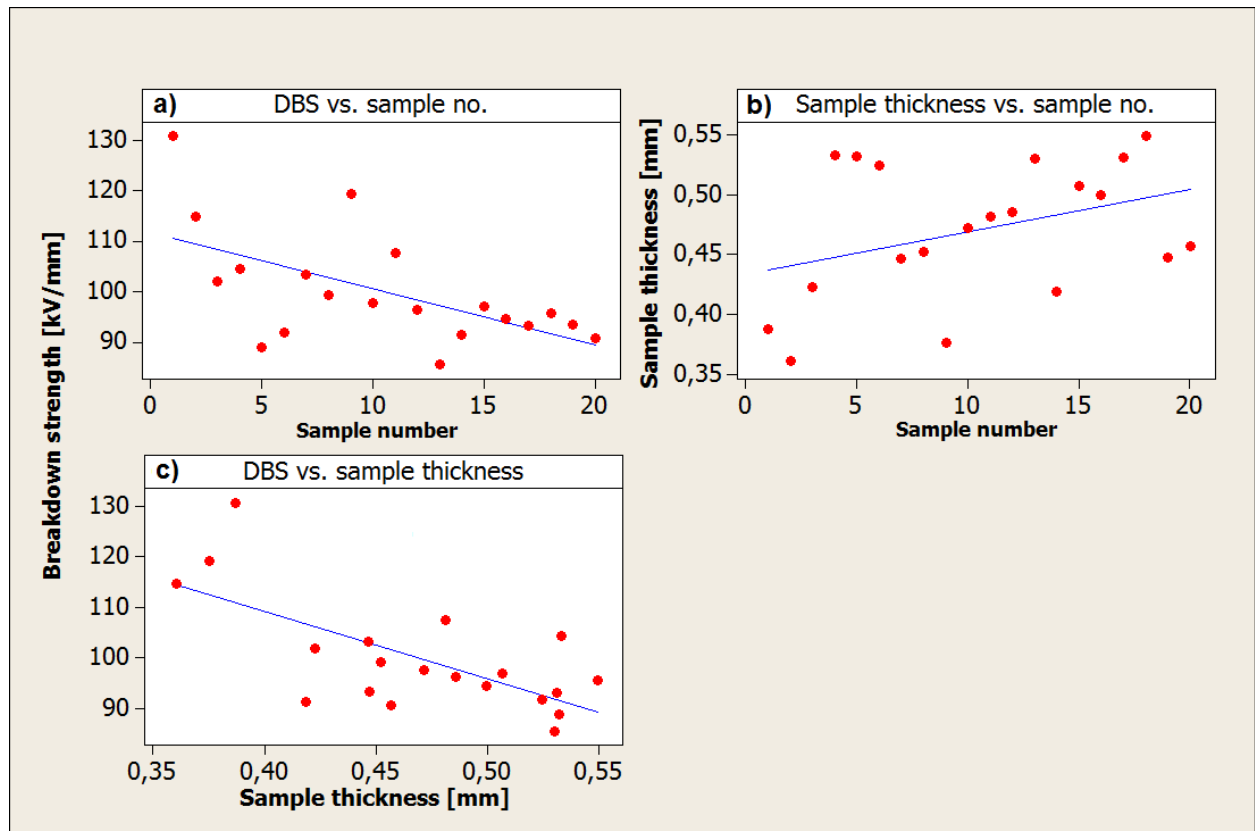


Figure 24. a) DBS as a function of sample number b) Sample thickness as a function of sample number c) DBS as a function of sample thickness. This is an example of the evaluation of PE+30% MgO without any drying of the pellets before the pressing process. Blue lines indicate linear regression fits.

4 RESULTS AND DISCUSSION

4.1 Stability of AC DBS measurements

The variations of the AC DBS for the same material dried, pressed and tested at different occasions have been investigated for neat PE. This was not possible to investigate on nanocomposites during this thesis work, due to the limited amount of accessible material. The variation of scale and shape parameters and confidence intervals in a Weibull plot for the same material is important, especially for references used for comparison with other materials.

The DBS of two extruded PE references that are extruded, dried, pressed and tested at different occasions are showed in a Weibull plot, as can be seen in **Figure 25**. The black values are from measurements on PE extruded in this thesis, while the red values were obtained from PE extruded in an earlier project at ABB. The same extrusion, drying and pressing parameters were used for those two extruded PE samples. No significant difference of the DBS can be seen in **Figure 25**. However, the PE sample extruded in this thesis (black values) shows less scattered DBS data indicated by the higher value of the shape parameter.

Figure 26 shows the DBS in a Weibull plot of PE references dried, pressed and measured at different occasions. All three samples were dried at 40°C for 17 h before the pressing process. The DBS as a function of sample thickness for extruded PE dried at 70°C (black values from **Figure 25**) and the three PE samples in **Figure 26** are shown in **Figure 27**. The DBS of these four samples are influenced by the sample thickness so that thinner samples results in higher DBS than thicker samples. This can be seen by the linear regression fits (blue lines) in **Figure 27**, which have a negative slope. This dependency agrees with the literature that thinner samples have a smaller probability to contain defects and therefore have higher DBS. The PE references in **Figure 26** have similar lowest DBS ~100 kV/mm except for the red reference that has one DBS value of ~80 kV/mm. The highest DBS values for these three references vary from ~130-170 kV/mm. It can also be concluded that the scatter of the DBS for PE reference samples are quite high, which is reflected in the low beta values (around six for the green PE reference in **Figure 26**).²²

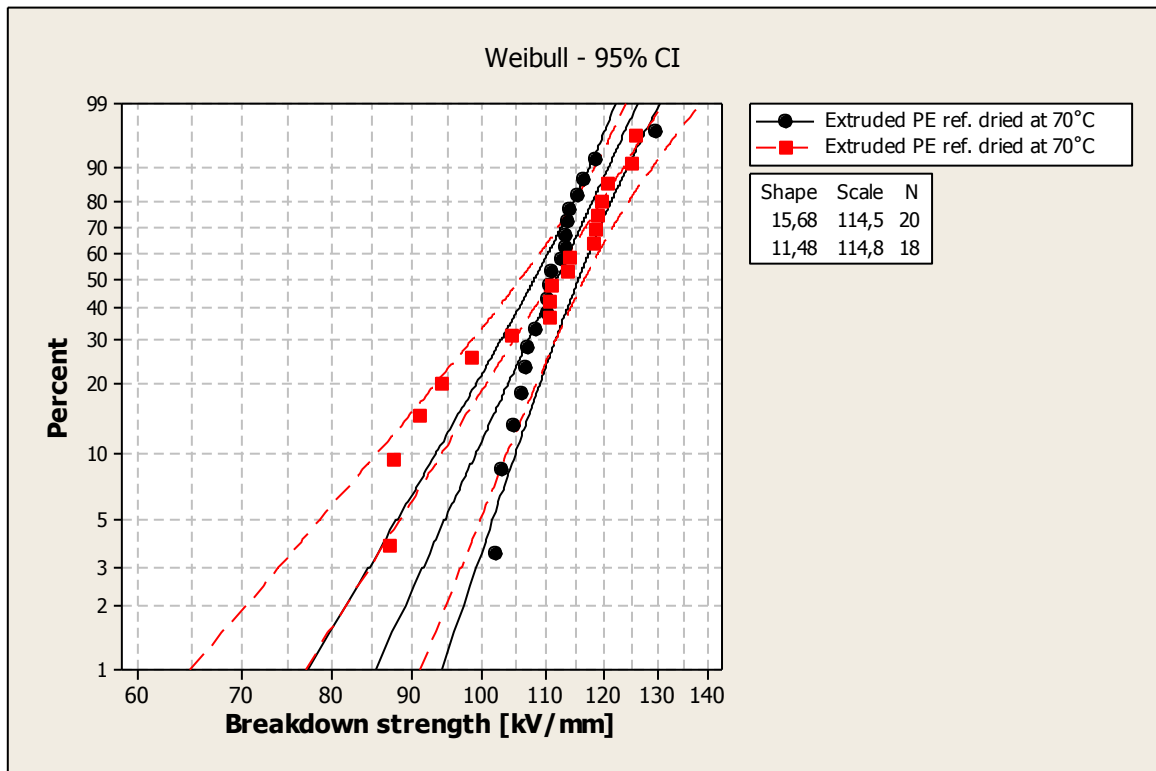


Figure 25. Weibull plot of two extruded PE references dried at 70°C for 24 h after the extrusion process. The black values are from the extrusion described in this thesis and the red values from an extrusion in an earlier project at ABB. The same process parameters were used for these two extrusion processes. 95% confidence intervals and linear regressions are indicated by the lines.

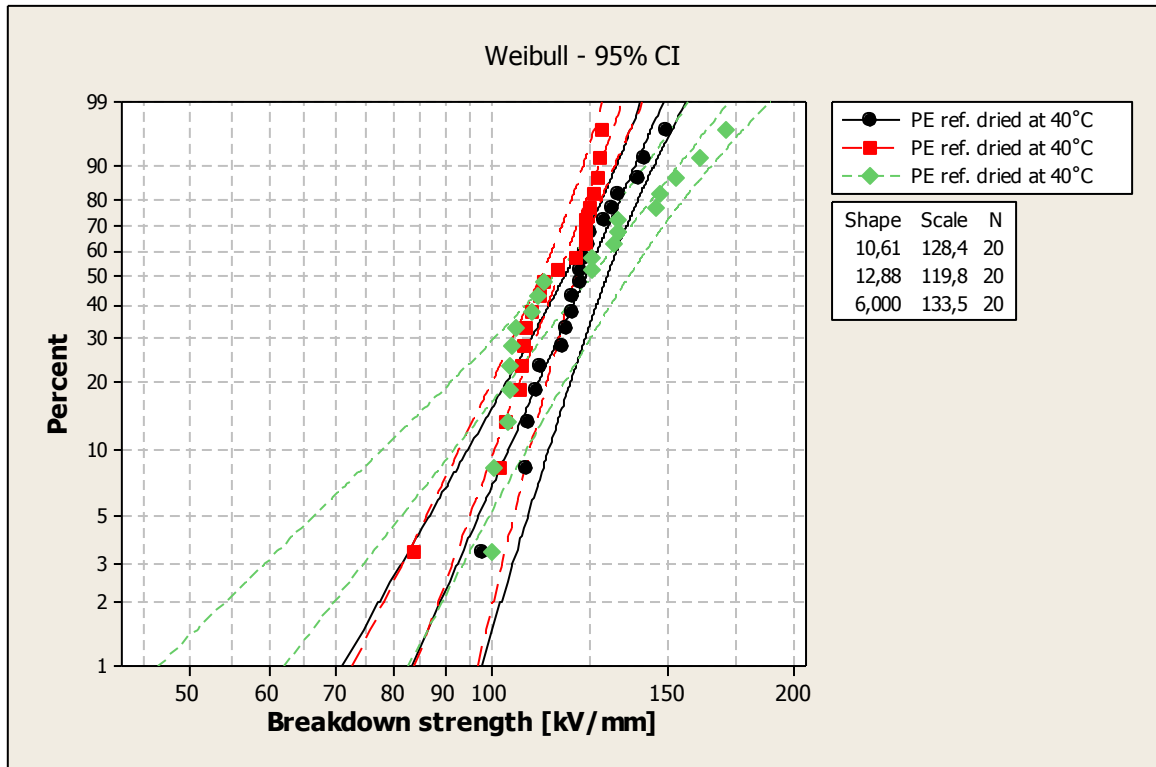


Figure 26. Weibull plot of three PE references dried at 40°C for 17 h. Those materials were dried, pressed and tested at different occasions. 95% confidence intervals and linear regressions are indicated by the lines.

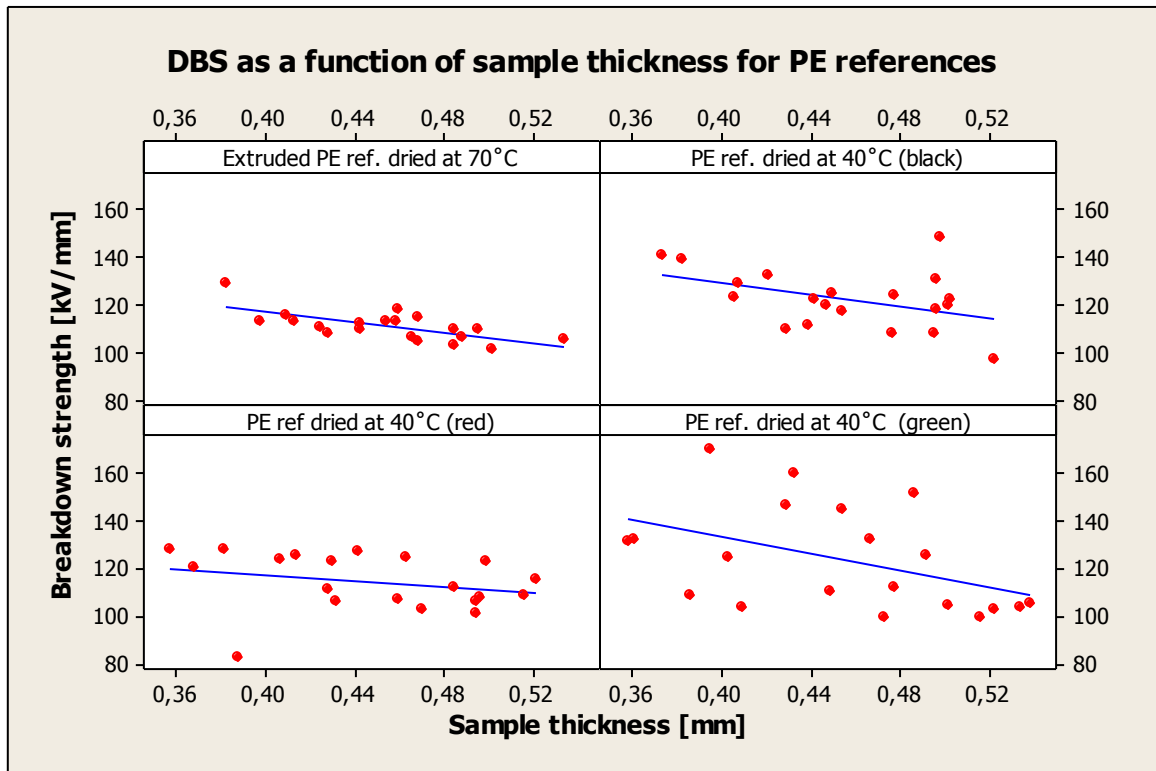


Figure 27. DBS of neat extruded PE dried at 70 °C for 24 h (black values from **Figure 25**) and three PE samples dried at 40 °C for 17 h (**Figure 26**) as a function of sample thickness. The blue lines are linear regression fits.

4.2 Influence of process parameters on breakdown strength

4.2.1 Different drying conditions

Different process parameters during sample preparation and compounding can influence the DBS. All materials were therefore extruded and pressed with the same process parameters. The drying temperatures and time of the drying process in vacuum varied for extruded and swelled materials. Additives mixed with PE by extrusion were dried at 70 °C for 24 h to evaporate moisture from the material before the pressing process. Additives mixed with PE by swelling were dried at 40°C for 17 h to evaporate the organic solvent while minimizing the migration of additives from the materials before the pressing process. Weibull plots of neat PE and neat PE nanocomposites dried at 70 °C for 24 h in vacuum, 40 °C for 17 h in vacuum or pressed to plates without drying are shown in **Figures 28-30** and the results are summarized in **Table 7**. Neat PE and PE+30% MgO dried at 40 °C showed higher scale parameters than the references dried at 70 °C but the increase in DBS was not significant. However, almost all breakdown values for these two references dried at 40 °C were higher than the references dried at 70 °C, i.e. the scale parameters are higher while they almost have the same shape parameters. However, it can be concluded from **Figures 28-30** that different amounts of moisture have no influence on the DBS for neat PE and the PE nanocomposites dried in 70 °C and without drying before the pressing process. This because an increased amount of moisture should decrease the DBS but the DBS remain unchanged for samples without drying compared to samples dried at 70 °C. One exception is the DBS on neat PE pellets without drying which have a slightly increased DBS at high probability of failure compared to pellets dried at 70 °C. This result further confirms that the amount of moisture in these samples have no influence on the DBS.

This increase in DBS was therefore deeper investigated for the neat PE. This was done with DSC analysis to determine any differences in thermal history or degree of crystallinity and FTIR spectroscopy to determine the amount of a process stabilizing additive present in the materials. The results of the DSC analysis are shown in **Figure 31** and **Figure 32**. No significant difference in melting or crystallization temperature, degree of crystallinity or thermal history could be seen. Reference samples swelled covered in heptane or cyclohexane and then dried at 40 °C were also analyzed with DSC but showed no significant difference either. This shows that the drying and swelling of the PE did not degrade the material. The PE that was used contains small amounts of a process stabilizing additive used to prevent oxidation of the material. Consumption of this additive due to oxidation or migration during the different drying conditions was investigated with FTIR. The amount of the process stabilizing additive can be determined by measuring the peak height of a specific absorption peak in the IR absorption spectrum. The wavelength of the specific absorption peak, name and amount of the process stabilizing additive cannot be mentioned due to confidential reasons. The height of this specific absorption peak was determined to be the same for PE dried at 70 °C for 24 h and 40 °C for 17 h and both samples therefore contain the same amount of the process stabilizing additive.

The reason for the higher breakdown values for neat PE (**Figure 28**) and PE+30% MgO (**Figure 30**) dried at 40°C than dried at 70°C remain unclear. This could be further investigated by using samples with the same sample thickness to exclude different influence of sample thickness on the DBS. However, this was not possible to perform during this thesis work.

Table 7. Summary of the α and β parameters in **Figures 28-30**, which show Weibull plots of PE and PE nanocomposites references with different drying conditions.

Polymer matrix	Drying conditions	α [kV/mm]	β (shape factor)
PE	Dried at 70 °C for 24 h	121.1	11.1
PE	Dried at 40 °C for 17 h	128.4	10.6
PE	Not dried	131.4	7.5
PE+3% MgO	Dried at 70 °C for 24 h	117.1	10.7
PE+3% MgO	Dried at 40 °C for 17 h	115	8.8
PE+3% MgO	Not dried	123.4	7.3
PE+30% MgO	Dried at 70 °C for 24 h	102.8	13.1
PE+30% MgO	Dried at 40 °C for 17 h	112.4	10
PE+30% MgO	Not dried	105	8.2

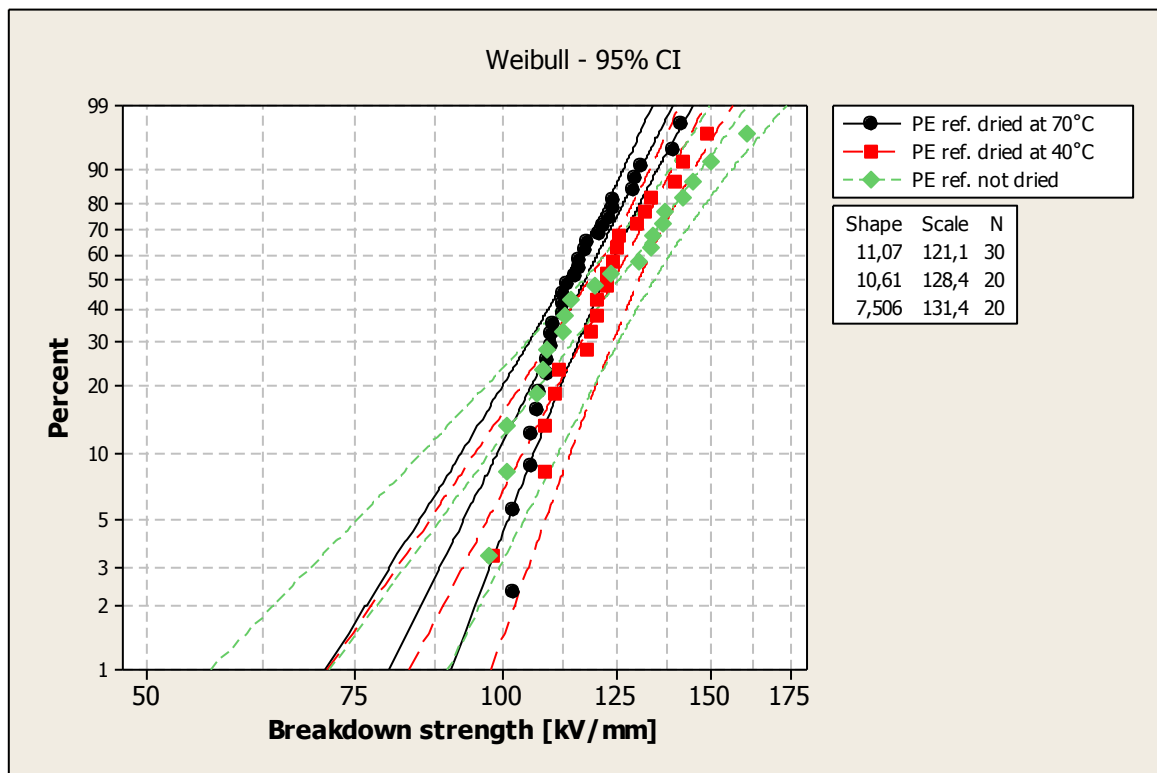


Figure 28. Weibull plot of neat PE references dried at 70°C for 24 h, 40°C for 17 h and without drying. 95% confidence intervals and linear regressions are indicated by the lines.

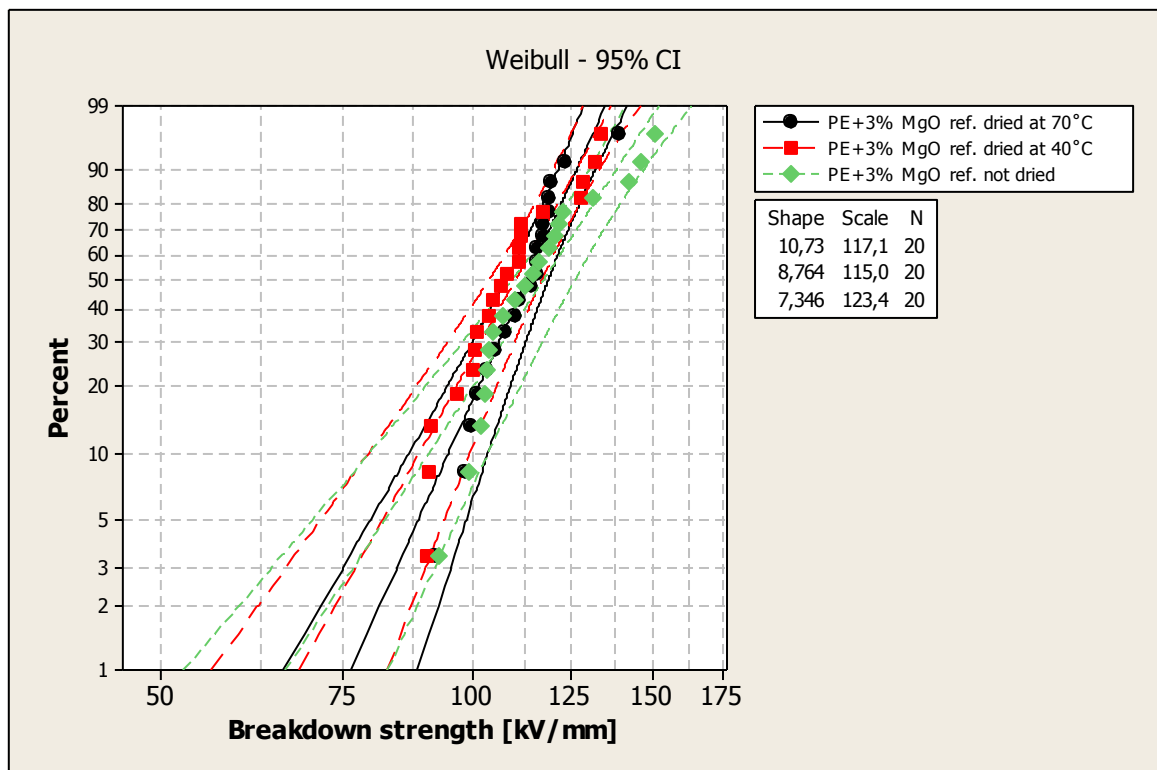


Figure 29. Weibull plot of PE nanocomposite references containing 3 wt% MgO nanoparticles dried at 70°C for 24 h, 40°C for 17 h and without drying. 95% confidence intervals and linear regressions are indicated by the lines.

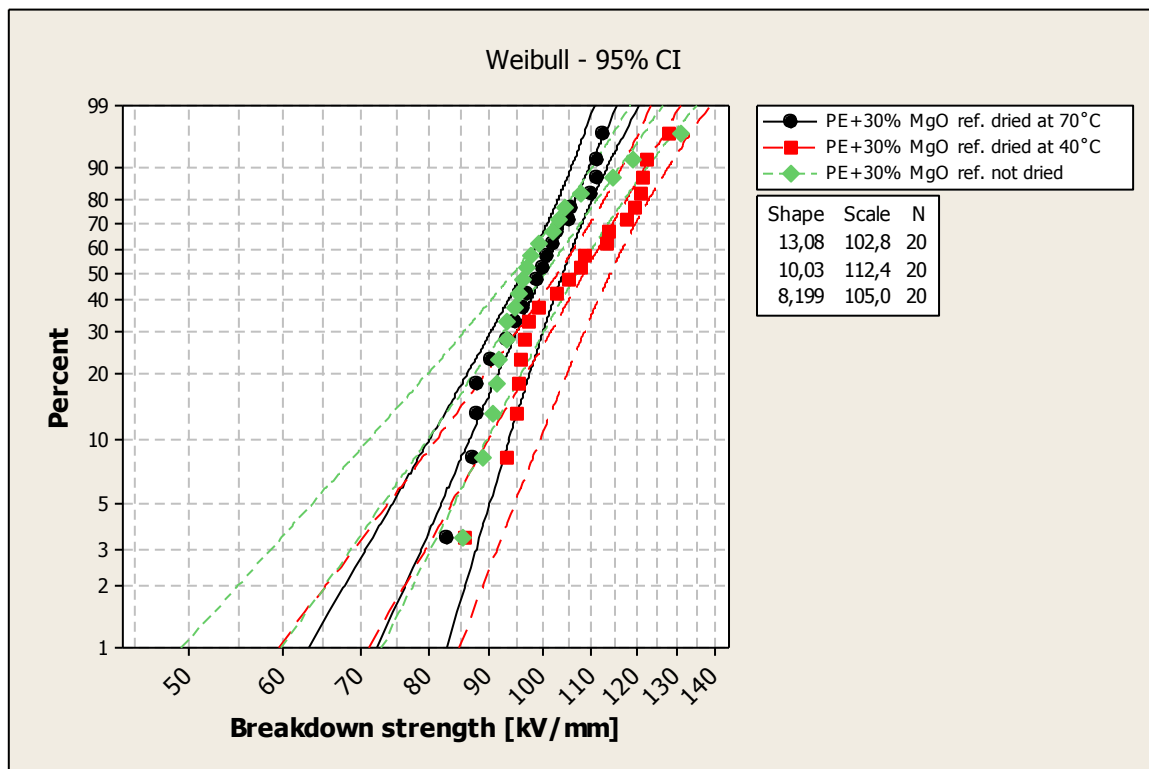


Figure 30. Weibull plot of PE nanocomposite references containing 30 wt% MgO nanoparticles dried at 70°C for 24 h, 40°C for 17 h and without drying. 95% confidence intervals and linear regressions are indicated by the lines.

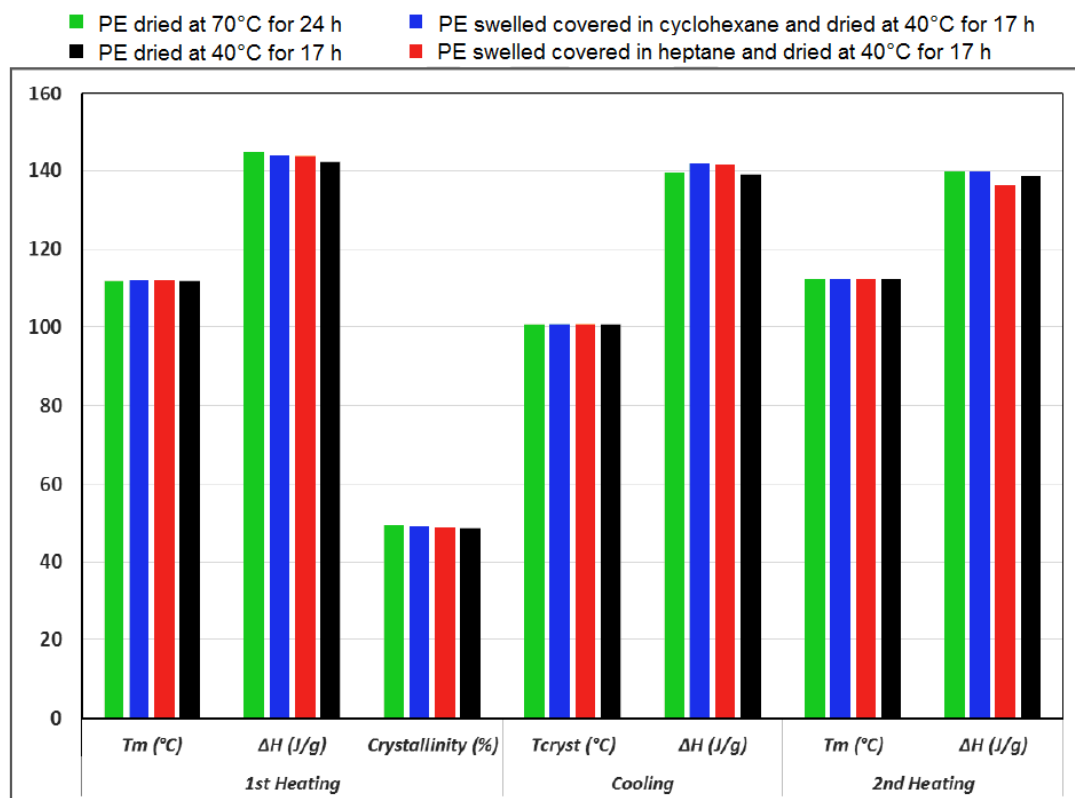


Figure 31. The results of the DSC measurements performed on PE samples after pressed in the hot press. The green and black bars shows the influence of drying parameters and the blue and red bars shows the influence of the swelling process on melting temperature, degree of crystallinity and crystallization temperature.

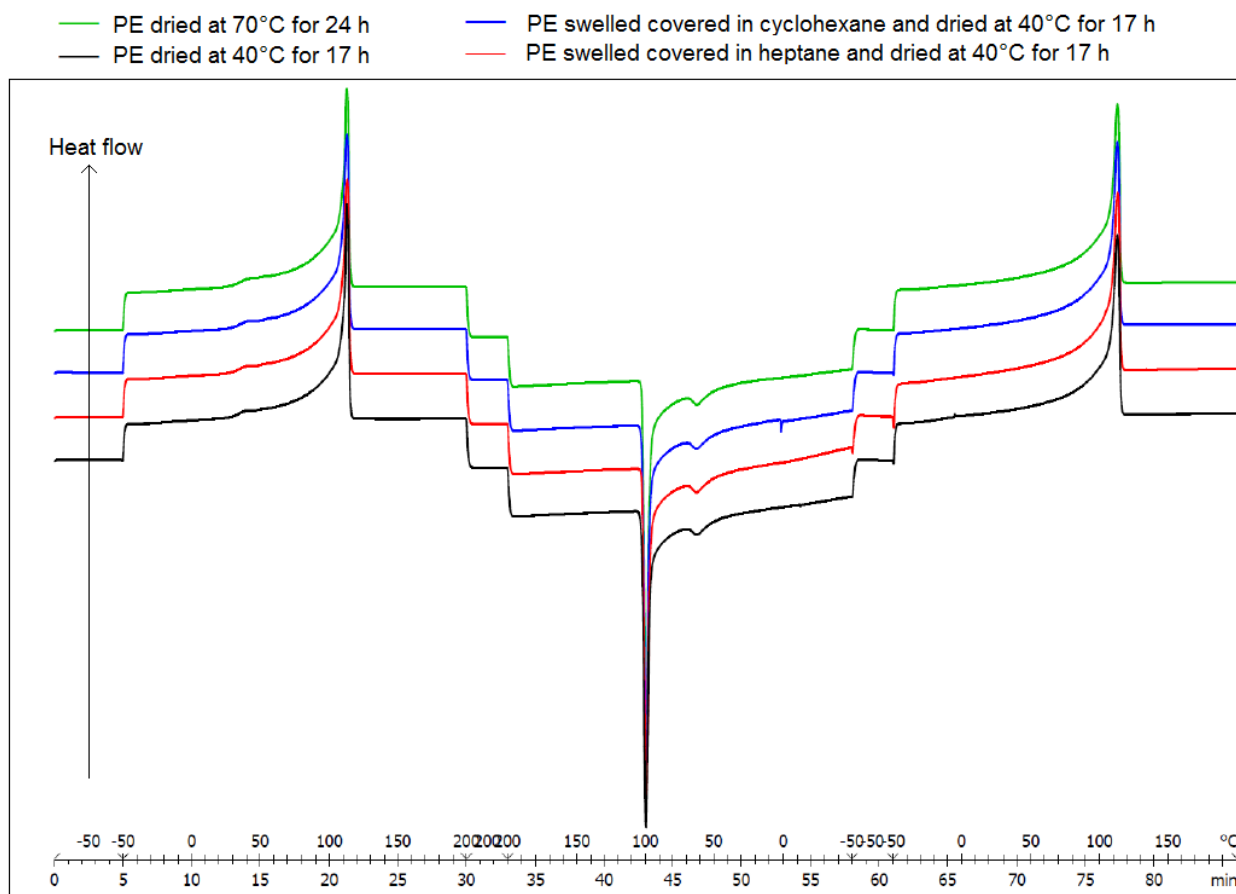


Figure 32. Heat flow as a function of time and temperature from the DSC measurements. An increased amount of heat flow indicates endothermic reactions (melting) while a decrease in heat flow indicates exothermic reactions (crystallization).

4.2.2 Influence of the extrusion process on breakdown strength

The DBS of extruded neat PE are compared to neat PE without extrusion, **Figure 33**, to investigate if this compounding process affects the DBS. No significant difference in DBS can be seen but the shape parameter of the extruded PE sample is higher, which indicates less scattering of DBS values. **Figure 34** shows the influence of sample thickness on the DBS for the extruded neat PE reference in **Figure 33** and the neat PE samples with different drying parameters, which are shown in a Weibull plot in **Figure 28**. All four samples in **Figure 34** show that the DBS (kV/mm) depends on the sample thickness, i.e. thinner samples results in higher DBS than thicker samples. This dependency agrees with the literature and is shown by the negative value of the linear regression fits (blue lines in **Figure 34**). All four samples in **Figure 34** also have similar lowest DBS values ~ 100 kV/mm, while the highest DBS values vary from ~ 130 - 160 kV/mm. The smallest scattering of DBS values were obtained for the extruded PE sample. The reason for different scattering of high DBS values and the similar lowest DBS values is unclear and not further investigated in this thesis.²²

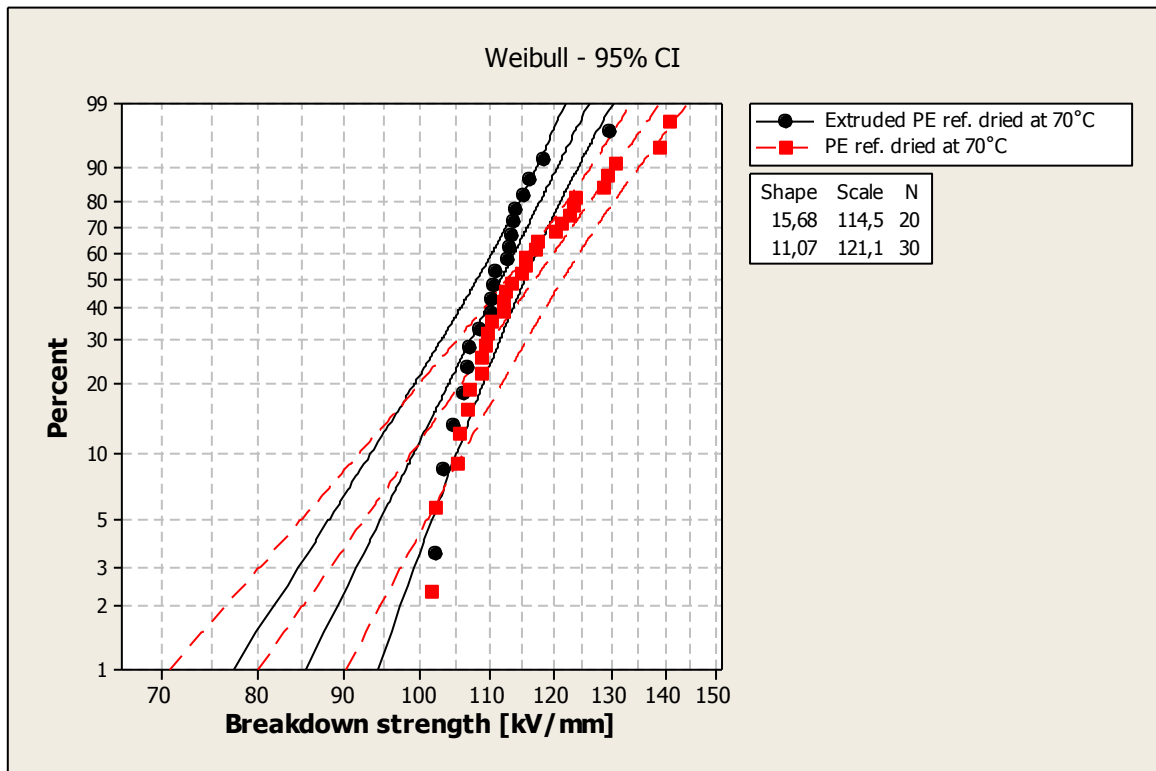


Figure 33. Weibull plot of extruded neat PE and neat PE without extrusion. Both samples were dried at 70°C for 24 h before the pressing process. 95% confidence intervals and linear regressions are indicated by the lines.

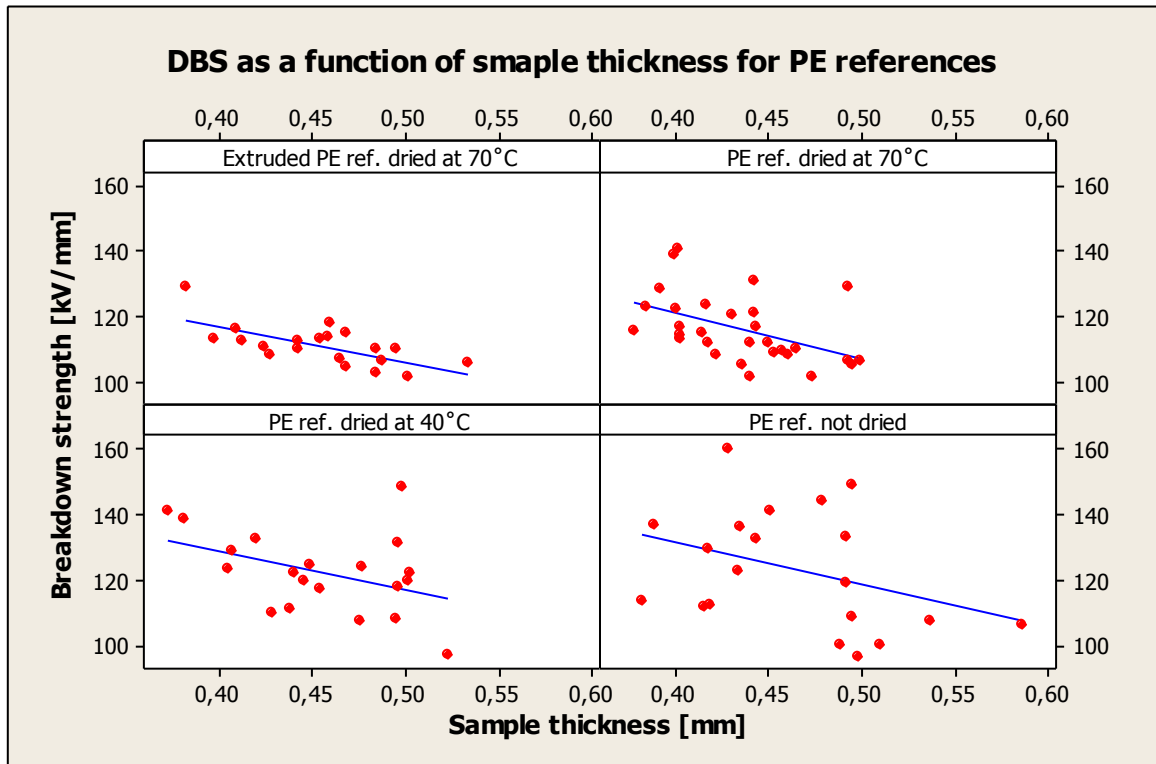


Figure 34. DBS of neat PE references as a function of sample thickness. The blue lines are linear regression fits.

4.3 Influence of nanofillers on breakdown strength

Nanocomposites of PE containing 3 and 30 wt% MgO nanoparticles are compared to neat PE in **Figure 35**. All three materials were extruded, dried in vacuum at 70°C for 24 h before plates were pressed and the AC DBS were measured. A significant difference can be seen between the lower DBS of PE+30% MgO compared to neat PE and PE+3% MgO. The amount of nanoparticles observed in literature that can improve the DBS is around a few wt%, so the lower DBS with 30 wt% MgO was expected. This since nanoparticles easily forms agglomerations, even at low loadings, and acts like micro sized particles and thus lowers the DBS. Such agglomerations can be minimized if the surface of the nanoparticles is modified with a suitable coating to become more compatible with the polymer matrix. However, in this investigation it was desirable to have an uncoated and polar surface of the MgO nanoparticles. This since the PE nanocomposite with 30 wt% MgO nanoparticles will be used as polymer matrix to investigate if voltage stabilizing additives can be adsorbed to the polar surfaces of the nanoparticles and thus improve the DBS. One other reason to use the 30 wt% MgO nanocomposite as polymer matrices is due to its lower DBS than neat PE and the DBS should therefore be easier to improve by addition of voltage stabilizing additives. The similar DBS of PE+3% MgO and neat PE are also believed to be the result of agglomeration of nanoparticles. This because the extrusion process parameters used in this thesis are not optimized in order to disperse nanoparticles but to mix additives with the polymer matrix.²

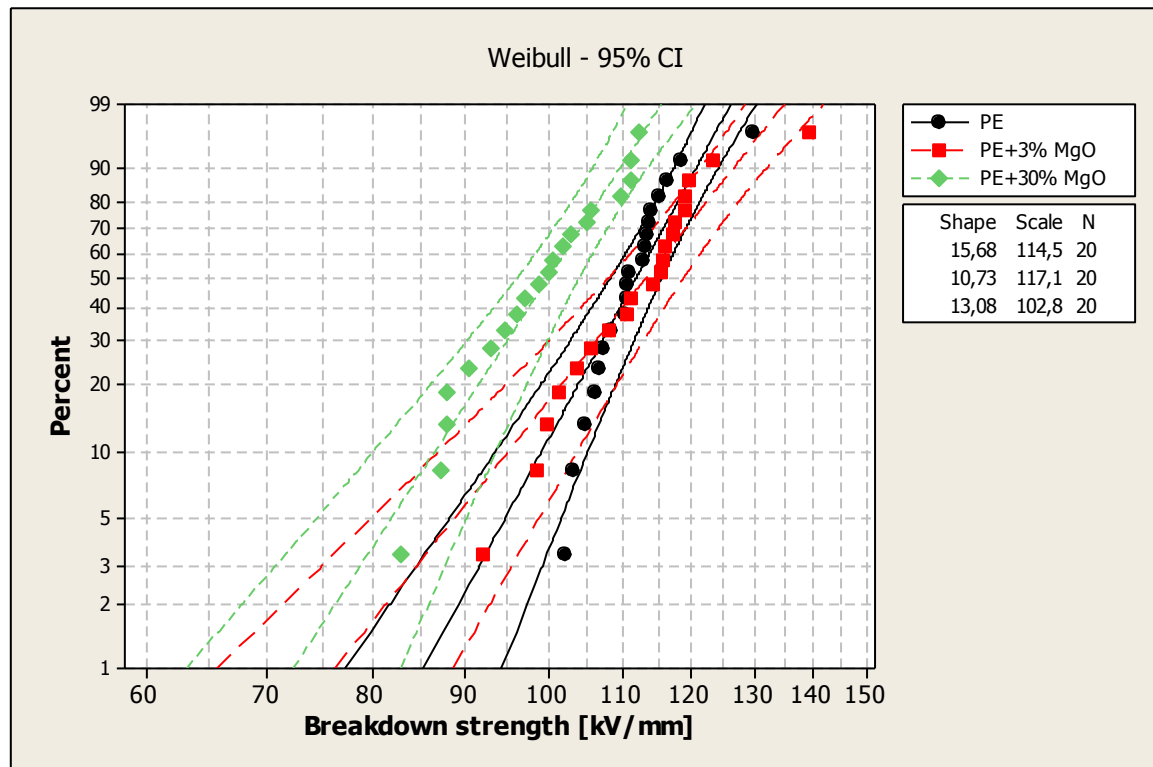


Figure 35. Weibull plot of neat PE and PE nanocomposites containing 3 and 30 wt% MgO nanofillers. 95% confidence intervals and linear regressions are indicated by the lines.

4.4 Influence of voltage stabilizing additives on breakdown strength

4.4.1 Additives mixed with PE matrices by extrusion

The DBS at 63.2% failure probability (α) and the slope of the Weibull plot (β) for materials where the voltage stabilizing additives were mixed with neat PE matrices by extrusion are summarized

in **Table 8**. All materials in this section were dried at 70°C for 24 h in vacuum after the extrusion process before they were pressed to plates. Weibull plots of PE with voltage stabilizing additives compared to neat extruded PE are shown in **Figures 36-38**. No significant difference in DBS could be seen for the various additives in this section. PE+1.5 wt% additive C shows a slight significant improvement over 50 % probability of failure but this is mainly due to the low shape parameter caused by the four highest DBS values. Scattering of some DBS values at high probability of failure resulting in a low shape parameter were also observed by the stability of PE references, as can be seen in **Figure 26**.

Table 8. Summary of the α and β parameters for voltage stabilizing additives mixed with neat PE matrices by extrusion. Weibull plots of these materials are shown in **Figures 36-38**.

Polymer matrix	Additive	α [kV/mm]	β (shape factor)
PE	None, reference sample	114.5	15.7
PE	1.5 % additive C	124.8	9.7
PE	3 % additive C	113.8	11
PE	0.2 % additive E	114.4	10.7
PE	0.5 % additive E	122	7.4
PE	0.2 % additive D	121.7	7.2
PE	3 % additive D	115.8	10.9

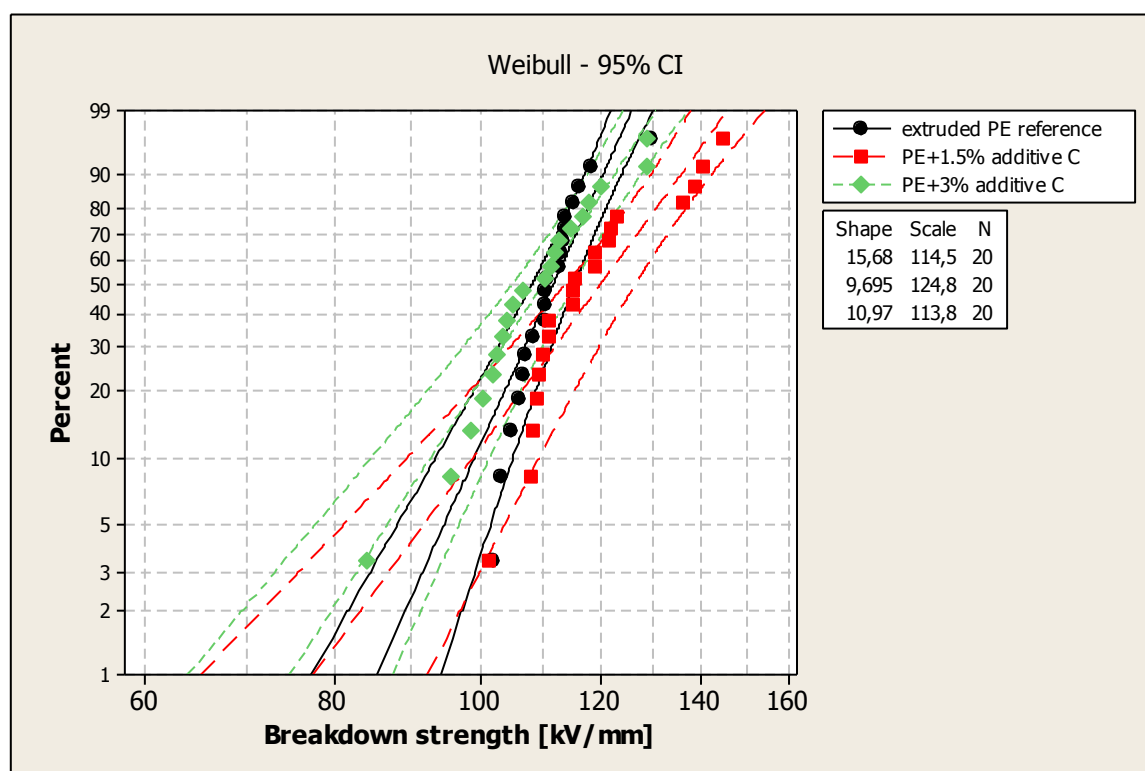


Figure 36. Weibull plot of neat PE and PE containing 1.5 and 3 wt% of the voltage stabilizing additive C. The additive was mixed with PE by extrusion and compared to neat extruded PE. 95% confidence intervals and linear regressions are indicated by the lines.

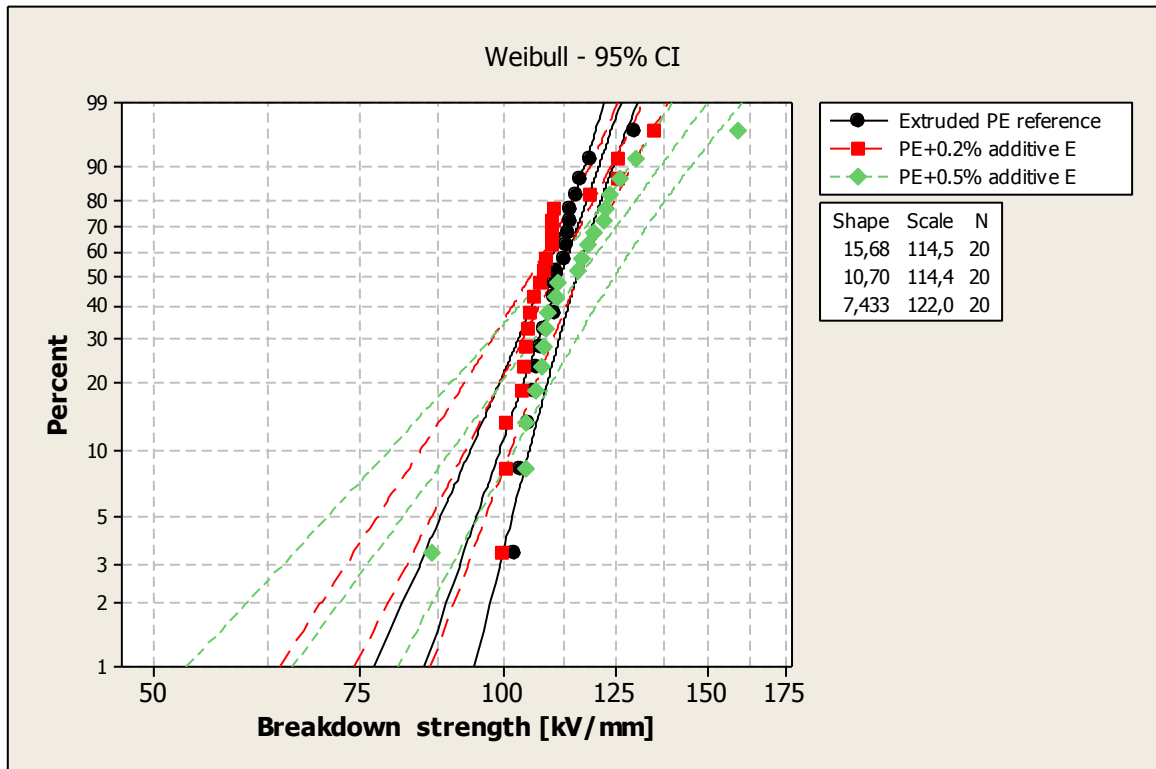


Figure 37. Weibull plot of neat PE and PE containing 0.2 and 0.5 wt% of the voltage stabilizing additive E. The additive was mixed with PE by extrusion and compared to neat extruded PE. 95% confidence intervals and linear regressions are indicated by the lines.

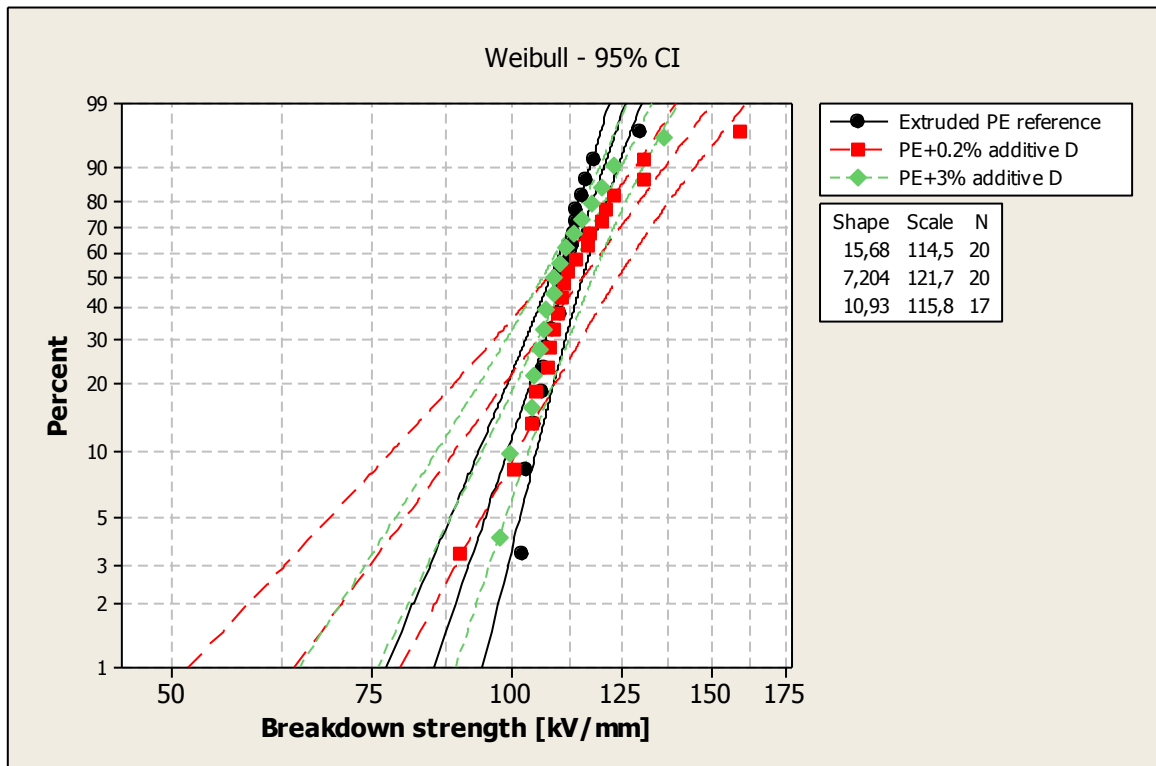


Figure 38. Weibull plot of PE containing 0.2 and 3 wt% of the voltage stabilizing additive D mixed with PE by extrusion and compared to neat extruded PE. 95% confidence intervals and linear regressions are indicated by the lines.

4.4.2 Additives mixed with PE matrices by swelling

The voltage stabilizing additive A was tried to be swelled into neat PE matrices with the organic solvents heptane and cyclohexane. The PE pellets in the size of ~5 mm in diameter were immersed in either solvent, which also contained 9 wt% of additive A. The swelled materials were dried at 40 °C, instead of 70 °C as for the extruded materials, to evaporate the organic solvent without diffusion of the additives out of the PE pellets. The swelled materials were thus compared to a PE reference dried at 40 °C to exclude the influence of different degree of moisture or different process parameters on the DBS. The details of the swelling parameters are previously summarized in **Table 5**. It is important to point out that the actual concentrations of the additives in the PE plates are currently unknown and needs to be quantified by chromatographic methods.

A summary of the α and β parameters of the Weibull plots in this section, **Figures 39-41**, are shown in **Table 9**. No significant improvement of the DBS can be seen in **Figure 39** where heptane was used as organic solvent to swell additive A into PE. In **Figure 40** cyclohexane was used and the higher DBS of the curve that contains additive A is significant over 50 % compared to the PE reference swelled with cyclohexane but not compared to the reference without any swelling. This improvement at high probability of failure is caused by a lower β value, which indicates more scattering of the DBS data. The DBS values of PE+9 wt% of additive A in **Figure 40** looks to fit better to two linear regressions with different slopes than one. This can be achieved by the use of a mixed Weibull distribution plot. This tendency can also be seen for other materials, e.g. all Weibull plots in **Figure 39**. However, a mixed Weibull distribution plot should only be used if the reasons for breakdown at high and low probability of failure are independent of each other. This can e.g. be the case if the breakdowns at low and high electrical fields are caused by two different independent breakdown mechanisms. The parameter estimation of a mixed Weibull distribution is more difficult to perform and therefore left out of this thesis work.⁴⁹

Figure 41 shows the influence of the organic solvents on the DBS. The organic solvents have a purity of ~99 % which means that contaminants could be swelled into the PE matrices during the swelling process. The swelled reference samples had a smell of organic solvents during the AC DBS tests, which indicate that the samples still contain some solvents even after the drying and pressing process. However, the organic solvents show no significant influence on the DBS despite these observations.

Table 9. Summary of α and β parameters for additive A swelled into neat PE matrices with different organic solvents. Weibull plots of these materials are shown in **Figures 39-41**.

Polymer matrix	Additive	Organic solvent	α [kV/mm]	β (shape factor)
PE	None ref.	None ref.	128.4	10.6
PE	None ref.	Heptane	134.3	8.4
PE	Additive A	Heptane	128.8	7.8
PE	None ref.	Cyclohexane	123.1	13.8
PE	Additive A	Cyclohexane	137	8.9

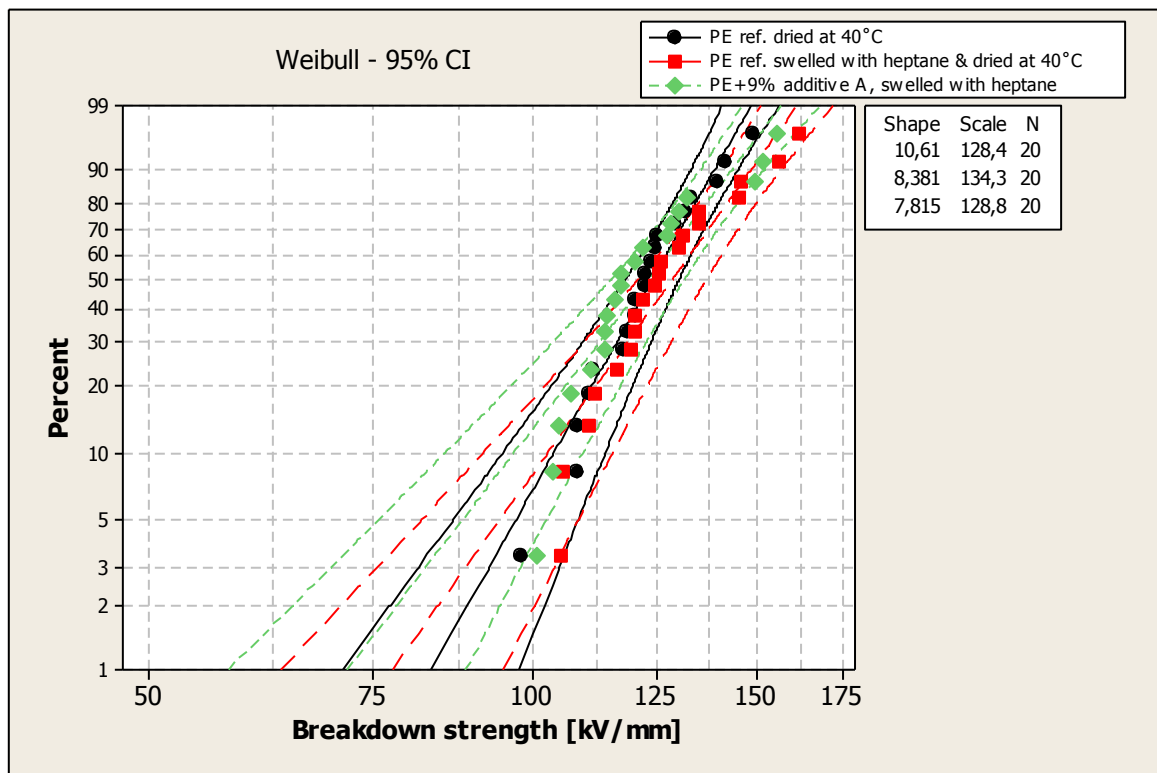


Figure 39. Weibull plot of PE swelled covered in a mixture of solvent and 9 wt% additive A compared to PE swelled covered in heptane and PE without swelling. 95% confidence intervals and linear regressions are indicated by the lines.

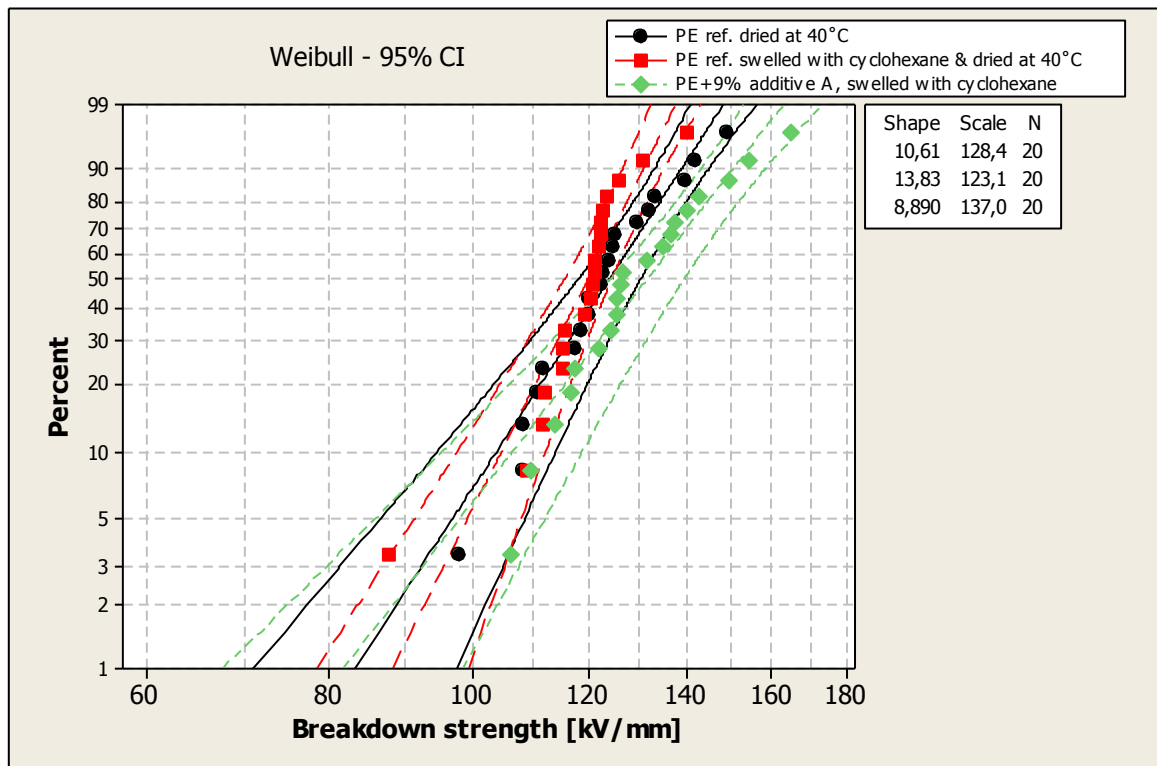


Figure 40. Weibull plot of PE swelled covered a mixture of cyclohexane and 9 wt% additive A compared to PE swelled covered in cyclohexane and PE without swelling. 95% confidence intervals and linear regressions are indicated by the lines.

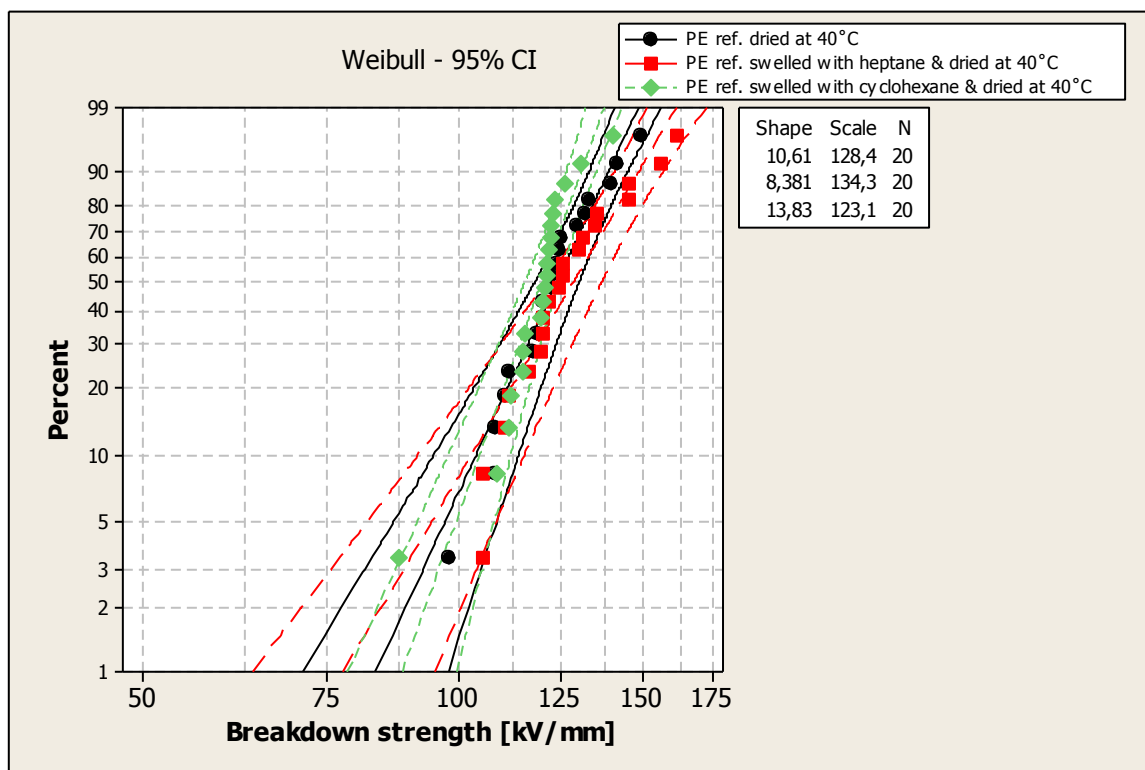


Figure 41. Influence of organic solvents on the DBS for PE swelled covered in heptane or cyclohexane compared to PE without swelling. 95% confidence intervals and linear regressions are indicated by the lines.

4.5 Influence of both nanofillers and voltage stabilizers on breakdown strength

4.5.1 Additives mixed with PE nanocomposite matrices by extrusion

The α and β parameters for voltage stabilizing additives mixed with PE nanocomposite matrices by extrusion are summarized in **Table 10**. All materials in this section were dried at 70°C for 24 h in vacuum after the extrusion process before they were pressed to plates. Weibull plots of the materials summarized in **Table 10** are shown in **Figures 42-43**. No significant differences in DBS for PE nanocomposites with and without additives could be seen in this section.

Neat PE containing additive A has also been AC DBS tested without any significant differences. Quantitative analysis of how much additives the pressed plates contain is interesting because additives mixed by extrusion with neat PE matrices in an earlier project at ABB showed that only a fraction (12-33 %) of the initial concentration additives that was added during the extrusion was present in the pressed plates. PE nanocomposites were therefore used, with the intention to adsorb the additives onto the nanoparticles surfaces. The conclusion of the results without any improvements in DBS is that the pressed plates of the materials in this section also only contained a fraction of the initial amount of additive added during the extrusion process. Compounding of the additives using the extrusion process was thus not believed to be sufficient. The additives were therefore tried to be swelled into the nanocomposite polymer matrices.

Table 10. Summary of the α and β parameters for voltage stabilizing additives mixed with PE nanocomposite matrices by extrusion. Weibull plots of these materials are shown in **Figures 42-43**.

Polymer matrix	Additive	α [kV/mm]	β (shape factor)
PE+30% MgO	None, reference	102.8	13.1
PE+30% MgO	1.5% additive C	104.5	15
PE+30% MgO	3% additive C	105.5	12.7
PE+30% MgO	1.5% additive A	106.2	11.4
PE+30% MgO	3% additive A	104.4	11.3

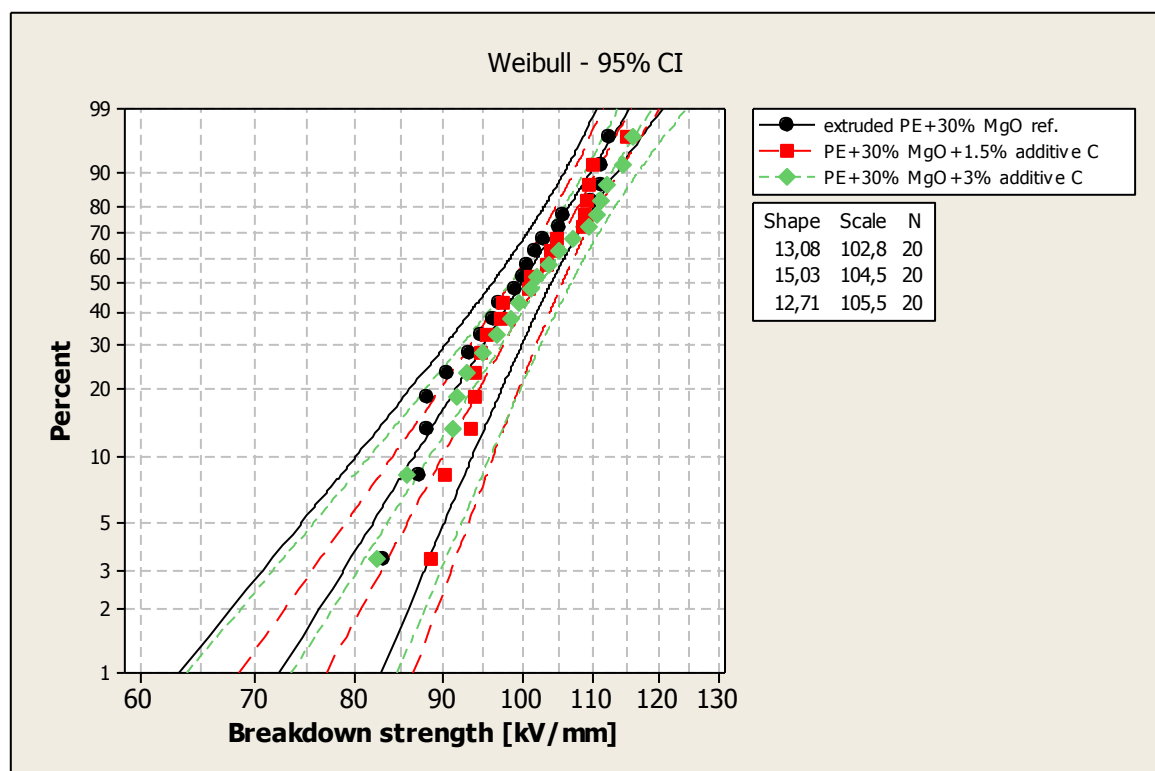


Figure 42. Weibull plot of nanocomposite matrices of PE+30% MgO containing 1.5 and 3 wt% of the voltage stabilizing additive C. The reference of PE+30% MgO was extruded to exclude the influence of different process parameters on the DBS. 95% confidence intervals and linear regressions are indicated by the lines.

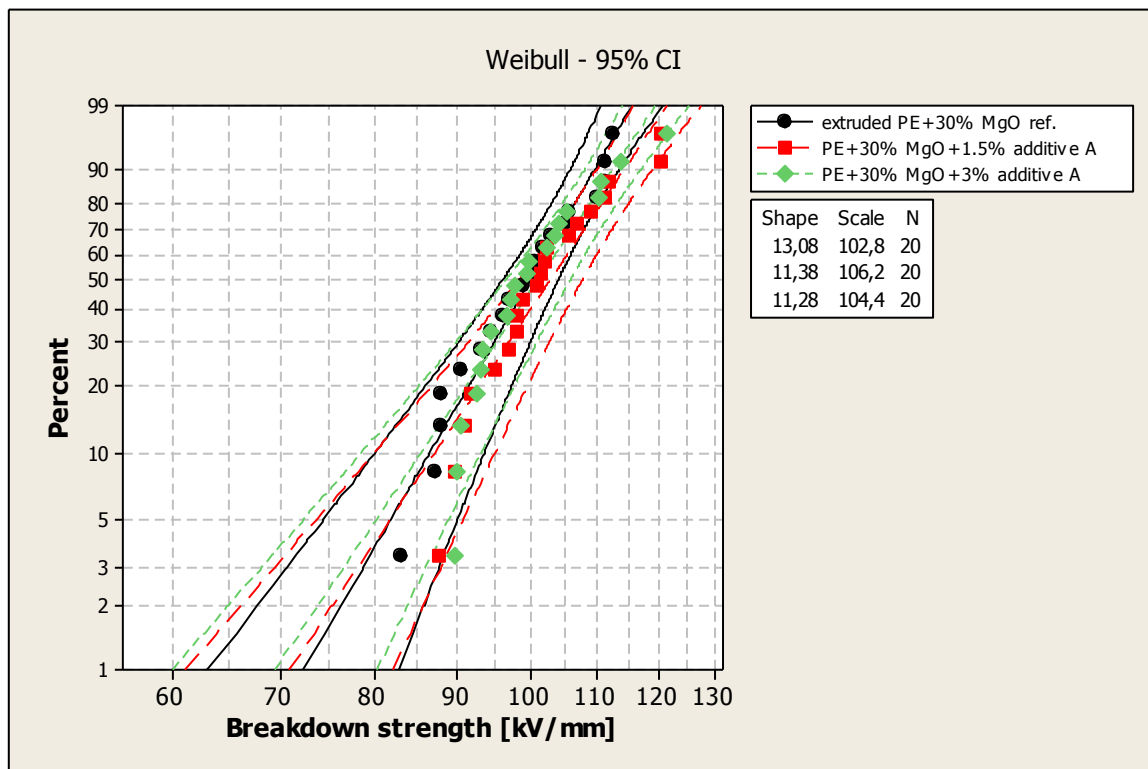


Figure 43. Weibull plot of nanocomposite matrices of PE+30% MgO containing 1.5 and 3 wt% of the voltage stabilizing additive A. The reference of PE+30% MgO was extruded to exclude the influence of different process parameters on the DBS. 95% confidence intervals and linear regressions are indicated by the lines.

4.5.2 Additives mixed with PE nanocomposite matrices by swelling

PE nanocomposite matrices with 3 and 30 wt% MgO nanoparticles were used as polymer matrices in attempts to swell additive A into the material with small amounts of heptane. A larger amount of the voltage stabilizing additive A were believed to be solved in nanocomposites than for neat PE, due to adsorption onto the surfaces of the highly polar MgO nanoparticles. The results of the nanocomposite matrix with 3 wt% and 30 wt% MgO are shown in **Figure 44** and **Figure 45**, respectively. The references for comparison were dried in vacuum with the same drying conditions, i.e. 40°C for 17 h, to exclude influence of different drying parameters on the DBS. Here the data indicate an increase of the electrical field required to initiate the breakdown process, with an increasing concentration of the Additive A. The actual amount of the additive present in the pressed samples must be quantified with chromatographic methods.

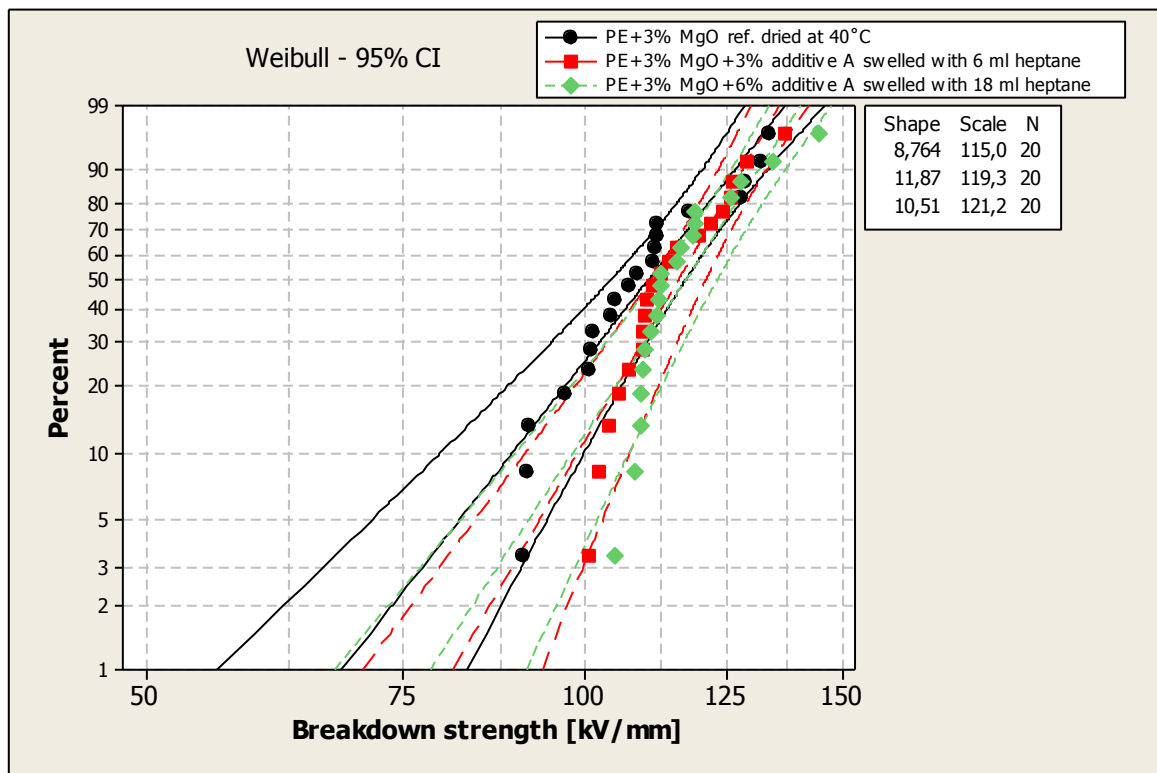


Figure 44. Weibull plot of nanocomposite matrices of PE+3% MgO nanoparticles containing 3 and 6 wt% additive A which was mixed by swelling with heptane. 95% confidence intervals and linear regressions are indicated by the lines.

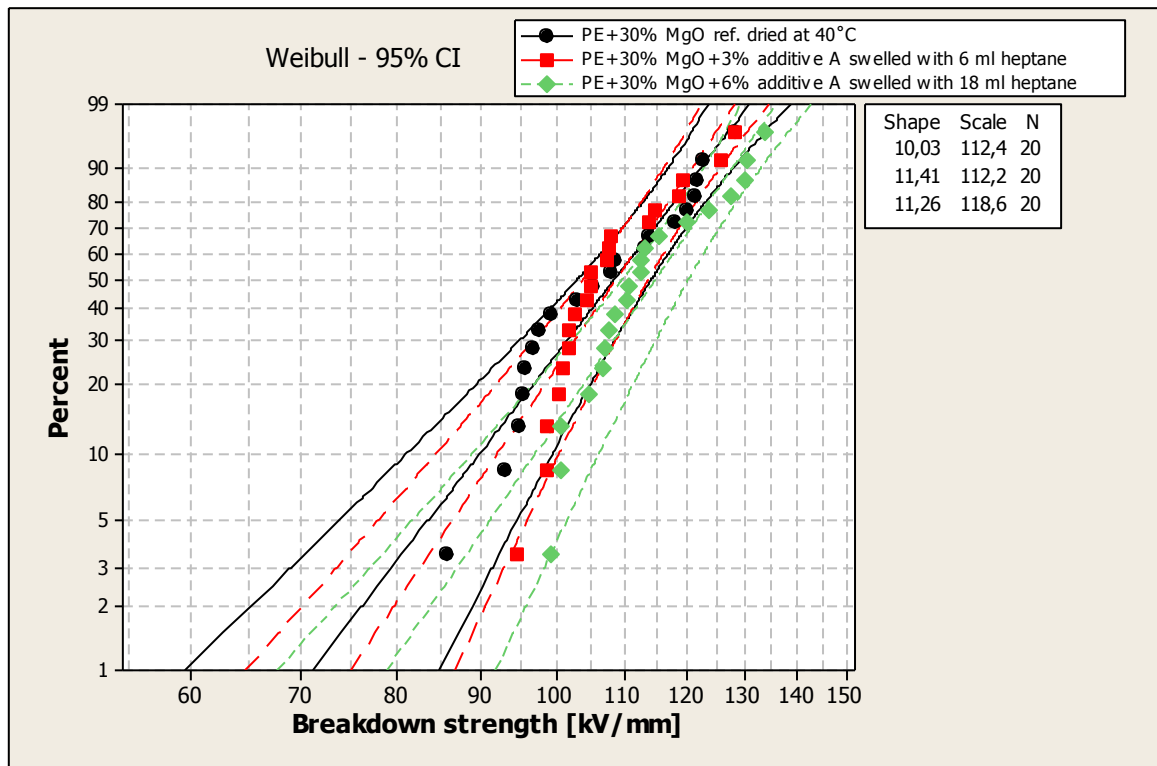


Figure 45. Weibull plot of nanocomposite matrices of PE+30% MgO nanoparticles containing 3 and 6 wt% additive A which was mixed by swelling with heptane. 95% confidence intervals and linear regressions are indicated by the lines.

5 CONCLUSIONS

The aim of this thesis work was to investigate if the dielectric breakdown strength (DBS) of pure low density polyethylene (LDPE) or LDPE magnesium oxide (MgO) nanocomposites can be improved by voltage stabilizing additives. In the first step the effect of various processing parameters on the breakdown strength were assessed. Different drying parameters of the materials before the pressing process show no significant difference on the alternating current DBS. There was however a trend that a few materials dried at higher temperatures (70 °C in vacuum for 24 h) exhibited lower breakdown strength compared with samples dried at lower temperatures (40 °C in vacuum for 17 h) or undried materials. This was further investigated by differential scanning calorimetry and infrared spectroscopy. No difference in crystalline structure (degree of crystallinity, melting point and crystallization temperature) was observed. No consumption of the process stabilizer was indicated by the infrared spectroscopy. Furthermore it was verified that potential remaining moisture in the materials on the breakdown data was negligible. The influence of various ways to add voltage stabilizers to the polymer matrix: mixing by extrusion or solvent swelling was investigated. Extruded materials show less scattering of AC DBS data, i.e. higher shape parameter in a two parameter Weibull plot, than materials without extrusion. The influence of sample thickness on breakdown data was carefully investigated. The breakdown value per millimeter increased with decreasing sample thickness in accordance with literature.

Voltage stabilizing additives were compounded into LDPE or LDPE nanocomposites with extrusion. No significant improvements in DBS with the addition of voltage stabilizers have been seen for neat LDPE compared to references of the same material, typical breakdown values ranged between 109-116 kV/mm. The solubility of additives was believed to be better in nanocomposites, due to the large polar surface of the particles. Since no improvements in DBS were found in the nanocomposites it is believed that the extrusion process was not sufficient to mix the additives with the polymer matrix, instead solution swelling was used. The influence of addition of voltage stabilizing additives on the DBS of LDPE MgO nanocomposites (3 and 30 wt% MgO) is currently inconclusive. Here the breakdown data indicate an increase in electrical field to initiate breakdown at low probability of failure with approximately 15-20% with increased amount of voltage stabilizing additive. However, it is not clear that these improvements are significant and further work is required to quantify the amount of additive present in the pressed samples.

6 FUTURE WORK

Recommended further attempts to increase the DBS of LDPE are to:

- Optimize the swelling process (temperature and time).
- Identify new types of voltage stabilizing additives with higher solubility in LDPE.
- Complement the AC breakdown tests with direct current breakdown measurements.
- Use a robust reference material with high shape parameter (>20) as quality check of the used oil and instrument.

7 ACKNOWLEDGEMENTS

I would like to thank my supervisor Henrik Hillborg for the opportunity to perform my thesis work at ABB and also all other co-workers at ABB who have helped me during the work. Special thanks to Anneli Jedenmalm, Mikael Unge and Joakim Jambeck. I would also like to thank all thesis workers at ABB for interesting things to talk about during lunches. Thanks to Gabriella Wallentin for help with a lot of breakdown measurements. I would also like to thank my reviewer Urban Wiklund for feedback on my thesis work and my examiner Åsa Kassman for the good administration during this thesis work.

8 REFERENCES

- ¹ F. Oldervoll, Electrical and thermal ageing of extruded low density polyethylene insulation under HVDC conditions, PhD thesis, Norwegian University of science and technology, Trondheim 2000.
- ² M. Takala, Electrical insulation materials towards nanodielectrics, PhD thesis, Tampere University of technology, Tampere 2010.
- ³ Y. Yamano, Roles of polycyclic compounds in increasing breakdown strength of LDPE film, IEEE Transactions on dielectrics and electrical insulation (2006) 774-781.
- ⁴ M. Ieda, M. Nagao and M. Hikita, High-field conduction and breakdown in insulating polymers, IEEE transactions on dielectrics and electrical insulation (1994) 934-945.
- ⁵ S. Li, G. Yin, G. Chen, J. Li, S. Bai, L. Zhong, Y. Zhang and Q. Lei, Short-term breakdown and long-term breakdown failure in nanodielectrics: a review, IEEE transaction on dielectrics and electrical insulation (2010) 1523-1535.
- ⁶ Z. Ma, X. Huang, P. Jiang and G. Wang, Effect of silane-grafting on water tree resistance of XLPE cable insulation, Journal of applied polymer science (2010) 3168-3176.
- ⁷ L. A. Dissado and J. C. Fothergill, Electrical degradation and breakdown in polymers, Peter Peregrinus Ltd., London 1992.
- ⁸ Y. Sun, C. Bealing, S. Boggs and R. Ramprasad, 50+ years of intrinsic breakdown, IEEE electrical insulation magazine (2013) 8-15.
- ⁹ Y. Tanaka, N. Ohnuma, K. Katsunami, and Y. Ohki, Effects of crystallinity and electron mean-free-path on dielectric strength of low-density polyethylene, IEEE Transactions on Electrical Insulation (1991) 258–265.
- ¹⁰ K. Stark and C. Garton, Electric strength of irradiated polythene, Nature (1955) 1225–1226.
- ¹¹ J. Claude, Y. Lu, and Q. Wang, Effect of molecular weight on the dielectric breakdown strength of ferroelectric poly(vinylidene fluoride-chlorotrifluoroethylene)s, Applied Physics Letters (2007) 2129041-2129043.
- ¹² A. von Hippel, Electric breakdown of solid and liquid insulators, Journal of Applied Physics (1937) 815–832.
- ¹³ Y. Sun, S. A. Boggs and R. Ramprasad, The intrinsic electrical breakdown strength of insulators from first principles, Applied physics letters (2012) 1329061-1329065.
- ¹⁴ A. Huazayyin, S. Boggs and R. Ramprasad, Depths of chemical impurity states in polyethylene; the big picture from first principles, in: IEEE international conference on solid dielectrics, Bologna, Italy, 2013 pp. 15-18.
- ¹⁵ B. Han, X. Wang, Z. Sun, J. Yang and Q. Lei, Space charge suppression induced by deep traps in polyethylene, Applied physics letters, (2013) 012902-012904.
- ¹⁶ D. Ma, et.al., Influence of nanoparticle surface modification on the electrical behavior of polyethylene nanocomposites, Nanotechnology (2005) 724–731.
- ¹⁷ Z. H. Fan and N. Yoshimura, The influence of crystalline morphology on the growth of water trees in PE, IEEE Transactions on dielectrics and electrical insulation (1996) 849-858.

-
- ¹⁸ T. Tanaka, Interface properties and surface erosion resistance, in: J. K. Nelson (Ed), Dielectric polymer nanocomposites, Springer US 2010.
- ¹⁹ K. C. Kao, Dielectric phenomena in solids, Academic press, Burlington 2004.
- ²⁰ E. Husain, R. S. Nema, Analysis of paschen curves for air, N₂ and SF₆ using the Townsend breakdown equation, IEEE transactions on electrical insulation (1982) 350-353.
- ²¹ D. B. Go and D. A. Pohlman, A mathematical model of the modified Paschen's curve for breakdown in microscale gaps, Journal of applied physics (2010) 1033031-1033039.
- ²² G. Chen, J. Zhao, S. Li and L. Zhong, Origin of the thickness dependent dc electrical breakdown in dielectrics, Applied physics letters (2012) 2229041-2229044.
- ²³ X. Huang, F. Liu, P. Jiang, Effect of nanoparticle surface treatment on morphology, electrical and water treeing behavior of LLDPE composites, IEEE transactions on dielectrics and electrical insulation (2010) 17-25.
- ²⁴ I. Radu, P. Notingher and J. Filippini, Influence of water trees on the electrical field distribution and breakdown in the point-point geometry, Journal of electrostatics (2000) 165-178.
- ²⁵ R. Sarathi, A. Nandini and T. Tanaka, Understanding electrical treeing phenomena in XLPE cable insulation under harmonic AC voltages adopting UHF technique, IEEE Transactions on dielectrics and electrical insulation (2012) 903-909.
- ²⁶ J. Catellon, I. Ramirez Vazquez, M. Frechette and D. Fabiani, Nanocomposite characterization and diagnostics tools, IEEE electrical insulation magazine (2013) 37-48.
- ²⁷ W. Yin, P. Irwin and D. Schweickart, Dielectric breakdown of polymer insulation aged at high temperatures, in: International power modulators and high voltage conference, Las Vegas, USA, 2008, pp. 537-542.
- ²⁸ C. Reddy, M. Gosityowaki, Y. Murata and Y. Sekiguchi, Superior thermal breakdown of MgO LDPE nanocomposite materials for HVDC insulation, International symposium on electrical insulation (2008) 661-664.
- ²⁹ J. Ho and T. R. Jow, High field conduction in biaxially oriented polypropylene at elevated temperature, IEEE transactions on dielectrics and electrical insulation (2012) 990-995.
- ³⁰ M. Nagao, T. Kimura, Y. Mizuno, M. Kosaki and M. Ieda, Detection of joule heating before dielectric breakdown in polyethylene films, IEEE transactions on electrical insulation (1990) 715-722.
- ³¹ X. Zhou, et.al., Electrical breakdown and ultrahigh electrical energy density in poly(vinylidene fluoride-hexafluoropropylene) copolymer, Applied physics letters (2009) 1629011-1629014.
- ³² J. Blok and D. G. LeGrand, Dielectric breakdown of polymer films, Journal of applied physics (1968) 288-293.
- ³³ X. Dou, et.al., Improved dielectric strength of barium titanate-polyvinylidene fluoride nanocomposite, Applied physics letters (2009) 1329041-1329043.
- ³⁴ J. K. Nelson, Backgrounds, principles and promise of nanodielectrics, in: J. K. Nelson (Ed), Dielectric polymer nanocomposites, Springer US 2010.

-
- ³⁵ R. C. Smith, C. Liang, M. Landry, J. K. Nelson and L. S. Schadler, The mechanisms leading to the useful electrical properties of polymer nanodielectrics, *IEEE transactions on dielectrics and electrical insulation* (2008) 187-196.
- ³⁶ M. Roy, J. K. Nelson, R. K. MacCrone and L. S. Schadler, Candidate mechanisms controlling the electrical characteristics of silica/XLPE nanodielectrics, *Journal of material science* (2007) 3789-3799.
- ³⁷ M. Roy et. al., Evidence for the role of the interface in polyolefin nanocomposites, *Proceedings of international symposium on electrical insulating materials* (2005) 223-226.
- ³⁸ M. Nagao, S. Watanabe, Y. Murakami and Y. Murata, Water tree retardation of MgO/LDPE and MgO/XLPE nanocomposites, *Electrical insulating materials* (2008) 483-486.
- ³⁹ K. Yu, Y. Niu, F. Xiang, Y. Zhou, Y. Bai and H. Wang, Enhanced electric strength and high energy density of barium titanite filled polymer nanocomposites, *Journal of applied physics* (2013) 1741071-1741075.
- ⁴⁰ T. P. Schuman and S. Siddabattuni, Improved dielectric breakdown strength of covalently-bonded interface polymer-particle nanocomposites, *Composite interfaces* (2010) 719-731.
- ⁴¹ S. Siddabattuni, T. P. Schuman, and F. Dogan, Improved polymer nanocomposite dielectric breakdown performance through barium titanate to epoxy interface control, *Material science and engineering B* (2011) 1422-1429.
- ⁴² S. P. Fillery, et.al., Nanolaminates: Increasing dielectric breakdown strength of composites, *ACS applied materials & interfaces* (2012) 1388-1396.
- ⁴³ H. Zhang, Y. Shang, X. Wang, H. Zhao, B. Han and Z. Li, Mechanisms on electrical breakdown strength increment of polyethylene by aromatic carbonyl compounds addition: a theoretical study, *Journal of molecular modeling* (2013) 5429-5438.
- ⁴⁴ A. Ashcraft, R. Eichhorn and R. Shaw, Laboratory studies of treeing in solid dielectrics and voltage stabilization of polyethylene, *IEEE International symposium on electrical Insulation* (1976) 6.
- ⁴⁵ M. jarvid, A. Johansson, V. Englund, S. Gubanski, M. R. Andersson, Electrical tree inhibition by voltage stabilizers, in: *Annual report conference on electrical insulation and dielectric phenomena*, Montreal, Canada, 2012, pp. 605-608.
- ⁴⁶ J. Woo Ko, K. S. Suh and S. H. Lee, Water treeing, AC breakdown, and dielectric loss characteristics of EVA-OH as a function of conversion rate, *Journal of applied polymer science* (2006) 420-424.
- ⁴⁷ S. Siddabattuni, T. P. Schuman, and F. Dogan, Dielectric properties of polymer-particle nanocomposites influenced by electronic nature of filler surfaces, *ACS applied materials & interfaces* (2013) 1917-1927.
- ⁴⁸ Y. Yamano and M. Iizuka, Improvement of electrical tree resistance of LDPE by mixed addition of nanoparticles and Phthalocyanine, *IEEE Transactions on dielectrics and electrical insulation*, (2011) 329-337.
- ⁴⁹ S. J. Laihonon, Polypropylene: Morphology, defects and electrical breakdown, PhD thesis, Royal institute of technology, Stockholm 2005.